Replies to review comments

We thank all the reviewers and the co-editor for the time and effort spent on the manuscript.

Considering all suggestions from three reviewers, we made the following major changes in the revision of the manuscript:

1. A detailed description of our MIPAS aerosol measurements is added.
2. The Sect. 3.2 that introduces the meteorological background is moved to Sect. 3.1. And Fig.4 that shows the meteorological background is the new Fig. 1.
3. In Fig. 1, ACI values no larger than 8 instead of 7 is shown to allow in a little more measurements, and it is moved to the new Fig. 5.
4. The Fig. 6 that shows the latitude and height cross section of the MIPAS median ACI values is removed, because contaminated by the background aerosol, the change of aerosol load after the Merapi eruption in 2010 and the poleward transport of the volcanic aerosol is not clear.
5. MIPAS aerosol measurements during the relatively volcanic eruption quiescent period in the Southern Hemisphere from 11/2007 to 03/ 2008 are used as the reference state to derive the change of aerosol load in the Southern Hemisphere after the Merapi eruption in 2010, so that the seasonal variations are removed. And the Fig.7 (the new Fig. 6 in the revised manuscript) and the Fig. 10 (the new Fig. 9 in the revised manuscript) are updated accordingly. Reference time period from November 2003 to March 2004 is also tested and they all showed qualitatively comparable results.
6. An appendix is added to compare the aerosol load in the tropical stratosphere during the selected reference period (11/2007 to 03/ 2008) and the time period of investigation (11/2010 to 03/ 2011).
7. The “transport efficiency“ may not be the accurate term to describe the proportion of sulfur that originated from the Merapi eruption and was transported to the Antarctic upper troposphere and lower stratosphere (UTLS), so we rephrase it in the abstract, discussion and conclusion..

Please find our point-by-point replies below in blue color. Other amendments can be found in the revised manuscript with tracked changes.

Anonymous Referee #1
Received and published: 1 June 2018

The Editor will have to decide if there is enough new science here to accept this paper. The paper needs some revisions, but the question is whether it is important science. This paper is well written and presents a new analysis of the poleward transport of the Merapi sulfur. But I'm not sure what is surprising in the conclusions. It is already known that stratospheric sulfur from volcanic eruptions gets transported to the poles, as we find it in ice cores.

Both the sulfate in the ice core record and observation of Antarctic ozone depletion have verified that major volcanic eruptions at low latitudes and volcanic eruptions at the Southern Hemisphere high latitudes may contribute to the sulfate in Antarctica, for instance, the low-latitude major eruptions of Agung in 1963 (Nicolas Patris, 2000), El Chichón in 1982 (Hofmann and Rosen, 1985), Pinatubo and Cerro Hudson in 1991 (Pitts et al., 1993) and high-latitude eruption Calbuco (Solomon et al., 2016; Ivy et al., 2017; Stone et al., 2017). However, there are discussions about the contributions over Antarctica from long range transport and local volcanic sources.

Meanwhile, due to the limit of spatial and temporal resolution of satellite data, and the spatial coverage of in-situ observations, it is difficult to investigate the transport process. We were not able to estimate the influence of the location of the eruption, the height of plume, and the atmospheric background conditions on the transport pathway, and thus not able to judge whether a volcanic eruption will contribute to the sulfate in Antarctica or how much if it does.

It is reasonable to believe that major low-latitude eruptions inject SO_2 directly into the upward branch of the BDC, and the SO_2 or aerosol ascend and flow slowly poleward along the BDC, which could be the main pathway of long-range transport from the tropics to the poles. The Merapi eruption in 2010 was a moderate eruption in the tropics that showed a poleward dispersion of aerosol to Antarctica whereas most other tropical eruptions did not. The fast dispersion of volcanic aerosol for the Merapi case did not seem to be caused by BDC.

This study is one step forward to reveal the transport process and the influence of background atmospheric conditions by combining satellite observations with model simulations in a case study. By carrying out model simulations, it was found that the transport of the volcanic aerosol from the Merapi eruption in 2010 was mainly driven by the relatively quick quasi-horizontal transport from the tropical tropopause layer to the upper troposphere and lower stratosphere at mid- and high latitudes. Based on simulations, the mechanism that influences the transport pathway could be analyzed, and the amount of sulfur transported could be quantified.

Is it that so little of the sulfur made it to the poles?

Based on our simulation and calculation, there was a maximum 8.80×10^3 tons of sulfur went to the south of 60°S between the isentropic surfaces of 350 and 480 K at the end of February 2011. If these were in form of a 75–25% H_2SO_4-H_2O solution, the total aerosol mass loading adds up to 2.15×10^4 tons. As seen in Fig.1 (Fig. 5 in the revised manuscript), except for the high-latitude volcanic eruptions, the moderate tropical eruption, Merapi eruption in 2010, made a most prominent contribution to the stratospheric aerosol at mid- and high latitudes.

Are there any observations to validate the model simulation?

In our study, MIPAS data are compared with model results. The altitude-resolved MIPAS aerosol observations are the best data to validate our model results. The CALIOP measurements captured some signals of sulfate aerosol and ash (not shown in the manuscript), but because the CALIOP aerosol data is very limited during the polar daytime, it did not complement to the MIPAS observations. We did not obtain ice core data later than 2001 to verify the disposition of sulfate.

Fig. 7 (confusing because the units are not defined) actually shows that the aerosol load was reduced at the South Pole.

Figure 7 shows the change in median ACI values in the tropics and the Southern Hemisphere corresponding to the same time period as Fig. 6. It is to demonstrate the increase in the aerosol load due to the eruption of Merapi. To calculate the values in Fig. 7, we first define the “reference state” of the aerosol load by calculating the median ACI in 1–4 November 2010 when there was no aerosol from the Merapi eruption. Then the median ACI values in Fig. 6 are subtracted from this “background” ACI. Since in the MIPAS retrievals, smaller ACI values represent larger aerosol extinction coefficients, in Fig. 7, the positive values indicate an increase in aerosol load and negative values indicate a decrease of the aerosol load. The values do not have units.

The negative values in the South Polar Region above 10 km are not caused by the transport of the volcanic aerosol. Because time period of 1–4 November 2010 is not an ideal “reference state” aerosol load, so there are seasonal variations in the Fig.7. Inspired by suggestions of referees, we used another time period to define the “reference state”. We removed the seasonal cycle in the aerosol data by using data from 11/2007-03/2008 (a relatively volcanically quiescent period in the Southern Hemisphere) instead of 4 days reference period. In this way, the change of the aerosol load after the Merapi eruption and the poleward transport of aerosol are clearer. For more details, please see reply to major comment 1 of referee #2 and the revised manuscript.

I am also confused about the initial stratospheric transport of the volcanic plume. If there was a westerly phase of the QBO, why was the transport toward the west?

Trajectory calculations of each air parcel in Lagrangian transport simulations are driven by wind fields at the location of each air parcel. Figure R1 shows the monthly mean zonal wind in November 2010. If the air parcels were in the area with easterlies, they would be transported towards west. The QBO index in Fig. 4f only shows the zonal wind anomalies over the Equator at 30 or 50 hPa, but can not show the wind directions at the location of each air parcels. Please note that in the revised manuscript, Fig. 4 is move to Fig. 1.

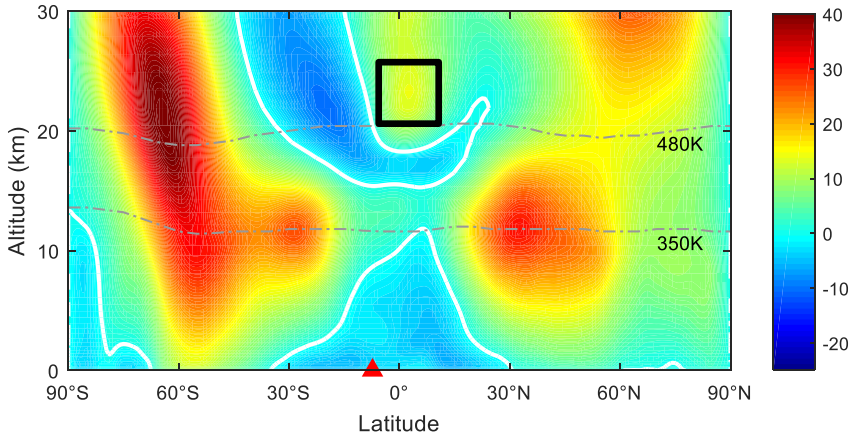

Figure R1: Monthly mean zonal wind (unit: m/s) in November 2010, overlapped the potential temperature of 350K and 480K. The thick white contour indicates the value of 0. The rectangle indicates the region over the equator between 30 hPa (~ 25 km) and 50hPa (~21 km). QBO indices (monthly mean zonal wind anomalies over the Equator) are usually defined at pressure levels of 30 and 50 hPa. The red triangle denotes the latitude of Mount Merapi.

I am confused by the discussion of transport barriers on page 12. The authors say there are PV boundaries, but never explain how this works nor what values of PV are used. Then they use potential temperature values to define transport boundaries. They have to explain how this works and make clear what “boundaries” are and why they chose the values of PV or potential temperature for those boundaries.

Rossby wave breaking is an important mechanism for the exchange of air masses between the tropical upper troposphere and the extratropical lower stratosphere. Potential vorticity (PV) streamers (e.g., poleward-moving filaments with low PV originating in the tropics) are indicators of Rossby wave breaking (RWB) and constitute important atmospheric transport pathways between the tropics and extratropics.

Kunz et al. (2015) derived a climatology of PV streamer boundaries on isentropic surfaces between 320 and 500K using ERA-Interim reanalyses for

the time period from 1979 to 2011. This boundary is defined as the maximum product of the meridional PV gradient and zonal wind speed on isentropic surfaces, which identifies a PV contour that best represents the dynamical discontinuity on each isentropic surface. It can be used as an isentropic transport barrier and to determine the isentropic cross-barrier transport related to Rossby wave breaking. There are seasonal variations in the location of PV boundaries as shown in Fig. R2 and the specific values of the PV boundaries on isentropic surfaces in each season can be found in Table R1.

In this study, the horizontal transport along the subtropical jet associated with Rossby wave breaking is a long-range transport mechanism from the tropical tropopause layer to the Southern Hemisphere lower stratosphere. The volcanic plume was transported along the subtropical jet and at the same time entered the extratropical lower stratosphere driven by Rossby wave breaking. The PV contours shown with gray dashed lines in Fig. 8 (the Fig. 7 in the revised manuscript) represent the isentropic transport barrier on 350 K isentropic surface (-3.33 PVU during November and -4.78 PVU during December) based on the climatology of the PV streamer boundaries derived by Kunz et al. (2015). Isentropic transport of air masses across these contours is due to Rossby wave breaking. In the polar stratosphere, PV boundaries on isentropic surfaces, e.g., around 480 K, can be considered as a barrier for cross polar vortex transport of air masses between the mid-latitudes and polar regions.

We have added more detailed explanations to Sect. 3.4 in the revised manuscript to make this term clearer.

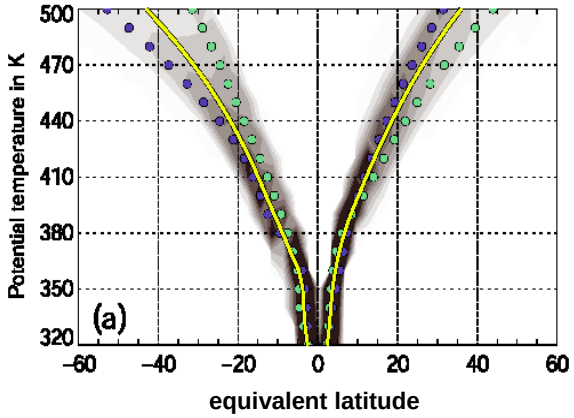

Figure R2. Probability density function of the 1979–2011 daily values of the (a) dynamically relevant contour of PV on isentropes between 320 and 500 K. The bin size is 3 PVU for PV and 5° for equivalent latitude. Blue and green dots represent the mean PV or mean equivalent latitude of the dynamically relevant contour in June, July and August (JJA) and December, January and February (DJF) respectively. The solid yellow line represents an annual mean. (Kunz et al., 2015)

	Northern Hemisphere				Southern Hemisphere			
Isentrope	MAM	JJA	SON	DJF	MAM	JJA	SON	DJF
320 K	2.22	2.44	2.60	2.21	−2.98	−2.25	−2.37	−2.53
330 K	2.59	3.08	3.28	2.65	−3.80	−2.52	−2.77	−3.59
340 K	2.85	3.62	3.74	2.91	−3.92	−2.79	−3.00	−4.48
350 K	2.98	4.46	4.10	3.24	−3.83	−3.17	−3.33	−4.78
360 K	3.64	5.51	4.91	3.80	−4.43	−3.93	−5.62	−5.18
370 K	4.63	6.36	5.99	4.65	−5.50	−6.20	−9.54	−6.24
380 K	5.88	7.24	7.20	6.07	−6.69	−9.57	−11.47	−7.61
390 K	7.76	8.56	8.54	8.58	−8.67	−12.52	−13.34	−9.23
400 K	9.63	10.04	9.99	11.36	−11.08	−14.37	−15.47	−10.92
410 K	11.50	11.67	11.51	13.93	−13.07	−16.20	−17.73	−12.64
420 K	13.53	13.44	13.21	16.55	−15.12	−18.39	−20.10	−14.51
430 K	15.68	15.33	15.15	19.20	−17.20	−21.17	−22.55	−16.51
440 K	17.85	17.28	17.26	21.94	−19.29	−24.60	−25.15	−18.50
450 K	20.15	19.28	19.52	24.95	−21.56	−28.61	−28.02	−20.50
460 K	22.55	21.38	22.01	28.17	−24.11	−32.81	−31.30	−22.52
470 K	25.09	23.65	24.82	31.69	−27.00	−37.38	−35.27	−24.52
480 K	27.80	26.08	27.85	35.46	−30.19	−42.20	−39.75	−26.64
490 K	30.62	28.55	31.16	39.47	−33.80	−47.35	−44.47	−28.93
500 K	33.64	31.44	34.80	43.90	−37.78	−52.86	−49.46	−31.47

Table R1 Seasonal Mean of the PV boundaries (in PVU) in isentropic surfaces between 320 and 500 K (Kunz et al., 2015)

It is not clear to me how the values of 8800 tons of sulfur (and are they sure this is S, and not SO2 or SO4?) and 4% were derived for transport into the south polar cap. The figures did not show much arriving south of 60◦S at all.

As Figure 10a (Fig. 9a in the revised manuscript) showed with black dots, it is calculated that there was a maximum of 4% of the plume south of 60°S between isentropic surfaces of 350 and 480 K at end of February 2011. The percentage is roughly calculated by dividing the number of SO_2 parcels between 350 and 480 K south of 60°S by the total number of SO_2 parcels released.

Based on previous research on the Merapi case, we assigned a total mass of SO_2 to all parcels released. There is not a chemical scheme in the Lagrangian particle dispersion model we used, so we assume that when the plume went to the high latitudes, the SO_2 are all converted to sulfate acid. And we multiplied the percentage of air parcels south of 60°S between isentropic surfaces of 350 and 480 K with the total mass of sulfur in the released plume and only calculated the mass of the part of sulfur (not SO_2 or sulfate acid). This result (8800 tons) is under the assumption that sulfate aerosol converted from SO_2 remained in the plume. And there are other factors that can affect this number have been discussed in Sect. 4.

It is possible that the confusions above came up because it was not very clearly explained in the manuscript. So we have added a further explanation

for each of them in the revised manuscript.

The authors need to address the 56 comments in the attached annotated manuscript, paying particular attention to issues with the figures.

Please see the supplement with comments.

Anonymous Referee #2
Received and published: 25 June 2018

General comments
This study investigates the transport of volcanic sulfur emissions from the 2010 eruption of Merapi. It uses both model simulations and satellite observations to investigate the poleward transport of sulfur to high latitudes. The topic is well suited to ACP.

Major comments
1. The study claims “good agreement” between the simulated trajectories and the MIPAS aerosol index measurements, and uses this “agreement” to underpin the conclusions of the work. Unfortunately, I just don’t see a good agreement between the satellite observations and the model results. The model results (Fig 5) show a strong sulfur presence at and above the tropical tropopause, and strong poleward transport along the 380 K PT surface. From Fig. 7, the observations show almost no aerosol above the tropical tropopause, and slight aerosol increases in the high latitude upper troposphere. If this slight high latitude aerosol increase is from the Merapi eruption, the transport pathway does not appear to be via the 380 K PT surface, as in the model simulation.
Plus, the observations show a highly elevated aerosol index in the SH high latitude stratosphere before the eruption, and some apparent descent of these aerosols, which could contribute to the elevated aerosol signal just below the tropopause in Jan and Feb 2010. I also worry about the choice of a very small reference period in the calculation of the anomalies in Fig 7, it seems likely that the anomalies shown might contain the influences of seasonal variations in aerosol and transport, for instance there are strong variations in UT aerosol in the NH, not associated with volcanic activity in Fig 6. The simulations presented here produce some clear results, but much more work would be required to be able to say that these results are supported or “validated” by the observations, this is simply not true.

We agree that we messed up a clear presentation of the satellite data showing the Merapi plume transport in Fig.7. We thank referee #2 for pointing out that 4 days before the eruption are too short for a reference period as there are seasonal variations in the aerosol signal. In order to bring the aerosol signal of the Merapi into the foreground, we selected a time period from 11/2007 to 03/2008 with no major SO_2 emission in the Southern Hemisphere UTLS (as shown in Fig. 5 in the revised manuscript) as a “reference state”, calculated the biweekly median ACI of the “reference state” and subtracted the biweekly ACI median between 11/2010 and 03/2011 from it. Now the aerosol signal due to the Merapi aerosol is shown clearly.

To test for inter-annual variations, we tested a second time period 11/2003 to 03/2004 without large or moderate volcanic eruptions in the Southern

Hemisphere and found qualitatively comparable results.

The Fig.6 does not show the poleward transport of the aerosol clearly with seasonal cycle in it, so we remove the Fig. 6 and the Fig.7 is the new Fig. 6 in the revised manuscript.

2. The authors claim to have investigated the transport efficiency of volcanic aerosol, for example stating that “the most efficient pathway for the quasi-horizontal mixing was in between the isentropic surfaces of 360 and 430 K”. They do not however define what they mean by “efficiency”–usually efficiencies correspond to some sort of ratio, e.g., the proportion of transported to injected material, but the analysis seems only to be based on the vertical levels where the largest numbers of trajectories existed, which is obviously strongly connected to the vertical level of the injections. It is also stated that transport from quasi-horizontal mixing is “more efficient” than the slow residual mass circulation of the Brewer-Dobson circulation, but this is a rather obvious result for an injection into the tropical UTLS especially when only short term simulations are performed. Is transport to Antarctica from a tropical UTLS injection more efficient than transport of background sulfate via the BDC? Such questions cannot be answered with this study.
Thank you for pointing this out. We agree that we can not compare the in-mixing with BDC in our study. We have rephrased the statement throughout the manuscript. Instead of “efficiency”, it is more accurate to say it is the proportion of sulfur that originated from the Merapi eruption and was transported to the Antarctic UTLS.

3. The connection between the aspects of the simulated aerosol transport and different dynamical regimes–the phase of the QBO or the strength of the subtropical jet–are not tested in any way, and so cannot be linked in a causal way. For example, the study does not show in any way that the transport of aerosol “was facilitated by the weakening of the subtropical jet during the seasonal transition from austral spring to summer and linked to the westerly phase of the quasi-biennial oscillation (QBO)” as stated in the conclusions. This is an assumption based on prior work, not a conclusion of the experiment presented here.
We agree that the role of QBO in the transport cannot be considered as the conclusions of this study. The influence of the QBO phase is rather described as the meteorological background. We have removed the statement of the QBO in the abstract and conclusions.

Specific comments:
P1, l16: usually present tense (“estimate”) is used to describe work done in the presented study. Check here and throughout.
Fixed. Thank you.

P1, l19: See major comment 1: “good agreement” is never quantified, and there is little evidence that the observations suggest a significant amount of aerosol transported to the SH high latitudes.
Please refer to the reply to major comment 1. The agreement between the simulations and the observations is significantly improved after we applied a new reference state.

P1, l26: Most efficient or strongest? Most efficient would imply calculation of some sort of efficiency index, which does not seem to have been done. These heights may have been where the strongest transport occurred just because of the height of the injection, not because the transport there is stronger than other heights.
We agree that most of the poleward transport is due to the in-mixing because the top of SO_2 injection is in the tropical tropopause layer. The words have been rephrased. Please also refer to the reply to major comment 2.

P1, l28: I guess less than 4% of the SO2 was transported to high SH latitudes since SO2 is decaying with a 1-month timescale, you probably mean 4% of the injected sulfur.
Yes, the 4% is the fraction of sulfur. It is fixed in the abstract.

P2, l8: The study by Aquila et al. (2014) presents model results of a geoengineering scenario: this is not strong proof for the kind of strong statement given here.
P2, l9: Similarly, the Pausata et al. (2015) study is also based on modeling results; this statement needs to be less conclusive to properly reflect current scientific understanding.
Because the QBO is not directly related to our results in this study, we removed these sentences in the introduction.

P2, l11: The impact of aerosol on polar ozone has been known about for a long time; a handful of references from 2008-2016 don’t properly support the statement made here.
A few earlier references are added here.

P2, l17: “a new record of the size...” is awkwardly phrased.
It is replaced with “an Antarctic ozone hole with the largest daily average size”.

P3, l11: Kravitz and Robock (2011) describe the impact of season on the impact of high latitude eruptions, and say little about the impact of the variation of quasi-horizontal mixing with season. Toohey et al. (2011) would be a more appropriate reference here.
Toohey, M., Krüger, K., Niemeier, U. and Timmreck, C.: The influence of

eruption season on the global aerosol evolution and radiative impact of tropical volcanic eruptions, Atmos. Chem. Phys., 11(23), 12351–12367, doi:10.5194/acp-11-12351-2011, 2011.
The reference is replaced. Thank you.

P4, l12: “product is sensitive: : :”
Fixed.

P6, l12: Some indication of what kinds of measurements have been used to build the “chronology of the Merapi eruption” would be useful for the reader here.

Thank you very much for your suggestion. We added the data source here as follows:

“According to the chronology of the Merapi eruption that combined satellite observations from AIRS, the Infrared Atmospheric Sounding Interferometer (IASI), the ozone monitoring instrument (OMI) and a limited number of Ground-based ultra-violet Differential Optical Absorption Spectroscopy (DOAS) measurements…”

P6, l25: The reconstructed SO2 injection between Nov 1 and Nov 3, which shows injection above the tropopause but little anywhere else–seems unlikely given the reported eruption chronology. This portion of the injection time series seems very uncertain, and the implications of possible errors here should be discussed.

Thank you for pointing this out. The SO_2 above the tropopause is quite robust in our simulation. We have checked the CALIOP profiles from 27 October 2010 to 10 November 2010 and found a few profiles that show some dust appeared over the location of Mount Merapi at the height from about 14 to 18 km on 2, 3, 5 November 2010 (no tracks over volcanic plume on 4 November 2010), and 3 to 17 km on 6 November 2010. It could be a fraction of the volcanic plume elevated by the updraft in the convection appeared with the tropical storm Anggrek. The center of the tropical storm Anggrek was on the Indian Ocean about 1000 km southwest of the Mount Merapi. So we consider this small fraction of SO_2 as real and prefer to keep it in our results. The fraction of SO_2 plume above the tropopause very small and our conclusions are not affected with or without it.

We have added some explanation in Sect. 3.2.

P7, l2: One should be clear that you are neglecting the impact of sedimentation completely, i.e., for all sulfate particles–it reads now like you are neglecting sedimentation for the small aerosol. Secondly, you need some words on the applicability of this assumption.

To avoid the ambiguity, this sentence is removed from Sect. 3. A few sentences are added in Sect.4 to discuss this assumption.

P7, l7: “parcels in the upper troposphere: : :”
Fixed.

P7, l21: The two sentences starting with “A more negative...” seem to be referring to conclusions from prior studies, which should be referenced. Also, the first sentence especially is confusing since the post-Merapi anomalies in Fig 4d imply a less negative eddy heat flux, best would be to adjust the description to be consistent with what is seen in Fig 4.
References are added.

P8, l21: please be clear that you refer to “the simulated plume” here and elsewhere.
It is fixed here and throughout the manuscript.

P8, l25: Till-> Until
Fixed.

P8, l30: I don’t see the “secondary upward transport” commented on here, either the description needs to be clearer, or this statement cut. P8, l31: Using the word “observable” when presenting simulation results is confusing.
This paragraph is rephrased. An appendix is added to show the upward transport of aerosol in the tropical stratosphere.

P9, l9: I don’t think you can conclude with all certainty that the transport was suppressed by the subtropical jets–it is likely, but you didn’t test it in any way in your analysis.
This paragraph has been removed together with the Fig. 6.

P9, l17: Four days is a very small sample to base a reference state on. How sensitive are the results to the choice of a reference? Better might be to define a clean climatology from prior years and subtract a seasonally varying climatology.
We changed the reference period. Please see reply to major comment 1 for the details.

P9, l22: Why does the zonal averaging “degrade” the ACI signal? Is this related to incomplete sampling and the plume being localized? What about the 1 month timescale of the conversion of SO2 to sulfate, does that play a role?

The global MIPAS measurements cover longitudes from -180 to 180° each day. After an eruption, only measurements around the longitude of the volcano indicate aerosol. When there are more than about 30 MIPAS measurements

between the Equator and 5°S, but only one or two of them sample the plume and the others sample clear air, the median and often the mean signal indicate clear air. Of course, the sampling also plays a role. In the tropics, MIPAS measures only down to about 12 km. Hence, the first eruption phase of Merapi (26 Oct - 3 Nov) will be missed. At higher altitudes, if the plume falls between the measurement tracks, it will be missed. The aged aerosol is usually dispersed, so the plume will not be missed due to the sampling.

The conversion of SO_2 to sulfate starts with the moment when the SO_2 enters the atmosphere, and the converted aerosol particles are present in detectable amounts right after the SO_2 injection.

The sentence in the manuscript "No significant change was observed during the first half month after the eruption due to the zonal averaging degrading the aerosol signal (Fig. 7a)" has been changed to:

“In the first half of November, the zonal median (Fig. 6a) does not show a signal of the Merapi eruption, because during the initial time period, the plume was confined to longitudes around the volcano (see Fig. 3), and the MIPAS tracks did not always catch the maximum concentration, so the median ACI values are large (low concentration or clear air). In the second half of November the plume was transported zonally around the globe and hence, the largest aerosol increase appeared in the upper troposphere at the latitude of the Mount Merapi (Fig. 6b) and then moved quasi-horizontally southward into the UTLS region at ~30–40°S (Figs. 6c–d), consistent with what Fig. 5c–d shows."

P9, l24: The strongest signal in the SH high latitudes is a large decrease in ACI, what is this?
This is a seasonal effect we observe every year in the MIPAS data. We followed your suggestion of using more data to define the reference state and to remove seasonal variations. For details and changes on the manuscript please see reply to the major comment 1.

P9, l25: How was the significance of this increase tested?
This paragraph is removed and new texts are added to describe the new Fig. 6.

P10, l2: “comparable” is a rather weak adjective, and in fact there are many important differences between the model results and observations (see major comments).
This sentence has been removed.

P10, l4: “in the surf zone”
Fixed.

P10, l6: What is “our data”? The statement here seems based on the simulation results, but not strongly supported by the observations.
It refers to the simulations. It is replaced with “The simulations”.

P10, l7: The conclusion regarding the main transport pathway stated here should apply only to the Merapi eruption–a large eruption like Pinatubo with a higher injection height will certainly have a different main transport pathway.
It is corrected in the manuscript

P11, l5: “the simulated poleward...”
Fixed.

P11, l14: observed->simulated
Fixed.

P11, l25: The impact of the QBO was not shown in any way by this study, only assumed based on prior work.
We have removed the statement of the QBO in the abstract and conclusions. Please refer to the reply to major comment 3.

P11, l28: No, Figure 4 shows there was weaker than usual wave activity after the eruption, and a colder, more stable vortex until the end of February.

The longitudinally averaged poleward eddy heat flux between 45 and 75◦ S was smaller than the long-term mean, indicating that the vortex was relatively unperturbed from mid-September to December. However, the polar vortex elongated and weakened gradually through November and was displaced off the pole in mid-December and broke down by mid-January 2011 as shown in Fig. R3.This decay of the polar vortex could also be seen in the Fig. 8 (the Fig. 7 in the revised manuscript), marked by the grey solid contour.

In Fig. R3, the breakdown was marked when the winds around the vortex edge decreased below 15 ms^{-1} on the 475 K potential temperature surface. Figure R4 shows the final warming started in mid-October with the development of strong zonal asymmetries in temperature. The cold pool over the South Pole declined and displaced. A warm pool with temperatures of 230–240 K dominated Antarctica from the end of December. This warming can also be observed in Fig. 4b (the new Fig.1b in the manuscript). Consistent with the warming, the zonal wind speed at 60°S at 150 hPa (Fig. 4c) showed a pronounced reduction in wind speed from 40ms^{-1} at the beginning of October to less than 20 ms-1from beginning of January.

In the revised manuscript, we add the temporal variations of the area of the polar vortex in Fig. 1 in the revised manuscript to show the change of intensity of the polar vortex.

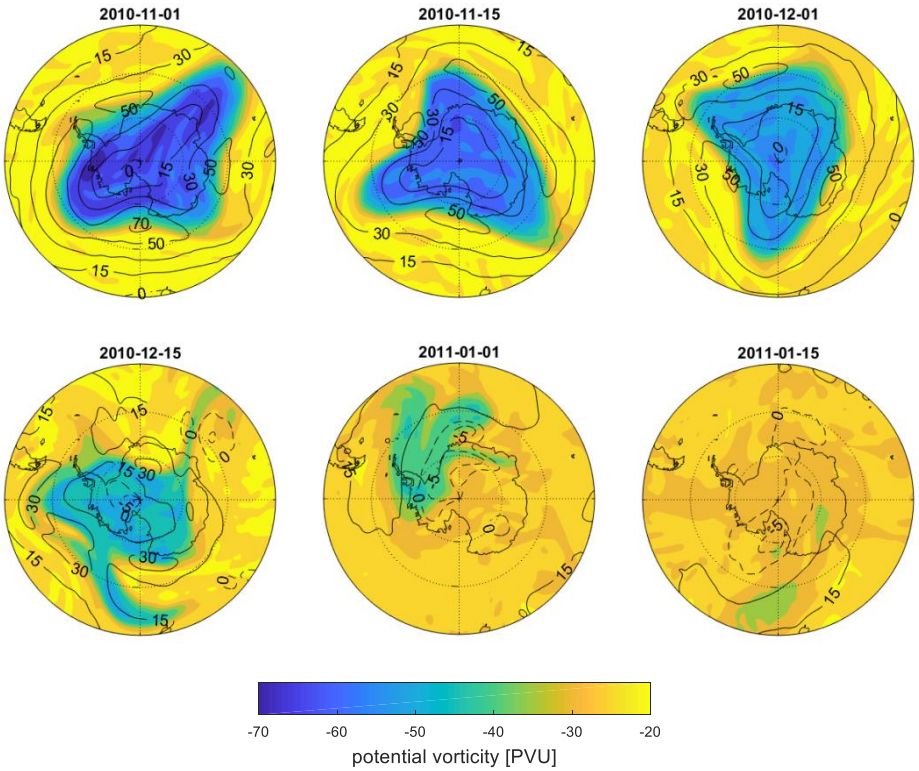

Figure R3: ERA-Interim potential vorticity (1PVU=10^{-6}Km^2 s^{-1} kg^{-1}; shaded) and zonal wind contours (m s^{-1}; black curves) on the 475 K isentropic surface. Data are shown for 00:00UTC on selected days. Outer circles of the polar maps indicate the latitude of 45°S. The prime meridian is oriented towards the top of the map.

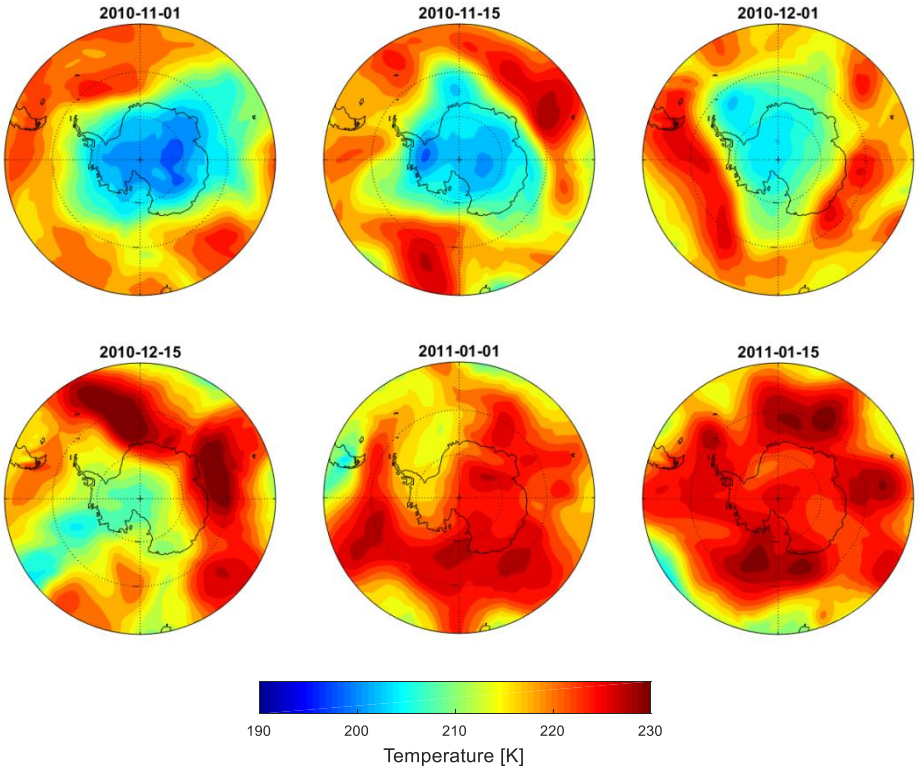

Figure R4: ERA-Interim temperature on the 150hPa pressure level. Data are shown for

00:00UTC on selected days. Outer circles of the polar maps indicate latitude of 45°S. The prime meridian is oriented towards the top of the map.

P12, l1: This paragraph is irrelevant, unless the authors have some evidence that the aerosol from Merapi was enough to produce enough heating to perturb the QBO.
This paragraph is removed.

P12, l9: This sentence, with the use of the word “contributed” is a rather strong statement given the observations don’t really support the strong degree of transport in the model.
The simulations agree much better to the observations after using a new reference state. But the assumptions in our simulation may overestimate the amount of aerosol transported to the Antarctica UTLS, so we rephrased this sentence and this estimation of the transported aerosol may be considered as an upper limit.

P12, l23: Again (see major comments), I don’t agree that the “MIPAS aerosol detections confirmed the MPTRAC simulations”.
Please refer to reply to major comment 1.

P13, l12: “validated” is too strong.
It is rephrased.

Anonymous Referee #3
Received and published: 5 July 2018

The paper contains a comparison between results of trajectory calculations for longrange transport of volcanic aerosol and a satellite derived qualitative quantity for aerosol, the aerosol cloud index (ACI). It might be of interest for ACP but it needs a lot of improvements to be useful.

1 General comments
It is often not clear what is from previous work or the actual study. Concerning the comparison and for model validation it would be much better to use the actual observations of H2SO4 aerosol and SO2 given in Günther et al., 2018 (ACP!) instead of the aerosol cloud index which cannot distinguish between PSCs and volcanic aerosol (e.g. Fig. 1) and where also important definitions are not provided. The figures are difficult to understand and contain too many frames. There are also several times contradictions between text and figures. The remarks on the interactions with the QBO should be corrected and shortened.

We agree that the current presentation of the MIPAS ACI data is not ideal for the comparison with the model results and we appreciate the suggestion to compare with the aerosol and SO_2 retrievals by Günther et al. (2018). However, after thorough analysis, we decide not to replace the ACI for the comparison but to improve the presentation of the ACI data. The reasons that lead to our decision are:

Before the retrieval of H_2SO_4 aerosol and SO_2, Günther et al. (2018) pre-processed the MIPAS data by filtering out optically thick clouds using the cloud index (CI) with a threshold of 1.7 and after the retrieval they filtered out thin ice clouds using with threshold ACI<7 and the same ice filter method as we did (Griessbach et al., 2016), and also the same ash filter to remove volcanic ash and mineral dust (Griessbach et al., 2014). In addition, Günther et al. (2018) removed all retrieved data points that were up to 4 km above any detected ice cloud. This was not necessary for the ACI as it is given on MIPAS 1.5 km vertical sampling grid in the UTLS, but the retrievals by Günther et al. (2018) had a vertical resolution of 3-4 km. Furthermore, Günther et al. (2018) filtered out PSCs based on latitude, time, and temperature criteria, i.e., if the temperature between 17–23 km dropped below the NAT existence temperature (195 K) poleward of 40° in NH winter (15 November to 15 April) and SH winter (1 April to 30 November) the retrieval results were discarded. But we would like to keep the non-ice PSC data in our figures to give an impression on the temporal and spatial extent of the PSCs. The PSC signal usually is stronger than the aerosol signal. It means that aerosol retrievals below PSCs are not possible.

Hence, generally our ACI data is representing the raw aerosol signal before

the volume density retrieval of Günther et al. (2018), with the main difference that we did not filter out PSCs. Filtering out PSCs based on time, latitude, and temperature criteria may also lead to a loss of clear air profiles, e.g., when the synoptic temperature is sufficiently low but no PSCs are present.

So instead of replacing our ACI data with retrievals of Günther et al. (2018), we first added a detailed description of the ACI and the filter methods we used in Sect. 2. Second, we significantly improved the representation of the ACI data in Fig. 7 (the new Fig. 6 in the revised manuscript) for the comparison with the simulations. Now the simulations agree much better with the MIPAS observations, and the poleward transport of the plume can be seen clearly.

2 Specific comments

Abstract: Please correct or remove the statements on QBO. Most of the calculations are for polar summer without vortex. Please mention the aerosol cloud index explicitly if you like to keep the main focus on it, just saying aerosol observations is misleading here.
The role of QBO in the transport cannot be considered as the conclusions of this study. The influence of the QBO phase is rather described as the meteorological background. We have removed the statement of the QBO in the abstract and conclusions. The aerosol cloud index is added in the abstract.

Introduction, L48: This might have some effect on ozone depletion in the next ozone hole season (2011).
It is added in the introduction. Thank you.

Section 2.1: Include more details on ACI from the Griessbach paper if you like to use this, including their Eq.3. The second paragraph is messy concerning the wavelength.

We revised Section 2.1 and described the ACI and what it is used for in our study in more detail. The paragraphs on the ACI read now:

"ACI is the maximum value of the cloud index (CI) and aerosol index (AI):

$$ACI = \max(CI; AI), \quad (1)$$

The CI method is an established method to detect clouds and aerosol with MIPAS data. The CI is the ratio between the mean radiance around the 792 cm^{-1} where a CO2 line is located and the atmospheric window region around 833 cm^{-1} (Spang et al., 2001):

$$CI = \frac{\overline{I_1}([788.25,796.25\ cm^{-1}])}{\overline{I_2}([832.31,834.37\ cm^{-1}])}, \quad (2)$$

where $\bar{I}_1$ and $\bar{I}_2$ are the mean radiances of each window. The AI is defined as the ratio between the mean radiances around the 792 cm^{-1} CO2 band and the atmospheric window region between 960 and 961 cm^{-1}:

$$AI = \frac{\bar{I}_1([788.25,796.25\ cm^{-1}])}{\bar{I}_3([960.00,961.00\ cm^{-1}])}, \qquad (3)$$

where $\bar{I}_1$ and $\bar{I}_3$ are the mean radiance of each window.

For the CI, Sembhi et al. (2012) defined a set of variable (latitude, altitude, and season) thresholds to discriminate between clear and cloudy air, and the most advanced set of altitude and latitude dependent thresholds allows for the detection of aerosol/clouds with IR extinction coefficients larger than 10^{-5} km^{-1}.

The ACI is a continuous unitless value, small values indicating a high cloud or aerosol particle load and higher values indicating a smaller cloud or aerosol particle load. For the CI, Sembhi et al. (2012) defined a set of variable (latitude, altitude, and season) thresholds to discriminate between clear and cloudy air. The most advanced set of altitude and latitude dependent thresholds allows for the detection of aerosol and clouds with IR extinction coefficients larger than 10-5 km-1. For the ACI, a comparable sensitivity is achieved when using a fixed threshold value of 7 (Griessbach et al. 2016). Variations in the background aerosol are also visible with larger ACI values.

To remove ice clouds and volcanic ash from the MIPAS aerosol measurements, we first separated the data into clear air (ACI>7) and cloudy air (ACI<=7). Then we applied the ice cloud filter (Griessbach et al., 2016) and the volcanic ash and mineral dust filter (Griessbach et al., 2014) to the cloudy part and removed all ice or ash detections. However, since the ice and ash cloud filters are not sensitive to non-ice PSCs, the resulting aerosol retrieval results still contain non-ice PSCs (supercooled ternary solutions and nitric acid trihydrate). We keep the non-ice PSCs in the MIPAS retrieval results in this study to show the temporal and spatial extent of the PSCs, when and where the identification of volcanic is not possible.

Section 2.3: Is the reanalysis ERA Interim (mentioned too late)?
Yes, the MPTRAC model in this study is driven by the ERA-interim reanalysis. The MPTRAC model can also be driven by other reanalyses. We added this information at the beginning of Sect. 2.3.

Section 3.1: Figure 2 and the text are in contradiction to each other and the given reference (Surono).
We checked the texts to fix a few mistakes in the description. Some sentences are added to explain the SO_2 around the tropopause during 1–3 November 2010. To avoid ambiguities, one sentence that describes the degassing in the chronology provided by Surono et al. (2012) is removed.

Section 3.2, L256ff: Effect on late spring or summer circulation?

The paragraph about the role of QBO that starts from Line 256 is removed in the revised manuscript.

Section 3.3: Figure 3 is difficult to read and interpret, especially in connection with the zonal wind (Singapore data). There is also some contradiction to Fig. 6 which does not contain ACI<7 in the regions of interest. Comparing Fig. 5 and 6 is like comparing apples and oranges. Here the clear poleward plume shown in Günther et al., 2018 would be much more useful.

Figure 3 compares the altitude of air parcels in the plume simulated with MPTRAC model and the latitude of the MIPAS ACI measurements. Both the simulations and observations use the same color scheme but the observations are marked additionally with circles. In this way, when the simulations do not agree with the observations, different colors may be observed.

In the MPTRAC model, trajectory calculations are driven by wind fields at the location of each air parcel. Air parcels at various altitudes may disperse towards different directions. Please refer to the reply to referee #1.

Figure 6 shows the median value of the MIPAS ACI in each latitude-altitude bin across all longitudes. The ACIs in each bin may contain small values that indicate large aerosol extinction and large values that indicate small aerosol extinction or even clear air. The median ACI value in each bin is probably larger than 7 when the majority of the ACI values in that bin are large.

We have used a new definition of the reference state to derive the change of aerosol load after the Merapi eruption. Please see Fig. 6 in the revised manuscript. The poleward transport is clearer and the simulations and observations agree better.

Section 4, line 403: It might be of interest to compare the sulfate input from Merapi to the Antarctic lower stratosphere with the contribution of the Puyehue-Cordon Caulle eruption in June 2011.

The Puyehue-Cordon Caulle is a mid-latitude eruption (40.59 °S) that has a higher chance to influence Antarctica than a volcanic eruption in the tropics. Although the amount of SO_2 injected was only 0.2 Tg, it is not difficult to estimate that the Puyehue-Cordon Caulle added more aerosol to Antarctica than Merapi based on Fig. 1 (Fig. 5 in the revised manuscript). It erupted during austral winter, had a direct influence on the formation of PSCs and affected the ozone concentration in the following austral spring, which can be seen in Fig. 4 in the study of Solomon et al. (2016). The Puyehue-Cordon Caulle eruption is one of the important cases that should definitely be investigated if we would like to study the influence of volcanic eruption on the Antarctic aerosols. So the accurate estimation of the effect of the Puyehue-Cordon Caulle eruption could be a whole new study.

3 Technical corrections

Please correct the plenty typos and grammar errors. In line 444 it should be 2011. Use consistent units. Don't use words like 'data', 'observed' for model results.
We have checked the typos and try to improve the grammar throughout the manuscript.

Figure 2, caption: Strange units. Is the time UTC or local? Longitude and latitude range for integration?
It is UTC. The explanation is added in the caption.

The spatial range for integration is within the radius of 75 km to the location of the Mount Merapi as described in Sect. 2.3.

Figure 4: For what latitude range is frame f? It would be more useful to provide data for 100hPa instead of 30hPa.
The QBO index is defined as the zonal wind anomalies over the Equator (0°) at 30 hPa or 50 hPa. But since the QBO is not directly related to the conclusion, the QBO index is removed from the figure. The temporal variation of the area of the polar vortex is added instead.

Figure 5: The labels are too small and the color scale is for large portions out of range.
The color scheme is improved. As the Southern Hemisphere is the area of interest, we only keep the figures for the Southern Hemisphere.

Figure 6, caption: Spell out ACI.
The Fig. 6 is removed in the revised manuscript.

Figure 7, caption: Is aerosol load here equal to ACI (without unit)?
Yes, the "aerosol load" in the caption is replaced with "MIPAS ACI values".

Figure 10: Labels missing.
The labels are added.

References:

Griessbach, S., L. Hoffmann, R. Spang and M. Riese: Volcanic ash detection with infrared limb sounding: MIPAS observations and radiative transfer simulations, Atmos. Meas. Tech. 7, 1487-1507, doi: 10.5194/amt-7-1487-2014, 2014.

Griessbach, S., Hoffmann, L., Spang, R., von Hobe, M., Müller, R., and Riese, M.: Infrared limb emission measurements of aerosol in the troposphere and stratosphere, Atmos.

Meas. Tech., 9, 4399-4423, doi:10.5194/amt-9-4399-2016, 2016.

Günther, A., Höpfner, M., Sinnhuber, B. M., Griessbach, S., Deshler, T., von Clarmann, T., and Stiller, G.: MIPAS observations of volcanic sulphate aerosol and sulphur dioxide in the stratosphere, Atmos. Chem. Phys., 2017, 1-32, doi: 10.5194/acp-18-1217-2018, 2018.

Hofmann, D. J., J. M. Rosen and W. Gringel: Delayed production of sulfuric acid condensation nuclei in the polar stratosphere from El Chichon volcanic vapors, J. Geophys. Res. Atmos., 90(D1), 2341-2354, doi: doi:10.1029/JD090iD01p02341, 1985.

Ivy, D. J., Solomon, S., Kinnison, D., Mills, M. J., Schmidt, A., and Neely, R. R.: The influence of the Calbuco eruption on the 2015 Antarctic ozone hole in a fully coupled chemistry-climate model, Geophys. Res. Lett., 44, 2556-2561, 10.1002/2016GL071925, 2017.

Kunz, A., Sprenger, M., and Wernli, H.: Climatology of potential vorticity streamers and associated isentropic transport pathways across PV gradient barriers, J. Geophys. Res. Atmos., 120, 3802-3821, doi: 10.1002/2014jd022615, 2015.

Nicolas Patris, R. J. D., Jean Jouzel Isotopic signatures of sulfur in shallow Antarctic ice cores, J. Geophys. Res. Atmos., 105, 7071-7078, doi:10.1029/1999JD900974, 2000.

Patris, N., R. J. Delmas and J. Jouzel: Isotopic signatures of sulfur in shallow Antarctic ice cores, J. Geophys. Res. Atmos., 105(D6), 7071-7078, doi: 0.1029/1999JD900974, 2000.

Pitts, M. C. and L. W. Thomason: The impact of the eruptions of Mount Pinatubo and CERRO Hudson on Antarctic aerosol levels during the 1991 austral spring, Geophys. Res. Lett., 20(22), 2451-2454, doi: doi:10.1029/93GL02160, 1993.

Solomon, S., Ivy, D. J., Kinnison, D., Mills, M. J., Neely, R. R., and Schmidt, A.: Emergence of healing in the Antarctic ozone layer, Science, 10.1126/science.aae0061, 2016.

Stone, K. A., Solomon, S., Kinnison, D. E., Pitts, M. C., Poole, L. R., Mills, M. J., Schmidt, A., Neely, R. R., Ivy, D., Schwartz, M. J., Vernier, J.-P., Johnson, B. J., Tully, M. B., Klekociuk, A. R., König-Langlo, G., and Hagiya, S.: Observing the Impact of Calbuco Volcanic Aerosols on South Polar Ozone Depletion in 2015, J. Geophys. Res. Atmos., 122, 11,862-811,879, 10.1002/2017JD026987, 2017.

Atmos. Chem. Phys. Discuss., https://doi.org/10.5194/acp-2018-332
Manuscript under review for journal Atmos. Chem. Phys.
Discussion started: 22 May 2018
© Author(s) 2018. CC BY 4.0 License.

Atmospheric Chemistry and Physics Discussions

Long-range transport of volcanic aerosol from the 2010 Merapi tropical eruption to Antarctica

Xue Wu[1,2], Sabine Griessbach[1], Lars Hoffmann[1]

[1]Jülich Supercomputing Centre, Forschungszentrum Jülich, Jülich, Germany
[2]Key Laboratory of Middle Atmosphere and Global Environment Observation, Institute of Atmospheric Physics, Chinese Academy of Sciences, Beijing, China

Correspondence to: Xue Wu (xu.wu@fz-juelich.de)

Abstract

Volcanic sulfate aerosol is an important source of sulfur for Antarctica where other local sources of sulfur are rare. Mid- and high latitude volcanic eruptions can directly influence the aerosol budget of the polar stratosphere. However, tropical eruptions can also enhance polar aerosol load following long-range transport. In the present work, we analyze the volcanic plume of a tropical eruption, Mount Merapi in October 2010, using the Lagrangian particle dispersion model Massive-Parallel Trajectory Calculations (MPTRAC), Atmospheric Infrared Sounder (AIRS) SO_2 observations and Michelson Interferometer for Passive Atmospheric Sounding (MIPAS) aerosol observations. We investigate the pathway and transport efficiency of the volcanic aerosol from the tropical tropopause layer (TTL) to the lower stratosphere over Antarctica. We first estimated the time- and height-resolved SO_2 injection time series over Mount Merapi during the explosive eruption using the AIRS SO_2 observations and a backward trajectory approach. Then the SO_2 injections were tracked for up to 6 months using the MPTRAC model. The Lagrangian transport simulation of the volcanic plume was compared to MIPAS aerosol observations and showed good agreement. Both of the simulation and the observations presented in this study suggest that a significant amount of aerosols of the volcanic plume from the Merapi eruption was transported from the tropics to the south of 60°S within one month after the eruption and even further to Antarctica in the following two months. This relatively fast meridional transport of volcanic aerosol was mainly driven by quasi-horizontal mixing from the TTL to the extratropical lower stratosphere, which was facilitated by the weakening of the subtropical jet during the seasonal transition from austral spring to summer and linked to the westerly phase of the quasi-biennial oscillation (QBO). When the plume went to southern high latitudes, the polar vortex was displaced from the south pole, so the volcanic plume was carried to the south pole without penetrating the polar vortex. Based on the model results, the most efficient pathway for the quasi-horizontal mixing was in between the isentropic surfaces of 360 and 430 K. Although only 4% of the initial SO_2 load was transported into

Summary of Comments on acp-2018-332-RC1-supplement.pdf

Page: 1

Number: 1 Author: Subject: Highlight Date: 5/31/2018 8:53:47 PM
delete

Author: Administrator Subject: Sticky Note Date: 6/2/2018 4:12:04 PM
fixed

Number: 2 Author: Subject: Highlight Date: 5/31/2018 8:54:31 PM
needs to be quantified. Significant by what standard?

Author: wuxue Subject: Sticky Note Date: 8/27/2018 1:56:55 AM
The sentence is rephrased.

Number: 3 Author: Subject: Highlight Date: 5/31/2018 8:55:25 PM
delete. Acronym is not used again.

Author: Administrator Subject: Sticky Note Date: 6/2/2018 4:12:19 PM
fixed

Number: 4 Author: Subject: Highlight Date: 5/31/2018 8:55:59 PM
South Pole

Author: Administrator Subject: Sticky Note Date: 6/2/2018 4:14:31 PM
fixed

Number: 5 Author: Subject: Highlight Date: 5/31/2018 8:56:06 PM
south pole

Author: Administrator Subject: Sticky Note Date: 6/2/2018 4:14:48 PM
fixed

Number: 6 Author: Subject: Highlight Date: 5/31/2018 8:56:29 PM
delete

Author: Administrator Subject: Sticky Note Date: 6/2/2018 4:14:54 PM
fixed

Atmos. Chem. Phys. Discuss., https://doi.org/10.5194/acp-2018-332
Manuscript under review for journal Atmos. Chem. Phys.
Discussion started: 22 May 2018
© Author(s) 2018. CC BY 4.0 License.

Atmospheric Chemistry and Physics Discussions

the lower stratosphere south of 60°S, the Merapi eruption contributed about 8800 tons of sulfur to the Antarctic lower stratosphere. This indicates that the long-range transport under favorable meteorological conditions enables tropical volcanic eruptions to be an important remote source of sulfur for the Antarctic stratosphere.

1 Introduction

Over the past two decades, multiple volcanic eruptions injected sulfur into the upper troposphere and lower stratosphere, which has been the dominant source of the stratospheric sulfate aerosol load (Vernier et al., 2011), preventing true background levels from other sources ever being seen (Solomon et al., 2011). Stratospheric sulfate aerosol mainly reflects solar radiation and absorbs infrared radiation, causing cooling of the troposphere and heating of the stratosphere. It contributes to the largest uncertainties to estimates and interpretations of the Earth's changing energy budget (Boucher et al., 2013). Further, by modulating the stratospheric and tropospheric temperature it has an impact on stratospheric dynamics, e. g. it can lead to dramatic phase changes of the quasi-biennial oscillation (Aquila et al., 2014) and alter the spatiotemporal characteristics of the El Niño–Southern Oscillation (ENSO) on both short (few years) and long (decades) timescales (Pausata et al., 2015). Stratospheric sulfate aerosol also has an impact on chemical processes in the lower stratosphere (Jäger and Wege, 1990; Solomon et al., 1993), in particular on polar ozone depletion (Tilmes et al., 2008; Drdla and Müller, 2012; Solomon et al., 2016). The presence of H_2SO_4 in the polar stratosphere in combination with cold temperatures facilitates the formation of polar stratospheric clouds (PSCs), which increase heterogeneous ozone depletion chemistry (Solomon et al., 1999; Zuev et al., 2015). Recent healing of Antarctic ozone depletion was constantly disturbed by moderate volcanic eruptions (Solomon et al., 2016). Mid- and high latitude explosive volcanic eruptions may directly influence the polar stratosphere. For example, the aerosol plume from the Calbuco eruption in 2015, including various volcanic gases, penetrated the polar vortex and caused a new record of the size of the Antarctic ozone hole after the eruption (Solomon et al., 2016; Ivy et al., 2017; Stone et al., 2017).

Usually, Antarctica is relatively free of local aerosol sources, but aerosols from low latitudes can reach Antarctica through long-range transport (Sand et al., 2017). Some of the sulfate found in the ice cores can be attributed to volcanic eruptions (Mazzera et al., 2001; Gao et al., 2007; Sigl et al., 2015). Measurements of enhanced aerosol in the lower Antarctic stratosphere right above the tropopause were made in October/November 1983, 84 and 85. These enhanced aerosol number concentrations were

Page: 2

Number: 1 Author: Subject: Highlight Date: 5/31/2018 8:57:19 PM
But we already know this happens for large eruptions. What is new here?

Author: Administrator Subject: Sticky Note Date: 6/3/2018 12:04:58 PM
Please refer to the reply for details.

Number: 2 Author: Subject: Highlight Date: 5/31/2018 8:58:18 PM
Not correct. What do you mean by "uncertainties?" Largest compared to what?

Author: Administrator Subject: Sticky Note Date: 6/3/2018 3:56:45 PM
This sentence is removed from the texts.

Number: 3 Author: Subject: Highlight Date: 5/31/2018 8:59:20 PM
dynamics;

Author: Administrator Subject: Sticky Note Date: 6/2/2018 4:15:59 PM
fixed

Number: 4 Author: Subject: Highlight Date: 5/31/2018 9:01:00 PM
new record size [record for what? Monthly mean? All time size?]

Author: Administrator Subject: Sticky Note Date: 8/27/2018 10:47:27 PM
Fixed. The sentence is rewritten as: ... in October 2015 caused a Antarctic ozone hole with the largest daily averaged size in record.

Number: 5 Author: Subject: Highlight Date: 5/31/2018 9:01:38 PM
aerosols [you use both singular and plural in the paper. Choose one and stick to it.]

Author: Administrator Subject: Sticky Note Date: 6/2/2018 4:16:37 PM
fixed

Number: 6 Author: Subject: Highlight Date: 5/31/2018 9:02:52 PM
Most

Author: Administrator Subject: Sticky Note Date: 6/2/2018 4:17:45 PM
fixed

Number: 7 Author: Subject: Highlight Date: 5/31/2018 9:03:02 PM
in ice

Author: Administrator Subject: Sticky Note Date: 6/2/2018 4:19:19 PM
fixed

Number: 8 Author: Subject: Highlight Date: 5/31/2018 9:03:32 PM
1984 and 1985

Author: Administrator Subject: Sticky Note Date: 6/2/2018 4:18:36 PM
fixed

Atmos. Chem. Phys. Discuss., https://doi.org/10.5194/acp-2018-332
Manuscript under review for journal Atmos. Chem. Phys.
Discussion started: 22 May 2018
© Author(s) 2018. CC BY 4.0 License.

Atmospheric Chemistry and Physics Discussions

attributed to aerosol transported to Antarctica from the eruption of the tropical volcano El Chichon in 1982 (Hofman and Rosen, 1985; Hofmann et al., 1988). Tropical volcanic eruptions can also enhance polar aerosols by long-range transport. Model results indicate that numerous moderate eruptions have affected ozone distributions over Antarctica, including the Merapi tropical eruption in October 2010 (Solomon et al., 2016). However, the transport mechanism is not well represented in present global climate models, and the uncertainties in modeled AOD in both polar regions are large (Sand et al., 2017).

The Mount Merapi (7.5°S, 110.4°E, elevation: 2930 m) is an active stratovolcano located in Central Java, Indonesia. Merapi has a long record of eruptive activities. The most recent large eruption with a volcanic explosivity index (VEI) of 4 occurred between 26 October and 7 November 2010 (Pallister et al., 2013), with SO_2 emission rates being a few orders of magnitude higher than previous eruptions. Following the Merapi eruption in 2010, evidence of poleward transport of sulfate aerosol towards southern hemisphere high latitudes was found in time series of aerosol observations by the Michelson Interferometer for Passive Atmospheric Sounding (MIPAS) (Günther et al., 2017) and Cloud-Aerosol Lidar with Orthogonal Polarization (CALIOP) (Khaykin et al., 2017) .

There are three main ways for transport out of the tropical tropopause layer (TTL): the deep and shallow branches of the Brewer-Dobson circulation (BDC) and horizontal mixing (Vogel et al., 2011). There is considerable year-to-year seasonal variability in the amount of irreversible transport from the tropics to high latitudes, which is related to both the phase of the QBO and the state of the polar vortex (Olsen et al., 2010). The BDC plays a large role in determining the distributions of many constituents in the extratropical lower stratosphere. And the faster quasi-horizontal transport between the tropics and polar regions also significantly contributes to determining these distributions. The efficiency of transporting constituents quasi-horizontally depends on wave breaking patterns and varies with time of year (Kravitz and Robock, 2011; Wu et al., 2017). Better knowledge of the transport pathways and an accurate representation of volcanic sulfur injections into the upper troposphere and lower stratosphere (UTLS) are key elements for understanding the global stratospheric aerosol budget is key to understanding the cooling effects and ozone loss linked to volcanic activity.

The aim of the present study is to investigate the quasi-horizontal transport by tracing the volcanic plume of the Merapi eruption from the tropics to Antarctica and quantifying its contribution to the sulfur load in the Antarctic lower stratosphere. In Sect. 2, the new Atmospheric Infrared Sounder (AIRS) SO_2 observations (Hoffmann et al., 2014), the MIPAS aerosol observations (Griessbach et al., 2016) and the method for reconstructing the SO_2 injection time series of the Merapi eruption are introduced. In

Page: 3

Number: 1 Author: Subject: Highlight Date: 6/2/2018 4:18:47 PM
Chichón

Author: Administrator Subject: Sticky Note Date: 6/2/2018 4:19:10 PM
fixed

Number: 2 Author: Subject: Highlight Date: 5/31/2018 9:04:25 PM
delete

Author: Administrator Subject: Sticky Note Date: 6/2/2018 4:19:36 PM
fixed

Number: 3 Author: Subject: Highlight Date: 5/31/2018 9:05:43 PM
delete [not used again]

Author: Administrator Subject: Sticky Note Date: 6/2/2018 4:19:45 PM
fixed

Number: 4 Author: Subject: Highlight Date: 5/31/2018 9:05:18 PM
needs to be defined in the text [not abstract] before using.

Author: Administrator Subject: Sticky Note Date: 6/2/2018 4:20:20 PM
fixed

© Author(s) 2018. CC BY 4.0 License.

Sect. 3 the results are presented: first, the reconstructed time series of the Merapi eruption is discussed; second, the dispersion of the Merapi plume is investigated using up to 6 months long Lagrangian forward trajectories initialized with the reconstructed SO_2 time series; third, the simulation is compared to MIPAS volcanic aerosol measurements and the plume dispersion is investigated using MIPAS aerosol detections. In Sect.4 the results are discussed with the background of the meteorological conditions and conclusions are given in Sect. 5.

2 Satellite data, model and method

2.1 MIPAS instrument and aerosol measurements

MIPAS (Fischer et al., 2008) is an infrared limb emission spectrometer aboard the European Space Agency's (ESA's) Envisat, which provided nearly 10 years of measurements from July 2002 to April 2012. MIPAS spectral measurements cover the wavelength range from 4.15 to 14.6 microns. The vertical coverage of MIPAS' nominal measurement mode during the so-called `optimized resolution phase' from January 2005 to April 2012 was 7–72 km. The field of view of MIPAS was about 3 km × 30 km (vertically × horizontally) at the tangent point. The extent of the measurement volume along the line of sight was about 300 km, and the horizontal distance between two adjacent limb scans was about 500 km. On each day, ~14 orbits with ~90 profiles per orbit were measured. The vertical sampling was 1.5 km in the UTLS and 3 km above the UTLS. In 2010 and 2011, MIPAS measured for 4 days in nominal mode followed alternately by one day in middle atmosphere mode or upper atmosphere mode. In this study, we focussed on measurements in the nominal mode.

For the aerosol detections, we used the MIPAS altitude-resolved aerosol-cloud-index (ACI) products as introduced by Griessbach et al. (2016) to compare with the MPTRAC simulations and analyze the poleward transport of the Merapi volcanic plume. Small ACI values indicate large aerosol extinction coefficients and vice versa. For instance, MIPAS data points with ACI < 7 can cover infrared extinction coefficients larger than 1×10^{-4} km^{-1}, which corresponds to 3×10^{-4} km^{-1} in the visible wavelength range (Griessbach et al. 2016). Larger ACI values will show aerosol load with even smaller extinction coefficients. As ice clouds usually have extinction coefficients larger than 1×10^{-4} km^{-1}, we applied a brightness-temperature-correlation method, that serves as an ice cloud filter, to all MIPAS spectra with ACI<7 (Griessbach et al., 2016) to remove the ice clouds from the data set. The resulting aerosol product is be sensitive to different types of aerosol, in particular, volcanic ash, sulfate aerosol, mineral dust, as well as non-ice PSCs.

Page: 4

Number: 1 Author: Subject: Highlight Date: 5/31/2018 9:09:48 PM
detection,

Author: Administrator Subject: Sticky Note Date: 6/2/2018 4:22:18 PM
fixed

Number: 2 Author: Subject: Highlight Date: 5/31/2018 9:11:38 PM
delete

Author: Administrator Subject: Sticky Note Date: 6/2/2018 4:22:51 PM
fixed

Atmos. Chem. Phys. Discuss., https://doi.org/10.5194/acp-2018-332
Manuscript under review for journal Atmos. Chem. Phys.
Discussion started: 22 May 2018
© Author(s) 2018. CC BY 4.0 License.

Atmospheric Chemistry and Physics Discussions

2.2 AIRS

AIRS (Aumann et al., 2003) is an infrared nadir sounder with across-track scanning capabilities aboard the National Aeronautics and Space Administration's (NASA's) Aqua satellite. Aqua was launched in 2002 and operates in a nearly polar Sun-synchronous orbit at about 710 km with a period of 98 min. AIRS provides nearly continuous measurement coverage with 14.5 orbits per day and with a swath width of 1780 km it covers the globe almost twice a day. The AIRS footprint size is 13.5 km × 13.5 km at nadir and 41 km × 21.4 km for the outermost scan angles respectively. The along-track distance between two adjacent scans is 18 km. The AIRS observations provide good horizontal resolution and make it ideal for observing the fine filamentary structures of volcanic SO_2 plumes.

In this study, we use an optimized SO_2 index (SI, unit: K) to estimate the amount of SO_2 injected into the atmosphere by the Merapi eruption 2010. The SI is defined as the brightness temperature differences in the 7.3 µm SO_2 waveband.

$$SI = BT\left(1412.87\text{cm}^{-1}\right) - BT\left(1371.52\ \text{cm}^{-1}\right), \qquad (1)$$

where BT is the brightness temperature measured at wavenumber ν. This SI is more sensitive to low concentrations and performs better on suppressing background interfering signals than the SI provided in the AIRS operational data products. It is an improvement of the SI definition given by Hoffmann et al. (2014) by means of a better choice of the background channel (selecting 1412.87 cm^{-1} rather than 1407.2 cm^{-1}). The SI increases with increasing SO_2 column density and it is most sensitive to SO_2 at altitudes above 3-5 km. SO_2 injections into the lower troposphere are usually not detectable in the infrared spectral region because the atmosphere gets opaque due to the water vapor continuum. A detection threshold of 1 K was used in this study to identify the Merapi SO_2 injections. AIRS detected the Merapi SO_2 cloud from 3 November to 15 November 2010.

2.3 MPTRAC model and reconstruction of the volcanic SO_2 injection time series of the Merapi eruption

In this study, we used the highly scalable MPTRAC model to investigate the volcanic eruption event. In the [1]MPTAC model, air parcel trajectories are calculated based on numerical integration using wind fields from global meteorological [2]reanalyses (Hoffmann et al., 2016; Rößler et al., 2017). Diffusion is modeled by uncorrelated Gaussian random displacements of the air parcels with zero mean and standard deviations $\sigma_x = \sqrt{D_x \Delta t}$ (horizontally) and $\sigma_z = \sqrt{D_z \Delta t}$ (vertically). D_x and D_z are the horizontal and vertical diffusivities respectively, and Δt is the time step for the trajectory calculations. For the

Page: 5

Number: 1 Author: Subject: Highlight Date: 5/31/2018 9:16:28 PM
MPTRAC

Author: Administrator Subject: Sticky Note Date: 6/2/2018 4:22:57 PM
fixed

Number: 2 Author: Subject: Highlight Date: 5/31/2018 9:29:44 PM
specify which ones

Author: Administrator Subject: Sticky Note Date: 8/27/2018 1:59:44 AM
The MPTRAC model can be driven with reanalyses, i.e., ERA-Interim, Modern-Era Retrospective Analysis for Research and Applications (MERRA), and National Centers for Environmental Prediction (NCEP)/National Center for Atmospheric Research (NCAR) etc. In a previous study about the impact of reanalyses on the simulation results of the MPTRAC model (Hoffmann etl al., 2016), it shows that the ERA-interim data can ensure the performance of MPTRAC with a reasonable computing time. So in this study, our calculations are based on ERA-interim data, which is mentioned in the last paragraph of Sect. 2.3.
Explanations are added here in the revised manuscript.

© Author(s) 2018. CC BY 4.0 License.

Merapi simulation, D_x and D_z were set to 50 $m^2 s^{-1}$ and 0 $m^2 s^{-1}$ in the troposphere and 0 $m^2 s^{-1}$ and 0.1 $m^2 s^{-1}$ in the stratosphere, respectively. In addition, sub-grid scale wind fluctuations, which are particularly important for long-range simulations, are simulated by a Markov model (Stohl et al., 2005; Hoffmann et al., 2016). Loss processes of chemical species, SO_2 in our case, are simulated based on an exponential decay of the mass assigned to each air parcel. In the stratosphere a constant half lifetime of 7 days was assumed for SO_2. Considering that the Merapi eruption occurred in the humid tropics, with high concentration of hydroxyl radical, a half lifetime of 2.5 days was assumed for the troposphere.

To estimate the time- and altitude-resolved SO_2 injections, we follow the approach of Hoffmann et al. (2016) and Wu et al. (2017) and use backward trajectories calculated with the MPTRAC model together with AIRS SO_2 measurements. Observations from 3 to 7 November 2010 were used for estimating the SO_2 injection during the explosive eruption. Since the AIRS measurements do not provide altitude information, we established a column of air parcels at each AIRS SO_2 detection. The vertical range of the column was set to 0–25 km, covering the possible vertical dispersion range of the SO_2 plume in the first few days. The AIRS footprint size varies between 14 and 41 km, hence in the horizontal direction, we chose an average of 30 km as the full width at half maximum (FWHM) for the Gaussian scatter of the air parcels. In our simulation, a fixed total number of 100,000 air parcels was assigned to all air columns and the number of air parcels in each column was scaled linearly proportional to the SO_2 index. Then backward trajectories were calculated for all air parcels, and trajectories that were at least 2 days but no more than 5 days long and that passed the volcano domain were recorded as emissions of Merapi. The volcano domain was defined by means of a search radius of 75 km around the location of the Merapi and 0–20 km in the vertical direction, covering all possible injection heights. Sensitivity experiments have been conducted to optimize these pre-assigned parameters to obtain the best simulation results. Our estimates of the Merapi SO_2 injection are shown in Sect. 3.

Starting with the reconstructed altitude-resolved SO_2 injection time series, the transport of the Merapi plume is simulated for 6 months, covering the time period from the initial eruption on 26 October 2010 to 30 April 2011. The trajectory calculations are driven by the ERA–Interim data (Dee et al., 2011) interpolated on a 1°× 1° horizontal grid on 60 model levels with the vertical range extending from the surface to 0.1 hPa. The ERA–Interim data are provided at 00, 06, 12 and 18 UTC. Outputs of model simulations are given every 3 hours at 00, 03, 06, 09, 12, 15, 18 and 21 UTC. The impact of different meteorological analysis on MPTRAC simulations was assessed by Hoffmann et al. (2016, 2017). In both studies the ERA–Interim data showed good performance.

Page: 6

Number: 1 Author: Subject: Highlight Date: 5/31/2018 9:54:50 PM
what about removal by precipitation?

Author: Administrator Subject: Sticky Note Date: 6/3/2018 1:29:19 PM
Precipitation is a very important way of removal of SO2, but the time life of SO2 in the case of precipitation which could be very short is very difficult to define in the model we use. We can only roughly estimate the life of SO2 based on some parameters with a clear climatological trend, for example, the humidity and the concentration of oxidant. And we also compare the SO2 column density from our model results with AIRS SO2 observations, and in this way, we can adjust the life time of SO2 set up in our model to get a better agreement with the observations. This approach can not guarantee an accurate simulation of SO2 in the troposphere, but fortunately, the SO2 in lower troposphere and sulfate aerosol converted from these SO2 are not the interests in our study. We only focus on the SO2 injected into the upper troposphere and stratosphere.
Thank you for pointing this out. We added more detailed description of our model set-up in Sect. 2.3 in the revised manuscript.

Number: 2 Author: Subject: Highlight Date: 5/31/2018 9:55:18 PM
delete

Author: Administrator Subject: Sticky Note Date: 6/3/2018 12:05:54 PM
fixed

Number: 3 Author: Subject: Highlight Date: 5/31/2018 9:58:02 PM
analyses

Author: Administrator Subject: Sticky Note Date: 6/2/2018 5:01:21 PM
fixed

Atmos. Chem. Phys. Discuss., https://doi.org/10.5194/acp-2018-332
Manuscript under review for journal Atmos. Chem. Phys.
Discussion started: 22 May 2018
© Author(s) 2018. CC BY 4.0 License.

Atmospheric Chemistry and Physics Discussions

3 Results

Figure 1 displays the time-latitude section of MIPAS aerosol detections with median ACI value in each bin smaller than 7 and within the vertical range of 13 and 20 km, covering the tropical tropopause layer (TTL) and the extratropical lowermost stratosphere (LMS). The MIPAS data captured all the major events that contributed to the aerosol load in the UTLS, i.e., moderate volcanic eruptions from 2002 to 2012 and one large bushfire in 2009, as well as the subsequent dispersion and change of aerosol load over time. Particularly, after the Merapi eruption in 2010, marked by the red triangle in Fig. 1, the MIPAS data show an obvious poleward transport of aerosol from the tropics to Antarctica.

3.1 Merapi eruption and SO_2 injection time series

According to the chronology of the Merapi eruption (Surono et al., 2012), the explosive eruption first occurred between 10:00 and 12:00 UTC on 26 October and this eruption generated a plume that reached 12 km altitude. A period of relative small explosive eruptions continued from 26 October to 31 October. During the initial period of the dome growth (1–3 November), the level of SO_2 degassing was relatively low compared with the SO_2 degassing before 1 November. On 3 November, the eruptive intensity increased again accompanied by much stronger degassing and a series of explosions. The intermittent explosive eruptions occurred during 4–5 November with the climactic eruption on 4 November, producing an ash column that reached up to 17 km altitude. From 6 November, explosive activity decreased slowly and the degassing declined.

Figure 2 shows the time- and altitude-resolved SO_2 injections of the Merapi eruption retrieved using the AIRS SO_2 index data and the backward-trajectory approach. It successfully reproduced the chronology of the Merapi eruption as outlined by Surono et al. (2012). Significant SO_2 was injected into altitudes below 8 km during the initial explosive eruptions on 26–30 October. Starting from 30 October the plume reached up to 12 km. During 1–3 November the SO_2 injections into altitudes below 12 km continued but the mass was less than in the initial phase. On 3 November the intensity increased again and peaked in the climactic explosive eruptions of 4–5 November. Before 3 November the reconstruction indicates a minor fraction of SO_2 right above the tropopause.

To study the long-range transport of the Merapi plume, we initialized 100,000 air parcels at the SO_2 injection time series shown in Fig. 2 with a SO_2 mass of 0.44 Tg as provided in Surono et al. (2012) and calculated forward trajectories for 6 months. Here, we only considered the plume in the upper troposphere and stratosphere where the lifetime of both SO_2 and sulfate aerosol is longer than that in the lower troposphere. Further, the SO_2 was all converted into sulfate aerosol within a few weeks (von

Page: 7

Number: 1 Author: Subject: Highlight Date: 5/31/2018 10:05:50 PM
Not seen in Fig. 2. Why?

Author: Administrator Subject: Sticky Note Date: 6/3/2018 5:38:49 PM
In the study of Surono et al., 2012, it was claimed that between 10:00 UTC and 12:00 UTC on 26 October, there was an ash plume that reached 12 km altitude and released SO2 emissions, but they did not give the amount or the altitude of the SO2 injection. But it is clear that this period of time was the initial explosive phase, when only a small amount of SO2 was injected, about two orders of magnitude smaller than it was on 3 or 4 November (Surono et al., 2012). In our Fig. 2, there was a small amount of SO2 around 10-13 km on 26 October. Although its time of presence was a little earlier than 12:00 UTC 26 October, it would not bring notable error to the simulation later in this study.

Number: 2 Author: Subject: Highlight Date: 5/31/2018 10:07:07 PM
Also not seen in Fig. 2, particularly the 17 km signal.

Author: Administrator Subject: Sticky Note Date: 6/3/2018 4:01:59 PM
There is SO2 injection up to around 17 km on 4 November shown in Fig. 2.

© Author(s) 2018. CC BY 4.0 License.

Glasow et al., 2009; we could also see it in the AIRS SO_2 and MIPAS aerosol data), and we assumed that the sulfate aerosol converted from SO_2 remains collocated with the SO_2 plume, i.e., the sedimentation of small sulfate aerosol particles was negligible for the timescale considered.

Figure 3 shows the evolution of the simulated Merapi plume and compares the plume altitudes to the aerosol top altitudes measured by MIPAS between 7 and 23 November. Immediately after the eruption, the majority of the plume moved towards the southwest and was entrained by the anticyclonic circulation of the tropical cyclone Anggrek (not shown). After the Anggrek weakened and dissipated, the majority of the plume parcels in upper troposphere moved eastward and those in the lower stratosphere moved westward. In general, the altitudes of the simulated plume are comparable to the MIPAS observations. The remaining discrepancies of air parcel altitudes being higher than the altitudes of MIPAS aerosol detections can be attributed to the fact that the MIPAS tends to underestimate aerosol top cloud altitudes, which is about 0.9 km in case of low extinction aerosol layers and can reach down to -4.5 km in case of broken cloud conditions (Höpfner et al., 2009).

3.2 Meteorological background conditions after the Merapi eruption

The Merapi eruption in October 2010 occurred during the seasonal transition from austral spring to summer when the polar vortex typically weakens and the ozone hole shrinks. As depicted in Fig. 4, the meteorological conditions at the polar lower stratosphere (150hPa, ~12km) after the eruption deviated from the climatological mean. The minimum temperature south of 50°S (Fig. 4a) was much lower than the climatological mean during mid-November to mid-December but still higher than the low temperature necessary for existence of PSCs. The polar mean temperature in Fig. 4b, defined as the temperature averaged over latitudes south of 60°S, stayed lower than the climatological mean from November 2010 until February 2011. Corresponding to the low temperatures, the average zonal wind speed at 60°S (Fig. 4c) was significantly larger than the climatological mean value from November 2010 to mid-January 2011. The eddy heat flux in Fig. 4d is the product of meridional wind departures and temperature departures from the respective zonal mean values. A more negative value of eddy heat flux indicates that wave systems are propagating into the stratosphere and are warming the polar region. There is a strong anticorrelation between temperature and the 45-day average of the eddy heat flux lagged prior to the temperature. Comparing with the climatological mean state, the polar vortex was more disturbed during mid-July to end of August. But from mid-October to late November, the heat flux was much smaller than the long-term average, which meant a reduction in dynamical disturbances of the polar vortex as the QBO changed into a strong westerly phase. Considering the temperature, the

Page: 8

Number: 1 Author: Subject: Highlight Date: 5/31/2018 10:10:09 PM
delete

Author: Administrator Subject: Sticky Note Date: 6/2/2018 5:04:42 PM
fixed

Number: 2 Author: Subject: Highlight Date: 5/31/2018 10:10:44 PM
in the upper

Author: Administrator Subject: Sticky Note Date: 6/2/2018 5:04:47 PM
fixed

Number: 3 Author: Subject: Highlight Date: 5/31/2018 10:17:34 PM
This is an easterly phase of the QBO, not westerly as stated in the abstract. If the wind was westerly (Fig. 4f), how could the plume have moved westward?

Author: Administrator Subject: Sticky Note Date: 6/3/2018 12:06:54 PM
Please refer to the reply for details.

© Author(s) 2018. CC BY 4.0 License.

subpolar wind speed and the heat flux, the polar vortex was colder and stronger in November and December 2010 compared with the same time in other years. The study of Klekociuk et al. (2011) also confirmed that the polar vortex area was consistently larger than the climatological mean particularly during November and December (see their Fig. 9). Consistent with the strength of the polar vortex, in November and December 2010 the ozone hole area in Fig. 4e, defined as the region of ozone values below 220 Dobson Units (DU) located south of 40°S, was larger than the climatological mean. Meanwhile, the low polar mean temperature and stable polar vortex resulted in a long-lasting ozone hole, which disappeared in the last week of December. The polar vortex broke down by mid-January 2011 when subpolar wind speed decreased below 15 m/s (Fig. 4c).

The poleward transport from the tropics to the polar region is known to be modulated by the phase of the quasi-biennial oscillation (QBO) and the state of the polar vortex itself: Fig. 4f shows that just before the Merapi eruption in 2010, the QBO switched from easterly phase to westerly phase. The westerly phase of the QBO promotes meridional transport from the tropics to subtropics, especially into the winter hemisphere (O'Sullivan and Dunkerton, 1997; Shuckburgh et al., 2001; Jäger, 2005). However, it also results in zonal wind acceleration at the high latitudes (Watson and Gray, 2014; Holton and Tan, 1980) and a less dynamically disturbed polar vortex (Anstey and Shepherd, 2014; Baldwin and Dunkerton, 1999), which will make it less possible for air parcels to penetrate the polar vortex.

3.3 Lagrangian simulation and satellite observation of poleward transport of the Merapi plume

The early plume evolution until about one month after the initial eruption is shown on the maps in Fig. 3 together with MIPAS observations of volcanic aerosol (only aerosol detections with ACI<7 are shown). Within about one month after the initial eruption, the plume was nearly entirely transported around the globe in the tropics, moving west at altitudes of about 17 km. The lower part of the plume, below about 17 km was transported south-eastward and reached latitudes south of 30°S by mid-November. The simulated long-term transport of the Merapi plume is illustrated in Fig. 5, showing the relative number of air parcels reaching a latitude-altitude bin every half a month. To verify the model results, the poleward transport of aerosols as detected by MIPAS is shown in Fig. 6. For comparison, only simulation results above the minimum altitude of MIPAS aerosol detections in Fig. 6 are shown in Fig. 5. In this study, we only focus on aerosol distributions in the upper troposphere and stratosphere, where sulfate aerosol has a longer lifetime and potential climate impacts.

During the first month after the eruption (Figs. 5a–b), the majority of the plume was transported southward roughly along the isentropic surfaces. The most significant pathway is above the core of the

Page: 9

Number: 1 Author: Subject: Highlight Date: 5/31/2018 10:19:52 PM
delete

Author: Administrator Subject: Sticky Note Date: 6/2/2018 5:17:14 PM
fixed

Number: 2 Author: Subject: Highlight Date: 5/31/2018 10:20:57 PM
define once when first used, and then just use acronym.

Author: Administrator Subject: Sticky Note Date: 6/2/2018 5:17:29 PM
fixed

Atmos. Chem. Phys. Discuss., https://doi.org/10.5194/acp-2018-332
Manuscript under review for journal Atmos. Chem. Phys.
Discussion started: 22 May 2018
© Author(s) 2018. CC BY 4.0 License.

subtropical jet in the southern hemisphere. However, because of the transport barrier of the polar jet during austral spring, the plume was confined to the north of 60°S. In December 2010 (Figs. 5c–d), a larger fraction of the plume was transported southward above the subtropical jet core, and deep into the polar region south of 60°S as the polar jet broke up. Till the end of January 2011, the majority of the plume had entered the mid- and high latitudes in the southern hemisphere, whereas only a very small proportion of the plume was transported north of 30°N. Substantial quasi-horizontal poleward transport from the TTL towards the LMS in Antarctica was found from November 2010 to February 2011 (Figs. 5a–h), approximately between 350 and 480 K (~10–20 km). From March to April 2011(Figs. 5i–l), the proportion of the plume that went across 60°S stopped increasing and the maxima of the plume descended from 380 to 350 K. During this transport towards Antarctica, a secondary upward transport split from the plume, which was particularly observable from January 2011 till the end of the simulation in April 2011(Figs. 5e–l). This slow upward transport was mainly located around 15°S above the tropopause and can be attributed to the upward branch of the BDC.

The poleward transport in the MPTRAC simulations was confirmed by MIPAS aerosol detections. MIPAS ACI zonal median values are shown in Fig. 6 for all MIPAS measurements after filtering out ice clouds. Small ACI values indicate a large aerosol load and large ACI values indicate clear air. As seen in Fig. 6, the locally confined aerosol plume from the Merapi eruption did not dominate the zonal median during the first half month after the eruption (Fig. 6a), but became evident between 350 and 380 K around the latitude of 7.5°S by the end of November (Fig. 6b) as the plume was transported around the globe in the tropics. As shown in the MPTRAC simulations, the transport towards the northern mid- and high latitudes was suppressed by the strong subtropical jets. The transport of the volcanic plume towards Antarctica in the UTLS region was observed from December 2010 to February 2011 (Figs. 6c–h) consistent with the simulations. The MIPAS aerosol data also demonstrated the upward transport from the tropical upper troposphere to the stratosphere, which was observed after late January 2010. The aerosol transported upward had increased the aerosol load in the tropical stratosphere reservoir compared to the aerosol load before the Merapi eruption.

Fig. 6 verified aerosol transport from the tropics to Antarctica and upward into the tropical stratosphere. However, before the eruption of Merapi, the aerosol load in the tropical stratosphere was already elevated by several small and moderate-size volcanic eruptions, namely the Sarychev Peak (12 Jun 2009), Nyamuragira (20 Jan 2010), Soufriere Hills (11 Feb 2010) and Pacaya (28 May 2010). In order to infer the increase of the aerosol load due to the eruption of Merapi from the MIPAS data, we calculated the median ACI between 1–4 November 2010 when there was no aerosol from the Merapi

Page: 10

Number: 1 Author: Subject: Highlight Date: 5/31/2018 10:29:33 PM
Southern Hemisphere

Author: Administrator Subject: Sticky Note Date: 6/3/2018 1:30:14 PM
fixed

Number: 2 Author: Subject: Highlight Date: 5/31/2018 10:29:57 PM
southern hemisphere

Author: Administrator Subject: Sticky Note Date: 6/2/2018 5:17:34 PM
fixed

Number: 3 Author: Subject: Highlight Date: 5/31/2018 10:33:06 PM
June

Author: Administrator Subject: Sticky Note Date: 6/2/2018 5:17:48 PM
fixed

© Author(s) 2018. CC BY 4.0 License.

eruption, to define the "background" aerosol load and then remove this "background" from the median ACI in Fig. 6. The results shown in Fig.7 demonstrate the change of median ACIs in the tropics and southern hemisphere corresponding to the same time period as Fig. 6, with positive/negative values indicating an increase/decrease of aerosol load. No significant change was observed during the first half month after the eruption due to the zonal averaging degrading the aerosol signal (Fig. 7a). The largest increase first appeared in the upper troposphere directly above Mount Merapi (Fig. 7b) and then moved quasi-horizontally southward into the UTLS region to ~40°S (Figs. 7c–f), consistent with what Figs. 5 and 6 showed. A relatively small but still significant increase of aerosol south of 60°S in the tropopause region was found from January 2011 (Fig. 7e) and it lasted until mid- April 2011 (Fig. 7j). Six months after the eruption, the aerosol levels were still slightly elevated in the tropical upper troposphere above 350 K. There should have been a decrease of the aerosol load in the tropical stratosphere because of sedimentation and poleward transport of aerosol if there were no aerosol from the Merapi eruption. But the upward transport of the Merapi aerosol compensated the loss.

3.4 Efficiency of quasi-horizontal transport from the tropics to Antarctica

As the results of the Lagrangian transport simulations with the MPTRAC model were comparable to the MIPAS observations (Sect. 3.3), it was possible not only to demonstrate the transport pathways but also to estimate the efficiency of the transport. The MPTRAC simulations and the MIPAS observations have demonstrated transport on the "surf zone" that reaches from the subtropics to high latitudes (Holton et al., 1995), where air masses are affected by both fast meridional transport and the slow BDC. Our data show that quasi-horizontal mixing in the lower extratropical stratosphere between 350 and 480 K is the main transport pathway for the volcanic aerosol. Figure 8 illustrates how the volcanic plume between 350 and 480 K approached Antarctica over time. Gray dashed and solid lines mark potential vortices (PV) contours with the largest PV gradients on the 350 and 480 K isentropic surfaces. These dynamically relevant PV contours represent horizontal transport barriers for air masses on the respective isentropic surface. On isentropic surfaces below 380 K, the contours of maximum PV gradients represent the dynamical discontinuity near the core of the subtropical jet stream and thus represent a transport barrier between the tropics and midlatitudes (Haynes and Shuckburgh, 2000; Kunz et al., 2011a,b). Isentropic transport of air masses across these boundaries indicates exchange between the tropics and extratropics due to Rossby wave breaking. On isentropic surfaces above 400 K, the contours of maximum PV gradients represent a boundary in the lower stratosphere, in particular, due to the polar vortices in winter (Kunz et al., 2015). For comparison we have also shown contour lines of ozone

Page: 11

Number: 1 Author: Subject: Highlight Date: 5/31/2018 10:35:30 PM
compensated for

Author: Administrator Subject: Sticky Note Date: 6/2/2018 5:18:32 PM
fixed

Number: 2 Author: Subject: Highlight Date: 5/31/2018 10:39:24 PM
vorticity

Author: Administrator Subject: Sticky Note Date: 6/2/2018 5:23:25 PM
fixed

© Author(s) 2018. CC BY 4.0 License.

column density of 220 DU (black isolines in Fig. 8), indicating the location and size of the ozone hole. The PV boundary on 480 K is in most cases collocated with the area of the ozone hole, showing that both quantities provide a consistent representation of the area of the polar vortex.

The Merapi volcanic plume first reached the 350 K transport boundary in mid-November and went close to the 480 K transport boundary in December. The long-lasting polar vortex prevented the volcanic plume from crossing the transport boundary in the beginning of December, but from mid-December, the polar vortex became more disturbed and displaced from the south pole, together with a shrinking ozone hole. As mentioned in Sect.3.2, the ozone hole broke up at the end of December 2010 and the polar vortex broke down by mid-January 2011.

The fractions of the volcanic plume that crossed the individual transport boundaries or the latitude of 60°S on each isentropic surface are shown in Fig. 9. In both cases, the proportion increased from November 2010 to January 2011. In November and December 2010 the largest plume transport across the transport boundaries occurred between the 360 and 430 K isentropic surface (Fig. 9a), with a peak at 380–390 K. In January and February 2011 the peak was slightly elevated to 390–400 K. In November 2010, the volcanic plume did not cross the 480 K transport boundary of the polar vortex at high altitudes, especially above about 450 K. The high-latitude fraction kept increasing from December 2010 to February 2011 as the weakening of the polar vortex made the transport boundary more permeable. In March and April 2011, the total proportion decreased and the peak descended to 370 K in March and further to 360 K in April. The proportion of the volcanic plume south of 60°S (Fig. 9b) increased slightly from November to December 2010, and then increased significantly from December 2010 to January and February 2011 at all altitudes as the polar vortex displaced and broke down. Finally, the transport to south of 60°S started to decrease in March 2011. From November 2010 to February 2011 the peak was around 370–400 K, but in March and April 2011 the peak resided around 350–370 K.

Figure 10 summarizes the poleward transport of the volcanic plume between 350 and 480 K. The zonally resolved fractions derived from the Lagrangian MPTRAC simulations and the fraction of air parcels south of 60°S are shown in Fig. 10a. Figure 10b demonstrates the increasing and decreasing aerosol load in this vertical range for MIPAS aerosol detections relative to 1–4 November median (see Sect.3.3). The poleward transport trend in Fig. 10a is comparable to the poleward migration of the enhanced aerosol in Fig. 10b. The simulations show that the plume reached 60°S by the end of November 2010. Correspondingly, the aerosol load south of 60°S was elevated when the volcanic plume was transported there. The percentage fluctuated, but increased until the end of February 2011, with a maximum percentage of about 4%. A steep increase occurred from mid-December 2010 to end of

This page contains no comments

© Author(s) 2018. CC BY 4.0 License.

January 2011, following the displacement and breakdown of the polar vortex. The elevated aerosol load south of 60°S decreased from March 2011, because the plume descended to altitudes below 350 K as shown by Fig. 9b. Overall, enhanced aerosol due to Merapi eruption was observed mostly in the subtropics and midlatitudes, but the aerosol load in the south polar region was also significantly elevated for three months from December 2010 to February 2011.

4 Discussion

The results presented in Sect. 3 show that the meridional transport of the Merapi volcanic plume to Antarctica mostly occurred between the isentropic surfaces of 350 and 480 K (about 10 to 20 km), covering the TTL and the lower stratosphere at mid- and high latitudes. For this long-range transport on timescales of a few months, fast isentropic transport associated with quasi-horizontal mixing was found to be the most efficient pathway. The phase of QBO, subtropical Rossby wave breaking and the strength and stability of the polar vortex all have an impact on the transport efficiency. The Merapi eruption occurred in austral spring and fast poleward transport was facilitated by the weakening subtropical jet and active Rossby wave breaking events. The westerly QBO enhanced transport and mixing in the subtropics with implications on the position of the subtropical barrier (Shuckburgh et al., 2001; Palazzi et al., 2011). The QBO also modulated the ability of upward propagating planetary waves to influence the strength of the polar vortex. Although the polar vortex was relatively stable when the Merapi eruption occurred, after the volcanic plume reached the south polar region, the polar vortex was displaced from the south pole and distorted because more wave systems propagated into the polar stratosphere and warmed the polar region, so that the volcanic plume could be transported from the tropics deep into Antarctica under all these favourable conditions.

The phase of the QBO influences the amount of volcanic emissions transported out of tropics, while the heating effect of a large amount of sulfur injected by volcanic eruptions can change the pattern of the QBO (Niemeier and Schmidt, 2017). With increasing emission rates the velocity of the equatorial jet streams increases and less sulfate is transported out of the tropics. The amount of SO_2 injected during the Merapi eruption 2010 was 0.44 Tg, far less than the 5 TgS/yr required to shut down or reverse the QBO pattern (Niemeier and Schmidt, 2017), so that the westerly phase of the QBO that promote meridional transport was under minor influence of the heating effect of sulfur in this case.

Based on the simulations in Sect. 3.4, up to ~4% of air parcels composed of SO_2 and sulfate aerosol were transported from the TTL to the lower stratosphere in the south polar region till the end of

Page: 13

Number: 1 Author: Subject: Highlight Date: 6/3/2018 12:08:16 PM
not discussed or plotted above. If you are going to claim this, you have to show evidence.

Author: Administrator Subject: Sticky Note Date: 6/3/2018 12:08:12 PM
Please refer to the reply for details.

Number: 2 Author: Subject: Highlight Date: 5/31/2018 10:51:57 PM
That is a continuous emission. It cannot be compared to a one time emission.

Author: Administrator Subject: Sticky Note Date: 8/28/2018 3:47:40 PM
We rephrase this sentence: The amount of SO2 injected during the Merapi eruption 2010 was only 0.44 Tg, so that the westerly phase of the QBO that promotes meridional transport was under minor influence of the heating effect of sulfur in this case.
This sentence has been removed from the revised manuscript.

© Author(s) 2018. CC BY 4.0 License.

February 2011, which means the Merapi eruption contributed about 8800 tons of sulfur to the polar lower stratosphere within 4 months after the eruption, assuming that the sulfate aerosol converted from SO_2 remained in the plume. In the lower stratosphere, the atmosphere is relatively dry and clean compared with the lower troposphere, so the sulfate aerosols may have a smaller chance to interact with clouds or to be washed out. In fact, in the polar lower stratosphere usually sedimentation and downward transport by the BDC are the main removal processes. Clouds and washout processes usually cannot be expected in the lower stratosphere. However, the amount of sulfate aerosols in the plume could also be affected by other mechanisms that speed up the loss of sulfur, for example, coagulation in the volcanic plume, the absorption of sulfur onto fine ash particles etc. But for a moderate eruption, such as the Merapi eruption, sulphuric particle growth may not be as significant as it is in a large volcanic eruption, so the scavenging efficiency of sulfur will be low.

Besides, a kinematic trajectory model like MPTRAC, in which reanalysis vertical wind is used as vertical velocity, typically shows higher vertical dispersion in the equatorial lower stratosphere compared with a diabatic trajectory model (Schoeberl et al., 2003; Wohltmann and Rex, 2008; Liu et al., 2010; Ploeger et al., 2010, 2011). However, the ERA–Interim reanalysis data used in this study to drive the model may constrain the vertical dispersion much better than older reanalyses (Liu et al., 2010; Hoffmann et al., 2017). The meridional transport in this study was mainly quasi-horizontal transport in the mid- and high latitude UTLS region, so the effect of the vertical speed scheme is limited. Meanwhile, the MIPAS aerosol detections confirmed the MPTRAC simulations, so our results can be considered as a representative value.

The aerosol transported to the polar lower stratosphere will finally descend with the downward flow in the polar region to lower altitudes, and have a chance to become a nonlocal source of sulfur for Antarctica by dry and wet deposition, following the general precipitation patterns. Quantifying the sulfur deposition flux onto Antarctica is beyond the scope of this study, though. Model results of Solomon et al. (2016) suggest that the Merapi eruption made a small but significant contribution to ozone depletion over Antarctica in the vertical range of 200–100 hPa (~10–14 km). This altitude range is in agreement with our results, where we found transport into the Antarctic stratosphere between 10 and 20 km. When the volcanic plume was transported to Antarctica in December 2010, the polar synoptic temperature at these low height levels was already too high for the formation of PSCs. The additional ozone depletion found by Solomon et al. (2016) together with the fact that sulfate aerosol was transported from the Merapi into the Antarctic stratosphere between November and February where no PSCs are present during polar summer, may support the study which suggested that significant ozone

Page: 14

Number: 1 Author: Subject: Highlight Date: 5/31/2018 10:53:04 PM
DELETE. You can't use this with "for example," and anyway it has no information content.

Author: Administrator Subject: Sticky Note Date: 6/2/2018 5:23:57 PM
fixed

Number: 2 Author: Subject: Highlight Date: 5/31/2018 10:53:40 PM
sulfuric [stick to the standard spelling]

Author: Administrator Subject: Sticky Note Date: 6/2/2018 5:26:46 PM
fixed

© Author(s) 2018. CC BY 4.0 License.

depletion can also occur on cold binary aerosol (Drdla and Müller, 2012). The Merapi eruption in 2010 could be an interesting case study for more sophisticated geophysical models to study the aftermath of volcanic eruptions on polar processes.

5 Summary and conclusion

In this study, we analyzed the poleward transport pathway and the transport efficiency of volcanic aerosol released by the Merapi eruption in October 2010 from tropics to the Antarctic lower stratosphere. The analysis was based on AIRS SO_2 measurements, MIPAS sulfate aerosol detections and MPTRAC transport simulations. First, we estimated altitude-resolved SO_2 injection time series during the explosive eruption period using AIRS data together with a backward trajectory approach. Second, the long-range transport of the volcanic plume from the initial eruption to 30 April 2010 was simulated based on the derived SO_2 injection time series. Then the evolution and the poleward migration of the volcanic plume was analyzed and validated with MIPAS aerosol measurements.

Results of this study suggest that the volcanic plume from the Merapi eruption was transported from the tropics to south of 60°S within a time scale of one month. Later on a significant fraction of the volcanic plume crossed 60°S, even further to Antarctica until the end of February 2011. As a result, the aerosol load in the Antarctic lower stratosphere was significantly elevated for 3 months from December 2010 to February 2011. From March 2011, the aerosol transported to the polar lower stratosphere descended with the downward flow of the Brewer-Dobson circulation to lower altitudes. This relatively fast meridional transport and the distribution of volcanic aerosol was mainly carried out by quasi-horizontal mixing from the TTL to the extratropical lower stratosphere, which in turn was facilitated by the weakening of the subtropical jet in the seasonal transition from austral spring to summer. Based on the simulations, the most efficient pathway for this quasi-horizontal mixing occurred between isentropic surfaces of 360 to 430 K. The polar vortex in late austral spring 2010 was relatively strong compared to the climatological mean state. However, when the plume went to the south polar region, the polar vortex was displaced off the south pole, so that the volcanic plume was able to enter to the south pole without even penetrating the polar vortex.

Overall, after the Merapi eruption, the largest increase of aerosol load occurred in the southern hemisphere midlatitudes and a relatively small but significant fraction of the volcanic plume (4%) was further transported to the Antarctic lower stratosphere within 4 months after the eruption. This contributed 8800 tons of sulfur to the Antarctic stratosphere, which indicates that long-range transport

This page contains no comments

© Author(s) 2018. CC BY 4.0 License.

under favorable meteorological conditions enables tropical volcanic eruptions to be an important remote source of sulfur to Antarctica.

Code and data availability. AIRS data are distributed by the NASA Goddard Earth Sciences Data Information and Services Center. The SO_2 index data used in this study (Hoffmann et al., 2014) are available for download at https://datapub.fz-juelich.de/slcs/airs/volcanoes/ (last access: 17 December 2017). Envisat MIPAS Level-1B data are distributed by the European Space Agency. The ERA–Interim reanalysis data (Dee et al., 2011) were obtained from the European Centre for Medium-Range Weather Forecasts. The code of the Massive-Parallel Trajectory Calculations (MPTRAC) model is available under the terms and conditions of the GNU General Public License, Version 3 from the repository at https://github.com/slcs-jsc/mptrac (last access: 31 December 2017).

Competing interests. The authors declare that they have no conflict of interest.

Acknowledgments. This work was supported by National Natural Science Foundation of China under grant no. 41605023 and International Postdoctoral Exchange Fellowship Program 2015 under grant no. 20151006.

Reference

Anstey, J. A., and Shepherd, T. G.: High-latitude influence of the quasi-biennial oscillation, Q. J. R. Meteorol. Soc., 140, 1-21, doi: 10.1002/qj.2132, 2014.

Aquila, V., C. I. Garfinkel,P.A.Newman, L. D. Oman, and D. W. Waugh, Modifications of the quasi-biennial oscillation by a geoengineering perturbation of the stratospheric aerosol layer, Geophys. Res. Lett., 41, 1738-1744, doi: 10.1002/2013GL058818, 2014.

Aumann, H. H., Chahine, M. T., Gautier, C., Goldberg, M. D., Kalnay, E., McMillin, L. M., Revercomb, H., Rosenkranz, P. W., Smith, W. L., Staelin, D. H., Strow, L. L., and Susskind, J.: AIRS/AMSU/HSB on the Aqua mission: design, science objectives, data products, and processing systems, IEEE Trans. Geosci. Remote Sens., 41, 253-264, doi: 10.1109/TGRS.2002.808356, 2003.

Baldwin, M. P., and Dunkerton, T. J.: Propagation of the Arctic Oscillation from the stratosphere to the troposphere, J. Geophys. Res. Atmos., 104, 30937-30946, doi: 10.1029/1999JD900445, 1999.

Dee, D. P., Uppala, S. M., Simmons, A. J., Berrisford, P., Poli, P., Kobayashi, S., Andrae, U., Balmaseda, M. A., Balsamo, G., Bauer, P., Bechtold, P., Beljaars, A. C. M., van de Berg, L., Bidlot, J., Bormann, N., Delsol, C., Dragani, R., Fuentes, M., Geer, A. J., Haimberger, L., Healy, S. B., Hersbach, H., Holm, E. V., Isaksen, L., Kallberg, P., Kohler, M., Matricardi, M., McNally, A. P., Monge-Sanz, B. M., Morcrette, J. J., Park, B. K., Peubey, C., de Rosnay, P., Tavolato, C., Thepaut, J. N., and Vitart, F.: The ERA-Interim reanalysis: configuration and performance of the data assimilation system, Q. J. R. Meteorol. Soc., 137, 553-597, doi: 10.1002/qj.828, 2011.

Drdla, K., and Müller, R.: Temperature thresholds for chlorine activation and ozone loss in the polar stratosphere, Ann. Geophys., 30, 1055-1073, doi: 10.5194/angeo-30-1055-2012, 2012.

This page contains no comments

© Author(s) 2018. CC BY 4.0 License.

Fischer, H., Birk, M., Blom, C., Carli, B., Carlotti, M., von Clarmann, T., Delbouille, L., Dudhia, A., Ehhalt, D., Endemann, M., Flaud, J. M., Gessner, R., Kleinert, A., Koopman, R., Langen, J., López-Puertas, M., Mosner, P., Nett, H., Oelhaf, H., Perron, G., Remedios, J., Ridolfi, M., Stiller, G., and Zander, R.: MIPAS: an instrument for atmospheric and climate research, Atmos. Chem. Phys., 8, 2151-2188, doi: 10.5194/acp-8-2151-2008, 2008.

Gao, C., Oman, L., Robock, A., and Stenchikov, G. L.: Atmospheric volcanic loading derived from bipolar ice cores: Accounting for the spatial distribution of volcanic deposition, J. Geophys. Res. Atmos., 112, D09109, doi: 10.1029/2006JD007461, 2007.

Griessbach, S., Hoffmann, L., Spang, R., von Hobe, M., Müller, R., and Riese, M.: Infrared limb emission measurements of aerosol in the troposphere and stratosphere, Atmos. Meas. Tech., 9, 4399-4423, doi:10.5194/amt-9-4399-2016, 2016.

Günther, A., Höpfner, M., Sinnhuber, B. M., Griessbach, S., Deshler, T., von Clarmann, T., and Stiller, G.: MIPAS observations of volcanic sulphate aerosol and sulphur dioxide in the stratosphere, Atmos. Chem. Phys. Discuss., 2017, 1-32, doi: 10.5194/acp-2017-538, 2017.

Haynes, P., and Shuckburgh, E.: Effective diffusivity as a diagnostic of atmospheric transport: 2. Troposphere and lower stratosphere, J. Geophys. Res. Atmos., 105, 22795-22810, doi: 10.1029/2000JD900092, 2000.

Heng, Y., Hoffmann, L., Griessbach, S., Rößler, T., and Stein, O.: Inverse transport modeling of volcanic sulfur dioxide emissions using large-scale simulations, Geosci. Model Dev., 9, 1627-1645, doi:10.5194/gmd-9-1627-2016, 2016.

Hoffmann, L., Griessbach, S., and Meyer, C. I.: Volcanic emissions from AIRS observations: detection methods, case study, and statistical analysis, in: Remote Sensing of Clouds and the Atmosphere XIX and Optics in Atmospheric Propagation and Adaptive Systems XVII, edited by: Comeron, A., Kassianov, E. I., Schafer, K., Picard, R. H., Stein, K., and Gonglewski, J. D., Proceedings of SPIE, Spie-Int Soc Optical Engineering, Bellingham, doi: 92421410.1117/12.2066326, 2014.

Hoffmann, L., Hertzog, A., Rößler, T., Stein, O., and Wu, X.: Intercomparison of meteorological analyses and trajectories in the Antarctic lower stratosphere with Concordiasi superpressure balloon observations, Atmos. Chem. Phys., 17, 8045-8061, doi: 10.5194/acp-17-8045-2017, 2017.

Hoffmann, L., Rößler, T., Griessbach, S., Heng, Y., and Stein, O.: Lagrangian transport simulations of volcanic sulfur dioxide emissions: Impact of meteorological data products, J. Geophys. Res. Atmos., 121, 4651-4673, doi: 10.1002/2015JD023749, 2016.

Hofmann, D. J., Rosen, J. M., and Gringel, W.: Delayed production of sulfuric acid condensation nuclei in the polar stratosphere from El Chichon volcanic vapors, Journal of Geophysical Research: Atmospheres, 90, 2341-2354, doi:10.1029/JD090iD01p02341, 1985.

Hofmann, D. J., Rosen, J. M., and Harder, J. W.: Aerosol measurements in the winter/spring Antarctic stratosphere: 1. Correlative measurements with ozone, Journal of Geophysical Research: Atmospheres, 93, 665-676, doi:10.1029/JD093iD01p00665, 1988.

Holton, J. R., Haynes, P. H., McIntyre, M. E., Douglass, A. R., Rood, R. B., and Pfister, L.: Stratosphere-troposphere exchange, Reviews of Geophysics, 33, 403-439, doi: 10.1029/95RG02097, 1995.

Holton, J. R., and Tan, H. C.: The Influence of the Equatorial Quasi-Biennial Oscillation on the Global Circulation at 50 mb, J. Atmos. Sci., 37, 2200-2208, doi: 10.1175/1520-0469(1980)037<2200:tioteq>2.0.co;2, 1980.

Höpfner, M., Pitts, M. C., and Poole, L. R.: Comparison between CALIPSO and MIPAS observations of polar stratospheric clouds, Journal of Geophysical Research: Atmospheres, 114, doi:10.1029/2009JD012114, 2009.

This page contains no comments

© Author(s) 2018. CC BY 4.0 License.

548 Ivy, D. J., Solomon, S., Kinnison, D., Mills, M. J., Schmidt, A., and Neely, R. R.: The influence of the
549 Calbuco eruption on the 2015 Antarctic ozone hole in a fully coupled chemistry-climate model,
550 Geophys. Res. Lett., 44, 2556-2561, doi: 10.1002/2016GL071925, 2017.
551 Jäger, H.: Long-term record of lidar observations of the stratospheric aerosol layer at
552 Garmisch-Partenkirchen, J. Geophys. Res. Atmos., 110, D08106, doi: 10.1029/2004JD005506, 2005.
553 Jäger, H., and Wege, K.: Stratospheric ozone depletion at northern midlatitudes after major volcanic
554 eruptions, J. Atmos. Chem., 10, 273-287, doi: 10.1007/bf00053863, 1990.
555 Khaykin, S. M., Godin-Beekmann, S., Keckhut, P., Hauchecorne, A., Jumelet, J., Vernier, J. P.,
556 Bourassa, A., Degenstein, D. A., Rieger, L. A., Bingen, C., Vanhellemont, F., Robert, C., DeLand,
557 M., and Bhartia, P. K.: Variability and evolution of the midlatitude stratospheric aerosol budget from
558 22 years of ground-based lidar and satellite observations, Atmos. Chem. Phys., 17, 1829-1845, doi:
559 10.5194/acp-17-1829-2017, 2017.
560 Klekociuk, A., Tully, M., Alexander, S., Dargaville, R., Deschamps, L., Fraser, P., Gies, H., Henderson,
561 S., Javorniczky, J., and Krummel, P.: The Antarctic ozone hole during 2010, Aust. Meteorol. Ocean.
562 Journal., 61, 253, 2011.
563 Kravitz, B., and Robock, A.: Climate effects of high-latitude volcanic eruptions: Role of the time of
564 year, J. Geophys. Res. Atmos., 116, D01105, 10.1029/2010JD014448, 2011.
565 Kunz, A., Konopka, P., Müller, R., and Pan, L. L.: Dynamical tropopause based on isentropic potential
566 vorticity gradients, J. Geophys. Res. Atmos., 116, D01110, doi: 10.1029/2010JD014343, 2011a.
567 Kunz, A., Pan, L. L., Konopka, P., Kinnison, D. E., and Tilmes, S.: Chemical and dynamical
568 discontinuity at the extratropical tropopause based on START08 and WACCM analyses, J. Geophys.
569 Res. Atmos., 116, D24302, doi: 10.1029/2011JD016686, 2011b.
570 Kunz, A., Sprenger, M., and Wernli, H.: Climatology of potential vorticity streamers and associated
571 isentropic transport pathways across PV gradient barriers, J. Geophys. Res. Atmos., 120, 3802-3821,
572 doi: 10.1002/2014jd022615, 2015.
573 Liu, Y. S., Fueglistaler, S., and Haynes, P. H.: Advection-condensation paradigm for stratospheric water
574 vapor, J. Geophys. Res. Atmos., 115,D24307, doi: 10.1029/2010JD014352, 2010.
575 Mazzera, D. M., Lowenthal, D. H., Chow, J. C., and Watson, J. G.: Sources of PM10 and sulfate aerosol
576 at McMurdo station, Antarctica, Chemosphere, 45, 347-356, doi:
577 https://doi.org/10.1016/S0045-6535(00)00591-9, 2001.
578 Niemeier, U., and Schmidt, H.: Changing transport processes in the stratosphere by radiative heating of
579 sulfate aerosols, Atmos. Chem. Phys., 17, 14871-14886, doi: 10.5194/acp-17-14871-2017, 2017.
580 Olsen, M. A., Douglass, A. R., Schoeberl, M. R., Rodriquez, J. M., and Yoshida, Y.: Interannual
581 variability of ozone in the winter lower stratosphere and the relationship to lamina and irreversible
582 transport, J. Geophys. Res.-Atmos., 115, 10.1029/2009jd013004, 2010.
583 O'Sullivan, D., and Dunkerton, T. J.: The influence of the quasi-biennial oscillation on global
584 constituent distributions, J. Geophys. Res. Atmos., 102, 21731-21743, doi: 10.1029/97JD01689,
585 1997.
586 Palazzi, E., Fierli, F., Stiller, G. P., and Urban, J.: Probability density functions of long-lived tracer
587 observations from satellite in the subtropical barrier region: data intercomparison, Atmos. Chem.
588 Phys., 11, 10579-10598, doi: 10.5194/acp-11-10579-2011, 2011.
589 Pallister, J. S., Schneider, D. J., Griswold, J. P., Keeler, R. H., Burton, W. C., Noyles, C., Newhall, C.
590 G., and Ratdomopurbo, A.: Merapi 2010 eruption—Chronology and extrusion rates monitored with
591 satellite radar and used in eruption forecasting, J. Volcanol. Geotherm. Res., 261, 144-152, doi:
592 http://dx.doi.org/10.1016/j.jvolgeores.2012.07.012, 2013.

This page contains no comments

© Author(s) 2018. CC BY 4.0 License.

Pausata, F. S. R., Chafik, L., Caballero, R., and Battisti, D. S.: Impacts of high-latitude volcanic eruptions on ENSO and Asian monsoon, Proceedings of the National Academy of Sciences, 112, 13784-13788, doi: 10.1073/pnas.1509153112, 2015.

Ploeger, F., Konopka, P., Gunther, G., Grooss, J. U., and Muller, R.: Impact of the vertical velocity scheme on modeling transport in the tropical tropopause layer, J. Geophys. Res. Atmos., 115, 14, doi: 10.1029/2009jd012023, 2010.

Ploeger, F., Fueglistaler, S., Grooss, J. U., Gunther, G., Konopka, P., Liu, Y. S., Muller, R., Ravegnani, F., Schiller, C., Ulanovski, A., and Riese, M.: Insight from ozone and water vapour on transport in the tropical tropopause layer (TTL), Atmos. Chem. Phys., 11, 407-419, doi: 10.5194/acp-11-407-2011, 2011.

Rößler, T., Stein, O., Heng, Y., and Hoffmann, L.: Regional and seasonal truncation errors of trajectory calculations using ECMWF high-resolution operational analyses and forecasts, Geosci. Model Dev. Discuss., 2017, 1-27, doi: 10.5194/gmd-2016-314, 2017.

Sand, M., Samset, B. H., Balkanski, Y., Bauer, S., Bellouin, N., Berntsen, T. K., Bian, H., Chin, M., Diehl, T., Easter, R., Ghan, S. J., Iversen, T., Kirkevåg, A., Lamarque, J. F., Lin, G., Liu, X., Luo, G., Myhre, G., Noije, T. V., Penner, J. E., Schulz, M., Seland, Ø., Skeie, R. B., Stier, P., Takemura, T., Tsigaridis, K., Yu, F., Zhang, K., and Zhang, H.: Aerosols at the poles: an AeroCom Phase II multi-model evaluation, Atmos. Chem. Phys., 17, 12197-12218, doi: 10.5194/acp-17-12197-2017, 2017.

Schoeberl, M. R., Douglass, A. R., Zhu, Z. X., and Pawson, S.: A comparison of the lower stratospheric age spectra derived from a general circulation model and two data assimilation systems, J. Geophys. Res. Atmos., 108, 16, doi: 10.1029/2002jd002652, 2003.

Shuckburgh, E., Norton, W., Iwi, A., and Haynes, P.: Influence of the quasi-biennial oscillation on isentropic transport and mixing in the tropics and subtropics, J. Geophys. Res. Atmos., 106, 14327-14337, doi: 10.1029/2000JD900664, 2001.

Sigl, M., Winstrup, M., McConnell, J. R., Welten, K. C., Plunkett, G., Ludlow, F., Buntgen, U., Caffee, M., Chellman, N., Dahl-Jensen, D., Fischer, H., Kipfstuhl, S., Kostick, C., Maselli, O. J., Mekhaldi, F., Mulvaney, R., Muscheler, R., Pasteris, D. R., Pilcher, J. R., Salzer, M., Schupbach, S., Steffensen, J. P., Vinther, B. M., and Woodruff, T. E.: Timing and climate forcing of volcanic eruptions for the past 2,500 years, Nature, 523, 543-549, doi: 10.1038/nature14565http://www.nature.com/nature/journal/v523/n7562/abs/nature14565.html#supplementary-information, 2015.

Solomon, S.: Stratospheric ozone depletion: A review of concepts and history, Reviews of Geophysics, 37, 275-316, doi: 10.1029/1999RG900008, 1999.

Solomon, S., Daniel, J. S., Neely, R. R., Vernier, J.-P., Dutton, E. G., and Thomason, L. W.: The Persistently Variable "Background" Stratospheric Aerosol Layer and Global Climate Change, Science, 333, 866-870, doi: 10.1126/science.1206027, 2011.

Solomon, S., Ivy, D. J., Kinnison, D., Mills, M. J., Neely, R. R., and Schmidt, A.: Emergence of healing in the Antarctic ozone layer, Science, doi: 10.1126/science.aae0061, 2016.

Solomon, S., Sanders, R. W., Garcia, R. R., and Keys, J. G.: Increased chlorine dioxide over Antarctica caused by volcanic aerosols from Mount-Pinatubo, Nature, 363, 245–248, doi: https://doi.org/10.1038/363245a0, 1993.

Stohl, A., Forster, C., Frank, A., Seibert, P., and Wotawa, G.: Technical note: The Lagrangian particle dispersion model FLEXPART version 6.2, Atmos. Chem. Phys., 5, 2461-2474, doi:10.5194/acp-5-2461-2005, 2005.

Stone, K. A., Solomon, S., Kinnison, D. E., Pitts, M. C., Poole, L. R., Mills, M. J., Schmidt, A., Neely, R. R., Ivy, D., Schwartz, M. J., Vernier, J.-P., Johnson, B. J., Tully, M. B., Klekociuk, A. R.,

This page contains no comments

© Author(s) 2018. CC BY 4.0 License.

König-Langlo, G., and Hagiya, S.: Observing the Impact of Calbuco Volcanic Aerosols on South Polar Ozone Depletion in 2015, J. Geophys. Res. Atmos., 122, 11,862-811,879, doi: 10.1002/2017JD026987, 2017.

Surono, Jousset, P., Pallister, J., Boichu, M., Buongiorno, M. F., Budisantoso, A., Costa, F., Andreastuti, S., Prata, F., Schneider, D., Clarisse, L., Humaida, H., Sumarti, S., Bignami, C., Griswold, J., Carn, S., Oppenheimer, C., and Lavigne, F.: The 2010 explosive eruption of Java's Merapi volcano—A '100-year' event, J. Volcanol. Geotherm. Res., 241, 121-135, doi: http://dx.doi.org/10.1016/j.jvolgeores.2012.06.018, 2012.

Tilmes, S., Muller, R., and Salawitch, R.: The sensitivity of polar ozone depletion to proposed geoengineering schemes, Science, 320, 1201-1204, doi: 10.1126/science.1153966, 2008.

Vernier, J. P., Thomason, L. W., Pommereau, J. P., Bourassa, A., Pelon, J., Garnier, A., Hauchecorne, A., Blanot, L., Trepte, C., Degenstein, D., and Vargas, F.: Major influence of tropical volcanic eruptions on the stratospheric aerosol layer during the last decade, Geophys. Res. Lett., 38, L12807, 10.1029/2011GL047563, 2011.

Vogel, B., Pan, L. L., Konopka, P., Gunther, G., Muller, R., Hall, W., Campos, T., Pollack, I., Weinheimer, A., Wei, J., Atlas, E. L., and Bowman, K. P.: Transport pathways and signatures of mixing in the extratropical tropopause region derived from Lagrangian model simulations, J. Geophys. Res.-Atmos., 116, 16, doi: 10.1029/2010jd014876, 2011.

von Glasow, R., Bobrowski, N., and Kern, C.: The effects of volcanic eruptions on atmospheric chemistry, Chem. Geol., 263, 131-142, doi: http://dx.doi.org/10.1016/j.chemgeo.2008.08.020, 2009.

Watson, P. A. G., and Gray, L. J.: How Does the Quasi-Biennial Oscillation Affect the Stratospheric Polar Vortex?, J. Atmos. Sci., 71, 391-409, doi: 10.1175/jas-d-13-096.1, 2014.

Wohltmann, I., and Rex, M.: Improvement of vertical and residual velocities in pressure or hybrid sigma-pressure coordinates in analysis data in the stratosphere, Atmos. Chem. Phys., 8, 265-272, doi: 10.5194/acp-8-265-2008, 2008.

Wu, X., Griessbach, S., and Hoffmann, L.: Equatorward dispersion of a high-latitude volcanic plume and its relation to the Asian summer monsoon: a case study of the Sarychev eruption in 2009, Atmos. Chem. Phys., 17, 13439-13455, doi: 10.5194/acp-17-13439-2017, 2017.

Zuev, V. V., Zueva, N. E., Savelieva, E. S., and Gerasimov, V. V.: The Antarctic ozone depletion caused by Erebus volcano gas emissions, Atmos. Environ., 122, 393-399, doi: https://doi.org/10.1016/j.atmosenv.2015.10.005, 2015.

This page contains no comments

Atmos. Chem. Phys. Discuss., https://doi.org/10.5194/acp-2018-332
Manuscript under review for journal Atmos. Chem. Phys.
Discussion started: 22 May 2018
© Author(s) 2018. CC BY 4.0 License.

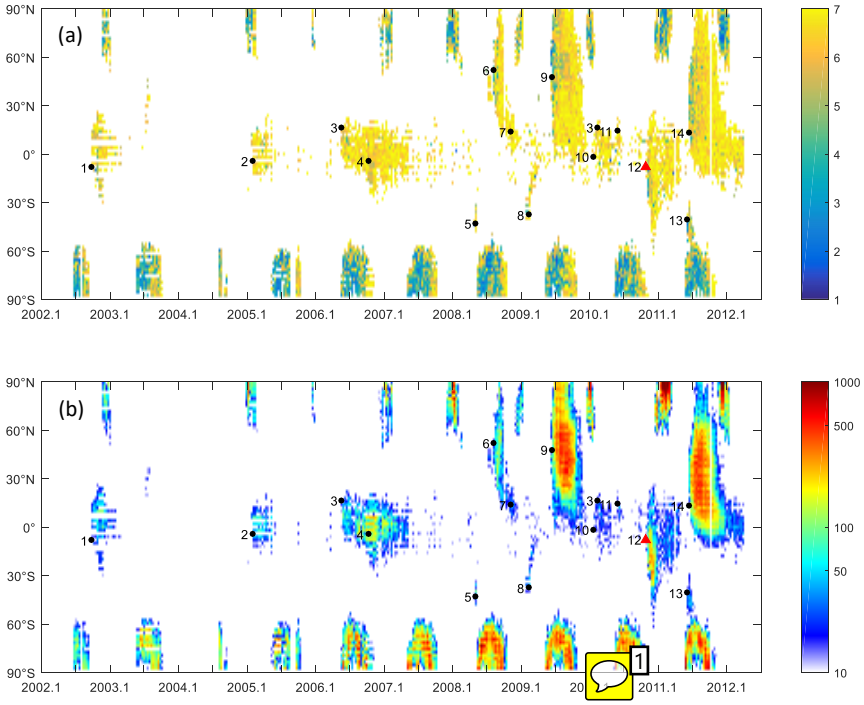

Figure 1: (a) Median value of ACI (ACI<7) and (b) number of MIPAS aerosol detections between 13 and 20 km (bin size 10 days and 2 ° in latitude). The red triangle indicates the eruption of Mount Merapi. The black dots indicate 1 Raung, 2 Manam, 3 Soufriere Hills, 4 Tavurvur (Rabaul), 5 Chaitén, 6 Kasatochi, 7 Dalaffilla, 8 Australian bushfire, 9 Sarychev Peak, 10 Nyamuragira, 11 Pacaya, 12 Mount Merapi, 13 Puyehue-Cordón Caulle, 14 Nabro.

Page: 21

Number: 1 Author: Subject: Sticky Note Date: 5/31/2018 10:04:22 PM

Explain label. Does 2010.1 mean January 2010?

Author: Administrator Subject: Sticky Note Date: 6/3/2018 3:02:31 PM

Yes, 2010.1 means January 2010. But we realize it is not necessary to include the '.1' in the tick labels, and it brought confusion too. So we replaced the '2010.1' with '2010' in the revised manuscript.

Atmos. Chem. Phys. Discuss., https://doi.org/10.5194/acp-2018-332
Manuscript under review for journal Atmos. Chem. Phys.
Discussion started: 22 May 2018
© Author(s) 2018. CC BY 4.0 License.

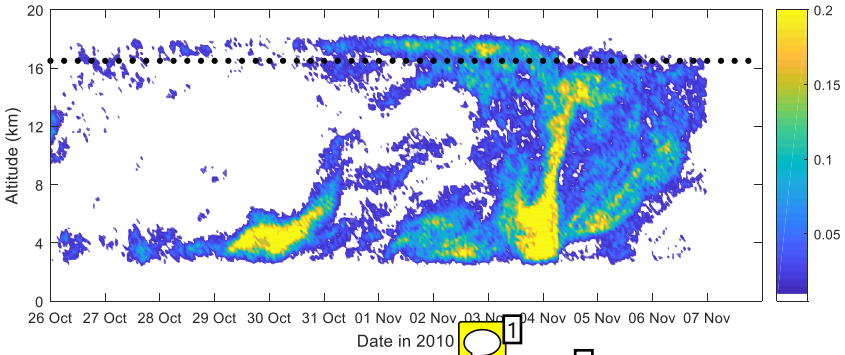

Figure 2: Merapi SO_2 emission time series (unit: kg m^{-2} s^{-1}) derived from AIRS measurements using a backward trajectory approach (see text for details). The emission data are binned every 1 h and 0.2 km. Gray dots denote the height of the thermal tropopause (based on the ERA–Interim reanalysis).

Page: 22

Number: 1 Author: Subject: Sticky Note Date: 5/31/2018 10:01:31 PM
What time of the day are the tick marks? OOZ?

Author: Administrator Subject: Sticky Note Date: 6/3/2018 12:17:21 PM
The tick marks show 0 UTC on each day. We add a one sentence in the figure caption to make it clear.

Number: 2 Author: Subject: Highlight Date: 5/31/2018 10:05:33 PM
Explain these units. How does length unit work?

Author: Administrator Subject: Sticky Note Date: 8/28/2018 3:57:24 PM
In our study, we considered the SO2 within a radius of 75 km to the location of volcano as the SO2 injected by the volcanic eruption. So the unit kg m-1 s-1 can be simply converted to kg m-3 s-1 by dividing the area. However, in the real case, the SO2 emission is not evenly distributed in this circular area, so we prefer to use the exact longitude, latitude, altitude of the SO2 to initialize the trajectories. In Fig. 2, we decide to group the SO2 emission only by time and altitude instead of showing the area-averaged value.
The choice of radius is verified by carrying out sensitivity simulation experiments and comparing the SO2 simulations with AIRS SO2 observations, which is not shown in the paper. If the radius is too large, it will include SO2 that was not necessarily injected by the volcanic eruption, and the simulated SO2 plume will be too dispersive compared with observations. But if the radius is too small, the injected SO2 will be underestimated. 75 km is considered as the best choice of radius for the Merapi case.

Atmos. Chem. Phys. Discuss., https://doi.org/10.5194/acp-2018-332
Manuscript under review for journal Atmos. Chem. Phys.
Discussion started: 22 May 2018
© Author(s) 2018. CC BY 4.0 License.

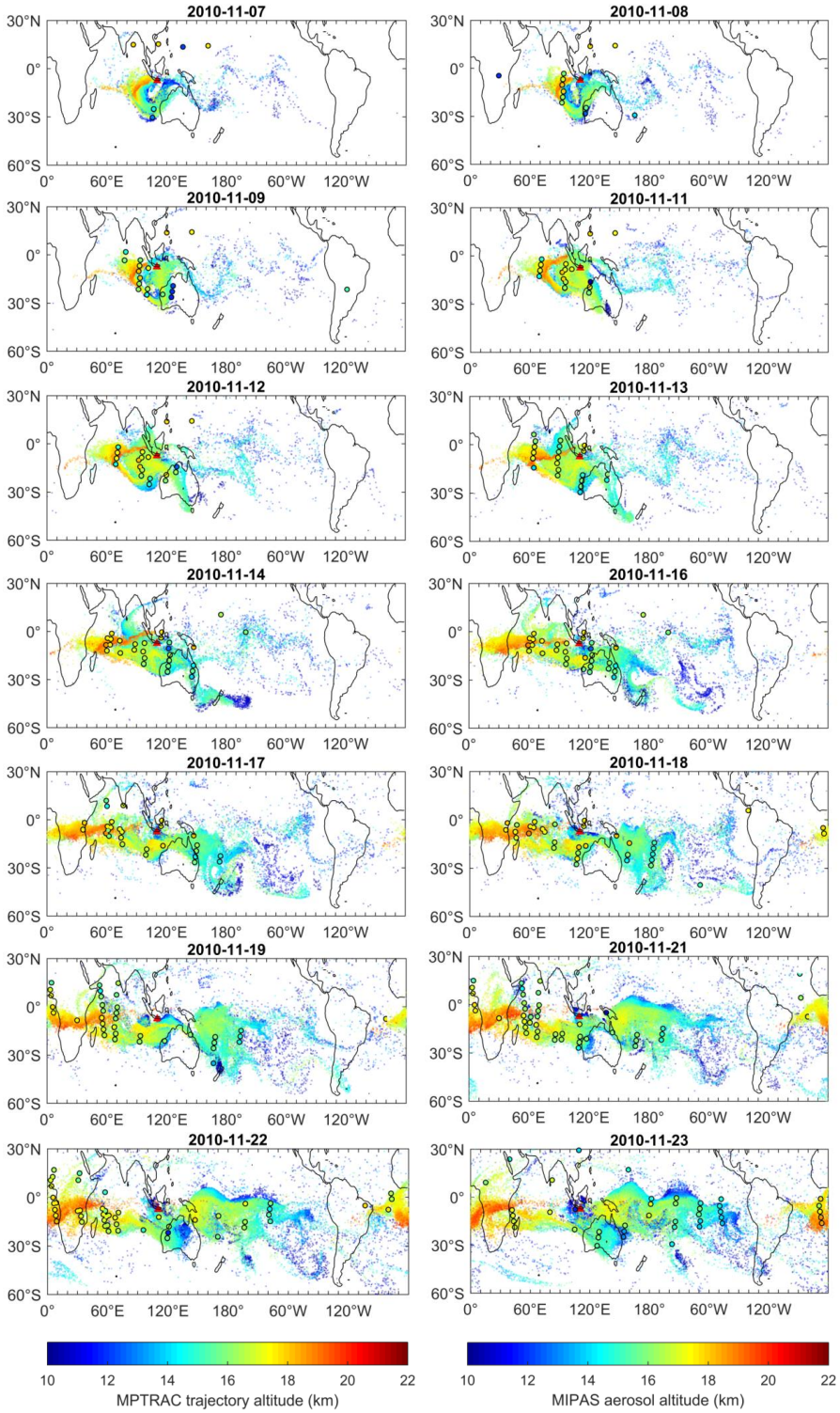

Figure 3: Distribution of the volcanic plume (showing only air parcels higher than 10 km, shading) from MPTRAC simulations (shown for 00:00UTC on selected days) and MIPAS aerosol detections (ACI < 7) within ±6 h (color-filled circles). The altitudes of all

This page contains no comments

Atmos. Chem. Phys. Discuss., https://doi.org/10.5194/acp-2018-332
Manuscript under review for journal Atmos. Chem. Phys.
Discussion started: 22 May 2018
© Author(s) 2018. CC BY 4.0 License.

Atmospheric Chemistry and Physics Discussions

air parcels, regardless of their SO_2 values, are shown. The red triangle denotes the location of Mount Merapi.

This page contains no comments

Atmos. Chem. Phys. Discuss., https://doi.org/10.5194/acp-2018-332
Manuscript under review for journal Atmos. Chem. Phys.
Discussion started: 22 May 2018
© Author(s) 2018. CC BY 4.0 License.

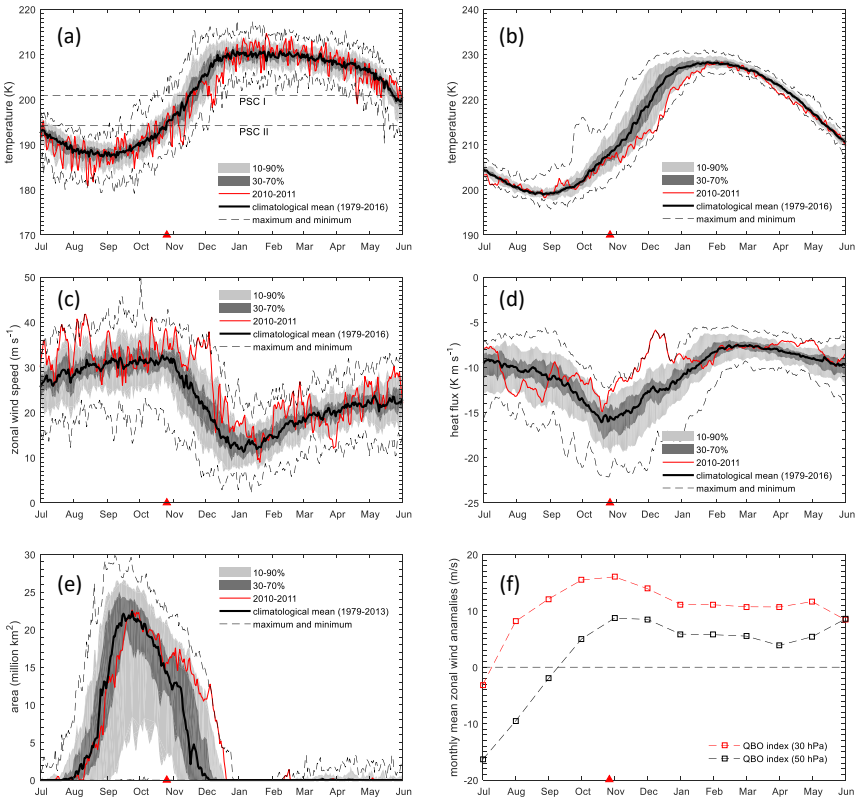

Figure 4: (a) Minimum temperature south of 50 ℃S at 150 hPa; (b) temperature averaged over the polar cap for latitudes south of 60 ℃S at 150 hPa; (c) zonal wind speed at 60 ℃S at 150 hPa; (d) eddy heat flux averaged between 45 ℃S and 75 ℃S for the 45-day period prior to the date indicated at 150 hPa; (e) ozone hole area from July 2010 to May 2011; (f) 1onthly mean zonal wind anomalies at 30 and 50 hPa. Temperatures for PSC existence in (a) are determined by assuming a nitric acid concentration of 6 ppbv and a water vapor concentration of 4.5 ppmv. (a)–(e) are based on 2IERRA2 data and (f) is based on 3CEP/NCAR reanalysis. The ozone hole area in (e) is determined from 4MI ozone satellite measurements. The red triangles indicate the time of the Merapi eruption.

Page: 25

Number: 1 Author: Subject: Highlight Date: 5/31/2018 10:18:02 PM
Where?

Author: Administrator Subject: Sticky Note Date: 6/3/2018 2:51:26 PM
fixed.

Number: 2 Author: Subject: Highlight Date: 5/31/2018 10:18:22 PM
reference?

Author: Administrator Subject: Sticky Note Date: 6/3/2018 2:51:32 PM
fixed

Number: 3 Author: Subject: Highlight Date: 5/31/2018 10:18:29 PM
reference?

Author: Administrator Subject: Sticky Note Date: 6/3/2018 2:51:37 PM
fixed

Number: 4 Author: Subject: Highlight Date: 5/31/2018 10:18:41 PM
reference?

Author: Administrator Subject: Sticky Note Date: 6/3/2018 2:51:44 PM
fixed

Atmos. Chem. Phys. Discuss., https://doi.org/10.5194/acp-2018-332
Manuscript under review for journal Atmos. Chem. Phys.
Discussion started: 22 May 2018
© Author(s) 2018. CC BY 4.0 License.

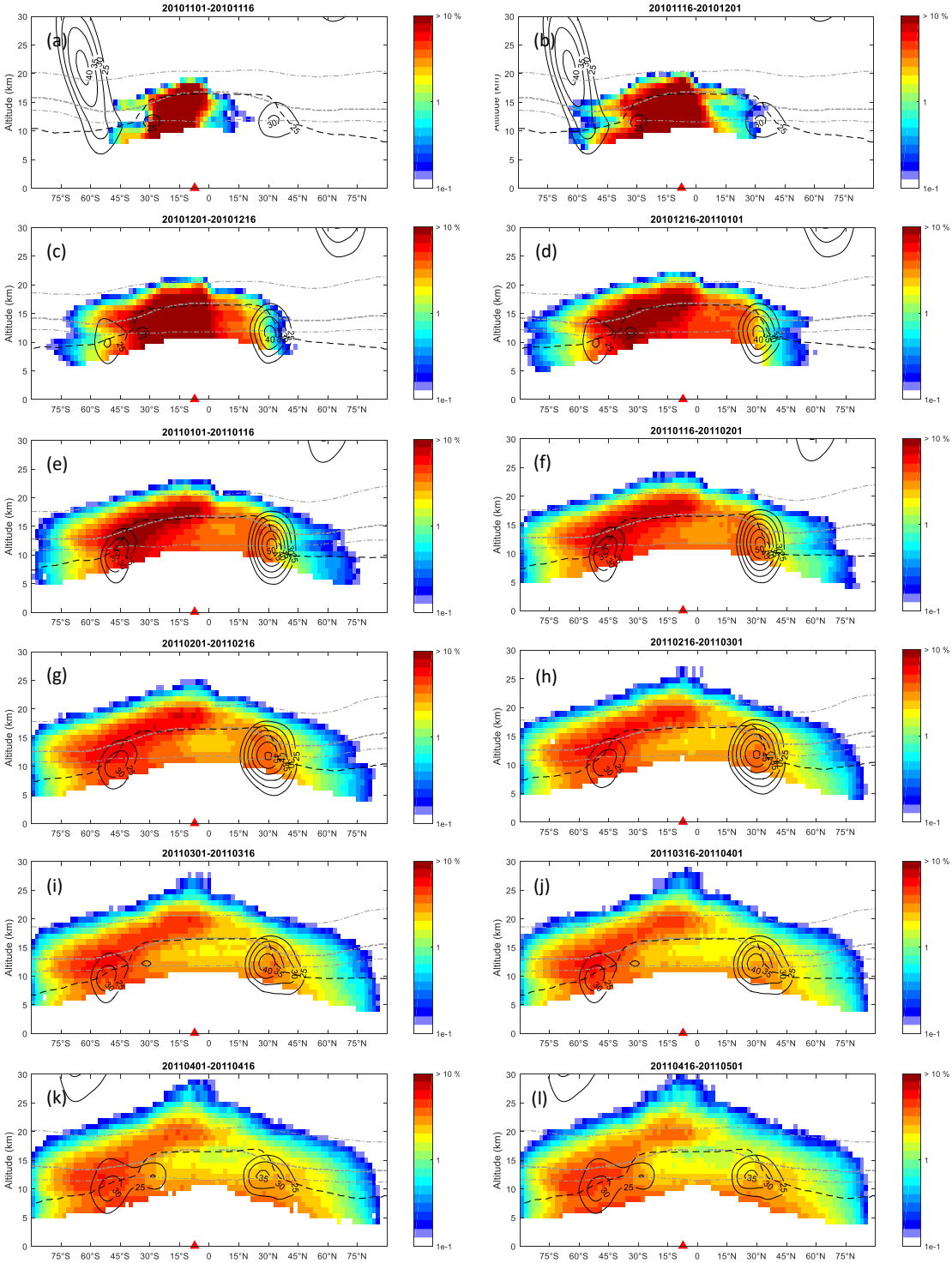

Figure 5: Percentage (%) of air parcels in proportion to the total number of air parcels from MPTRAC simulations, overlapped with monthly mean zonal winds (black contours), the thermal tropopause (black dashed line), the 380 K potential temperature isoline (thick gray dashed line) and 350 and 480 K potential temperature isolines (thin gray dashed lines). Results

This page contains no comments

Atmos. Chem. Phys. Discuss., https://doi.org/10.5194/acp-2018-332
Manuscript under review for journal Atmos. Chem. Phys.
Discussion started: 22 May 2018
© Author(s) 2018. CC BY 4.0 License.

Atmospheric Chemistry and Physics Discussions

are binned every 2 ° in latitude and 1 km in altitude. The red triangle denotes the latitude of the Merapi. Please see title of each figure for the time period covered.

This page contains no comments

Atmos. Chem. Phys. Discuss., https://doi.org/10.5194/acp-2018-332
Manuscript under review for journal Atmos. Chem. Phys.
Discussion started: 22 May 2018
© Author(s) 2018. CC BY 4.0 License.

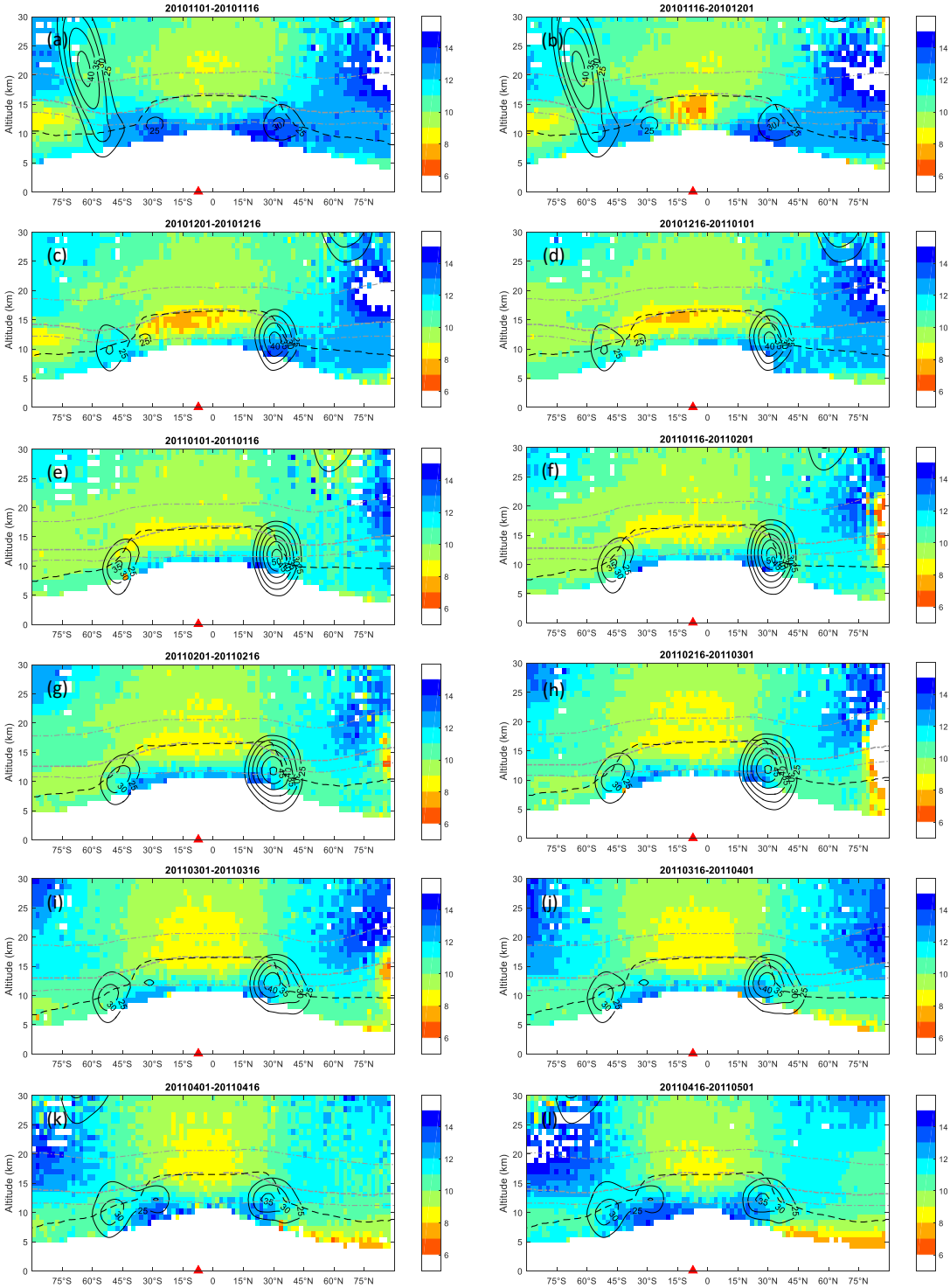

Figure 6: Median value of ACI of MIPAS aerosol detections (ice clouds filtered out), overlapped with monthly mean zonal winds (black contours), the thermal tropopause (black dashed line), the 380 K potential temperature isoline (thick gray dashed line) and 350 and 480 K potential temperature isolines (thin gray dashed lines). Results are binned

This page contains no comments

Atmos. Chem. Phys. Discuss., https://doi.org/10.5194/acp-2018-332
Manuscript under review for journal Atmos. Chem. Phys.
Discussion started: 22 May 2018
© Author(s) 2018. CC BY 4.0 License.

Atmospheric Chemistry and Physics Discussions

every 2 °in latitude and 1 km in altitude. Only median ACI values of 5–15 are shown. The red triangle denotes the latitude of the Merapi. Please see title of each figure for the time period covered.

This page contains no comments

Atmos. Chem. Phys. Discuss., https://doi.org/10.5194/acp-2018-332
Manuscript under review for journal Atmos. Chem. Phys.
Discussion started: 22 May 2018
© Author(s) 2018. CC BY 4.0 License.

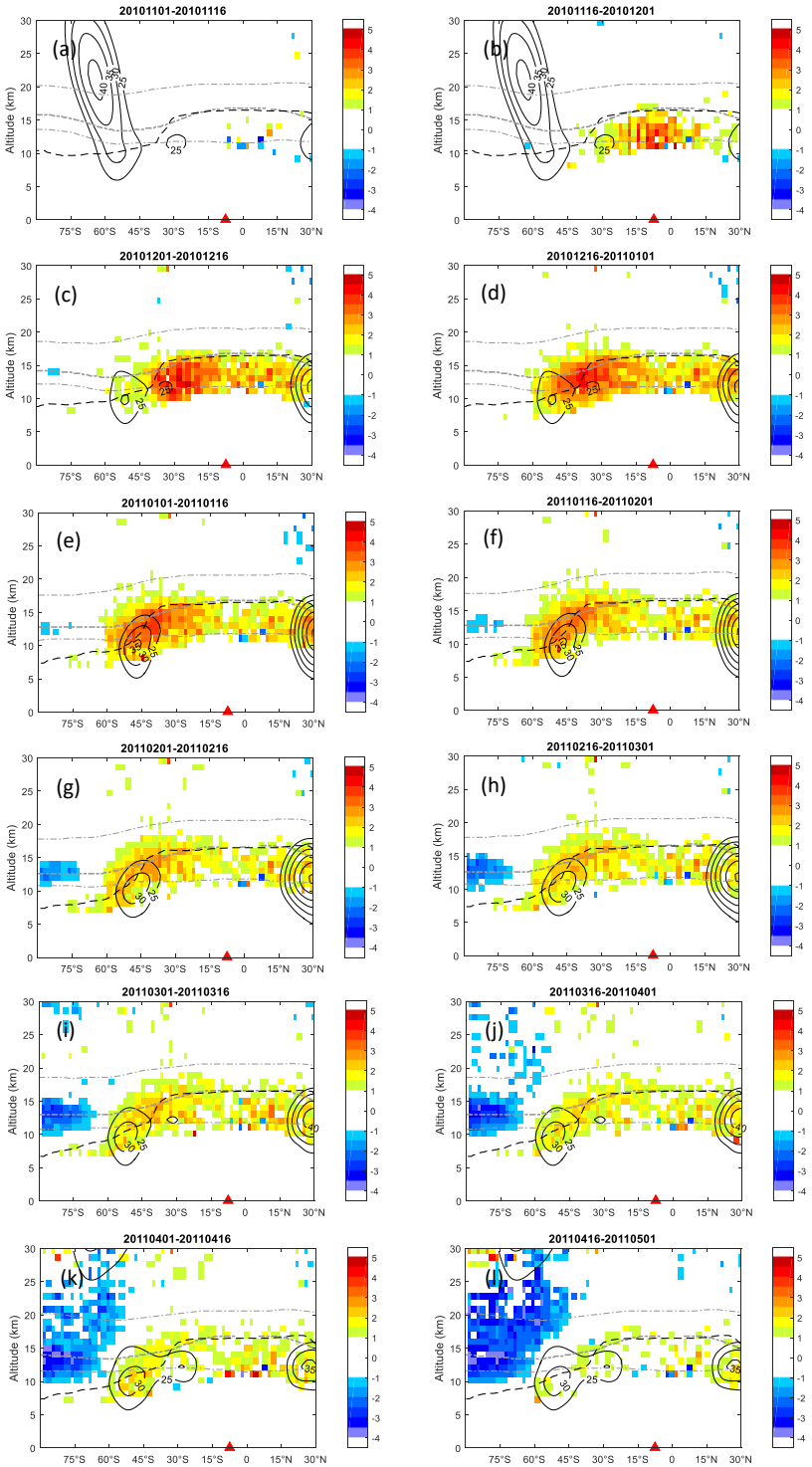

Figure 7: Change of aerosol load after the eruption of Merapi in 2010, overlapped with monthly mean zonal winds (black contours), the thermal tropopause (black dashed line), the 380 K potential temperature isoline (thick gray dashed line) and 350 and 480 K potential temperature isolines (thin gray dashed lines). Results are binned every 2 ° in

Page: 30

Number: 1 Author: Subject: Highlight Date: 5/31/2018 10:34:38 PM
What are the units? Are negative a higher load?

Author: Administrator Subject: Sticky Note Date: 8/28/2018 4:01:31 PM
It is explained in the main texts that the ACI is a unitless value. We edited the explanation to make it clearer and repeated the explanation in the figure caption in the revised manuscript. Please also pay attention that in the revised manuscript, we choose a volcanically quiescent year as the 'reference state' and regenerate this figure.Now is the new Fig. 6 in the revised manuscript.

Atmos. Chem. Phys. Discuss., https://doi.org/10.5194/acp-2018-332
Manuscript under review for journal Atmos. Chem. Phys.
Discussion started: 22 May 2018
© Author(s) 2018. CC BY 4.0 License.

Atmospheric Chemistry and Physics Discussions

latitude and 1 km in altitude. The red triangle denotes the latitude of the Merapi. Please see title of each figure for the time period covered.

This page contains no comments

Atmos. Chem. Phys. Discuss., https://doi.org/10.5194/acp-2018-332
Manuscript under review for journal Atmos. Chem. Phys.
Discussion started: 22 May 2018
© Author(s) 2018. CC BY 4.0 License.

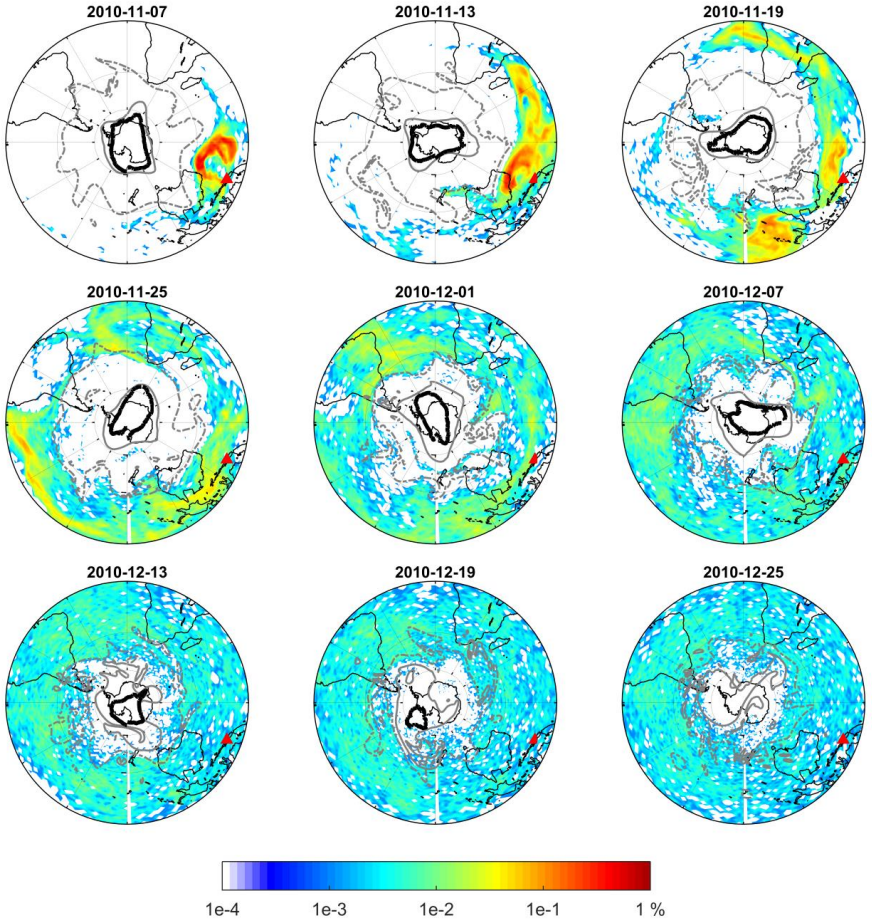

Figure 8: Percentage (%) of air parcels between the isentropic surfaces of 350 and 480 K in proportion to the total number of air parcels initialized in the Lagrangian transport simulation, at 12:00 UTC on selected dates. Results are binned every 2 °in longitude and 1 ° in latitude. The black contour indicates OMI daily mean ozone column density of 120 DU. 2V contours marked with gray dashed and solid lines show transport boundaries on the 350 and 480 K isentropic surfaces respectively (Kunz et al., 2015). The red triangle denotes the location of Mount Merapi

Page: 32

Number: 1 Author: Subject: Highlight Date: 5/31/2018 10:41:02 PM
Is it higher or lower inside the contour?

Author: Administrator Subject: Sticky Note Date: 6/3/2018 12:44:37 PM
220 DU contour is the boundary of the Antarctic ozone hole. The ozone column density is lower inside of the contour than outside of the contour.

Number: 2 Author: Subject: Highlight Date: 5/31/2018 10:40:05 PM
explain the units, and why these units correspond to transport boundaries.

Author: Administrator Subject: Sticky Note Date: 6/3/2018 12:47:11 PM
It is described in Sect. 3.4. We explain it with further details in the revised manuscript.

Atmos. Chem. Phys. Discuss., https://doi.org/10.5194/acp-2018-332
Manuscript under review for journal Atmos. Chem. Phys.
Discussion started: 22 May 2018
© Author(s) 2018. CC BY 4.0 License.

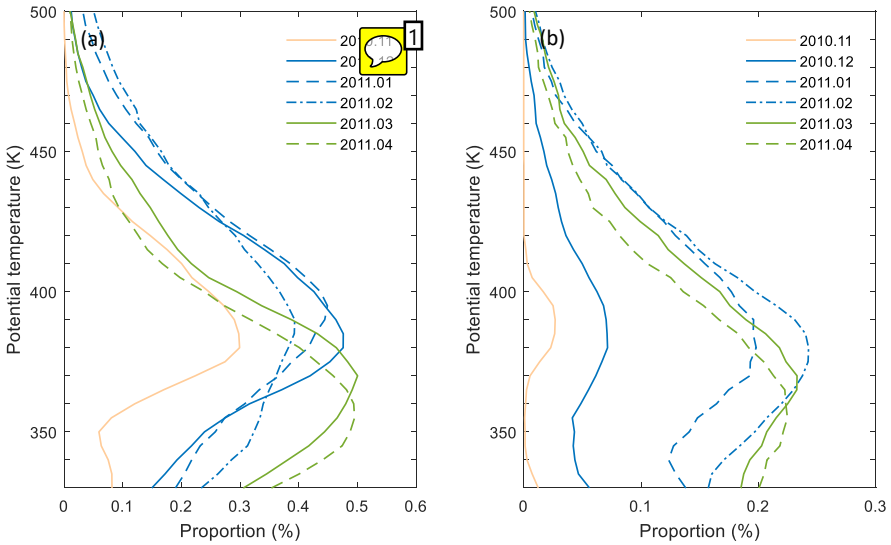

Figure 9: (a) Proportion (%) of the air parcels poleward of the PV-based transport boundaries at the end of each month; (b) proportion (%) of the air parcels south of 60 ℃S.

Page: 33

Number: 1 Author: Subject: Sticky Note Date: 5/31/2018 10:42:15 PM
What does this notation mean?

Author: Administrator Subject: Sticky Note Date: 6/3/2018 1:12:07 PM
It indicates the year and month. For example, 2010.11 indicates November 2011. To avoid the ambiguity, we replace it with Nov 2011 in the revised paper.

Atmos. Chem. Phys. Discuss., https://doi.org/10.5194/acp-2018-332
Manuscript under review for journal Atmos. Chem. Phys.
Discussion started: 22 May 2018
© Author(s) 2018. CC BY 4.0 License.

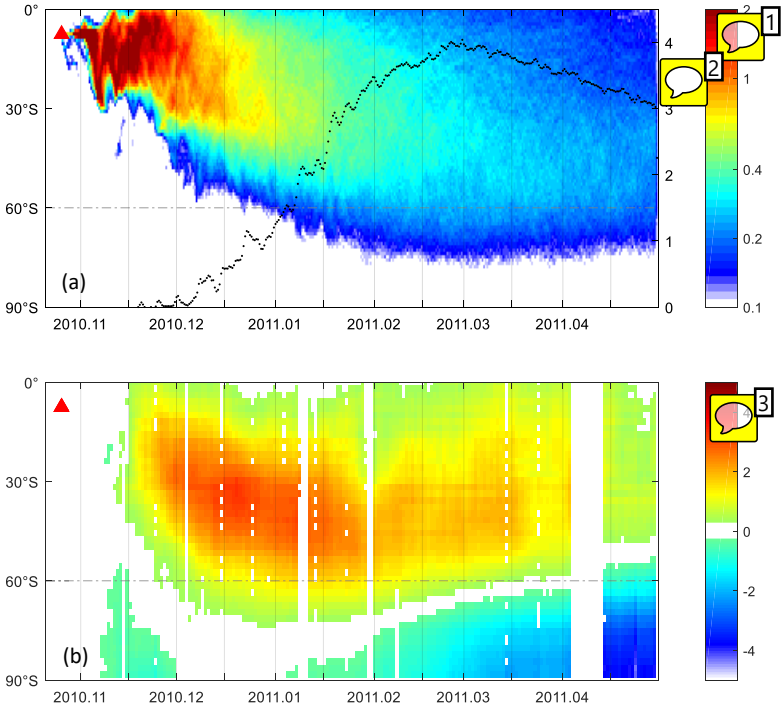

Figure 10: (a) Percentage (%) of air parcels between 350 and 480 K from MPTRAC simulations (shading, only percentages larger than 0.1% are shown; bin size: 12h and 1 ° in latitude), overlapped with proportion (%) of air parcels south of 60 °S (black dots); (b) Change of measured aerosol load between 350 and 480 K. 4 positive/negative values indicate increase/decrease of aerosol (bin size: 24h and 1 ° in latitude). The red triangle denotes the time and latitude of the Merapi eruption

Page: 34

Number: 1 Author: Subject: Sticky Note Date: 5/31/2018 10:46:31 PM
color scale needs label of variable and units.

Author: Administrator Subject: Sticky Note Date: 6/2/2018 5:53:27 PM
fixed

Number: 2 Author: Subject: Sticky Note Date: 5/31/2018 10:46:07 PM
axis needs label of variable and units.

Author: Administrator Subject: Sticky Note Date: 6/2/2018 5:56:00 PM
fixed

Number: 3 Author: Subject: Sticky Note Date: 5/31/2018 10:48:52 PM
color scale needs label of variable and units.

Author: Administrator Subject: Sticky Note Date: 6/2/2018 5:56:06 PM
fixed

Number: 4 Author: Subject: Highlight Date: 6/2/2018 5:36:42 PM
DON'T USE THIS CONFUSING CONSTRUCTION. WRITE IT OUT: Positive values indicate increase and negative values indicate decrease

Author: Administrator Subject: Sticky Note Date: 6/2/2018 5:36:19 PM
fixed

Long-range transport of volcanic aerosol from the 2010 Merapi tropical eruption to Antarctica

Xue Wu[1,2], Sabine Griessbach[1], Lars Hoffmann[1]

[1]Jülich Supercomputing Centre, Forschungszentrum Jülich, Jülich, Germany
[2]Key Laboratory of Middle Atmosphere and Global Environment Observation, Institute of Atmospheric Physics, Chinese Academy of Sciences, Beijing, China

Correspondence to: Xue Wu (xu.wu@fz-juelich.de)

Abstract

Volcanic sulfate aerosol is an important source of sulfur for Antarctica where other local sources of sulfur are rare. Mid- and high latitude volcanic eruptions can directly influence the aerosol budget of the polar stratosphere. However, tropical eruptions can also enhance polar aerosol load following long-range transport. In the present work, we analyze the volcanic plume of a tropical eruption, Mount Merapi in October 2010, and investigate the transport pathway of the volcanic aerosol from the tropical tropopause layer (TTL) to the lower stratosphere over Antarctica. We use the Lagrangian particle dispersion model Massive-Parallel Trajectory Calculations (MPTRAC) and Atmospheric Infrared Sounder (AIRS) SO_2 measurements to reconstruct the altitude-resolved SO_2 injection time series during the explosive eruption period and simulate the transport of the volcanic plume using the MPTRAC model. AIRS SO_2 and aerosol measurements, the aerosol-cloud-index values provided by Michelson Interferometer for Passive Atmospheric Sounding (MIPAS) are used to verify and complement the simulations. ~~We investigate the pathway and transport efficiency of the volcanic aerosol from the tropical tropopause layer (TTL) to the lower stratosphere over Antarctica. We first estimated the time- and height-resolved SO_2 injection time series over Mount Merapi during the explosive eruption using the AIRS SO_2 observations and a backward trajectory approach. Then the SO_2 injections were~~ are ~~tracked for up to 6 months using the MPTRAC model.~~ The Lagrangian transport simulation of the volcanic plume is~~was~~ compared with~~to~~ MIPAS aerosol measurements and show~~ed~~ good agreement. Both ~~of~~ the simulations and the observations presented in this study suggest that ~~aerosols of the volcanic plume~~ volcanic plumes from the Merapi eruption was transported to the south of 60 °S one month after the eruption and even further to Antarctica in the following months. This relatively fast meridional transport of volcanic aerosol was mainly driven by quasi-horizontal mixing from the TTL to the extratropical lower stratosphere and the most of the quasi-horizontal mixing occurred between the isentropic surfaces of 360 to 430 K.~~, which was facilitated by the weakening of the subtropical jet~~

~~during the seasonal transition from austral spring to summer and linked to the westerly phase of the quasi-biennial oscillation (QBO).~~ When the plume went to Southern Hemisphere high latitudes, the polar vortex was displaced from the ~~south pole~~South Pole, so that the volcanic plume was carried to the ~~south pole~~South Pole without penetrating the polar vortex. ~~Based on the model results, the most efficient pathway for the quasi-horizontal mixing was in between the isentropic surfaces of 360 and 430 K.~~ Although only 4% of the sulfur injected by the Merapi eruption~~initial SO_2 load~~ was transported into the lower stratosphere south of 60 °S, the Merapi eruption contributed up to 8800 tons of sulfur to the Antarctic lower stratosphere. This indicates that the long-range transport under favorable meteorological conditions enables a moderate tropical volcanic eruption~~s~~ to be an important remote source of sulfur for the Antarctic stratosphere.

1 Introduction

Over the past two decades, multiple volcanic eruptions injected sulfur into the upper troposphere and lower stratosphere, which has been the dominant source of the stratospheric sulfate aerosol load (Vernier et al., 2011), preventing the background level from other sources ever being seen (Solomon et al., 2011). Stratospheric sulfate aerosol mainly reflects solar radiation and absorbs infrared radiation, causing cooling of the troposphere and heating of the stratosphere. ~~It contributes to the largest uncertainties to estimates and interpretations of the Earth's changing energy budget (Boucher et al., 2013).by modulating the stratospheric and tropospheric temperature it has an impact on stratospheric dynamics, e. g. it can lead to dramatic phase changes of the quasi-biennial oscillation (Aquila et al., 2014) and alter the spatiotemporal characteristics of the El Niño Southern Oscillation (ENSO) on both short (few years) and long (decades) timescales (Pausata et al., 2015).~~Stratospheric sulfate aerosol also has an impact on chemical processes in the lower stratosphere (Jäger and Wege, 1990; Solomon et al., 1993), in particular on polar ozone depletion (e.g. McCormick et al., 1982; Solomon et al., 1986, 1999, 2016; Portmann et al., 1996; Tilmes et al., 2008; Drdla and Müller, 2012~~; Solomon et al., 2016~~). The presence of H_2SO_4 in the polar stratosphere in combination with cold temperatures facilitates the formation of polar stratospheric clouds (PSCs), which increase heterogeneous ozone depletion chemistry (Solomon et al., 1999; Zuev et al., 2015). Recent healing of Antarctic ozone depletion was constantly disturbed by moderate volcanic eruptions (Solomon et al., 2016). Mid- and high latitude explosive volcanic eruptions may directly influence the polar stratosphere and may have an effect on ozone depletion in the next austral spring. For example, the aerosol plume from the Calbuco eruption in

2015, including various volcanic gases, penetrated the polar vortex and caused an Antarctic ozone hole with the largest daily averaged size on record in October 2015 (Solomon et al., 2016; Ivy et al., 2017; Stone et al., 2017).

Usually, Antarctica is relatively free of local aerosol sources, but ~~aerosols~~aerosol from low latitudes can reach Antarctica through long-range transport (Sand et al., 2017). ~~Some~~ Most of the sulfate found in ~~the~~ ice cores can be attributed to volcanic eruptions (Mazzera et al., 2001; Gao et al., 2007; Sigl et al., 2015). Measurements of enhanced aerosol in the lower Antarctic stratosphere right above the tropopause were made in October/November 1983, 1984 and 1985. These enhanced aerosol number concentrations were attributed to aerosol transported to Antarctica from the eruption of the tropical volcano El Chichón ~~Chichon~~ in 1982 (Hofman and Rosen, 1985; Hofmann et al., 1988). ~~Tropical volcanic eruptions can also enhance polar aerosols by long-range transport.~~ Model results indicated that numerous moderate eruptions affected ozone distributions over Antarctica, including the Merapi tropical eruption in October 2010 (Solomon et al., 2016). However, due to the limit of spatial and temporal resolution of satellite data and in-situ observations, it is difficult to investigate transport process as well as the influence of the location of the eruption, the plume height and the background meteorological conditions. Thus the transport mechanism is not well represented in present global climate models and the uncertainties of the modeled AOD in polar regions are large (Sand et al., 2017).

~~The~~ Mount Merapi (7.5 °S, 110.4 °E, elevation: 2930 m) is an active stratovolcano located in Central Java, Indonesia. Merapi has a long record of eruptive activities. The most recent large eruption with a volcanic explosivity index ~~(VEI)~~ of 4 occurred between 26 October and 7 November 2010 (Pallister et al., 2013), with SO_2 emission rates being a few orders of magnitude higher than previous eruptions. Following the Merapi eruption in 2010, evidence of poleward transport of sulfate aerosol towards the Southern Hemisphere high latitudes was found in time series of aerosol measurements by the Michelson Interferometer for Passive Atmospheric Sounding (MIPAS) (Günther et al., 2018) and Cloud-Aerosol Lidar with Orthogonal Polarization (CALIOP) (Khaykin et al., 2017; Friberg et al., 2018) .

There are three main ways for transport out of the tropical tropopause layer (TTL): the deep and shallow branches of the Brewer-Dobson circulation (BDC) and horizontal mixing (Vogel et al., 2011). There is considerable year-to-year seasonal variability in the amount of irreversible transport from the tropics to high latitudes, which is related to the phase of the quasi-biennial oscillation (QBO) and the state of the polar vortex (Olsen et al., 2010). The BDC plays a large role in determining the distributions of many constituents in the extratropical lower stratosphere. The faster quasi-horizontal transport between the tropics and polar regions also significantly contributes to determining these distributions. The efficiency

of transporting constituents quasi-horizontally depends on wave breaking patterns and varies with the time of the year (Toohey et al., 2011~~Kravitz and Robock, 2011~~; Wu et al., 2017). Better knowledge of the transport pathways and an accurate representation of volcanic sulfur injections into the upper troposphere and lower stratosphere (UTLS) are key elements for estimating the global stratospheric aerosol budget, the cooling effects and the ozone loss linked to volcanic activity.

The aim of the present study is to~~–~~ reveal the transport process and the influence of meteorological conditions by combining satellite observations with model simulations in a case study. We investigate the quasi-horizontal transport by tracing the volcanic plume of the Merapi eruption from the tropics to Antarctica and quantifying its contribution to the sulfur load in the Antarctic lower stratosphere. In Sect. 2, the new Atmospheric Infrared Sounder (AIRS) SO_2 measurements (Hoffmann et al., 2014), the MIPAS aerosol measurements (Griessbach et al., 2016) and the method for reconstructing the SO_2 injection time series of the Merapi eruption are introduced. In Sect. 3 the results are presented: first, the reconstructed time series of the Merapi eruption is discussed; second, the dispersion of the Merapi plume is investigated using long Lagrangian forward trajectories initialized with the reconstructed SO_2 time series; third, the simulation results are compared with MIPAS aerosol measurements and the plume dispersion is investigated using MIPAS aerosol detections. In Sect.4 the results are discussed and the conclusions are given in Sect. 5.

2 Satellite data, model and method

2.1 MIPAS ~~instrument and~~ aerosol measurements

MIPAS (Fischer et al., 2008) is an infrared limb emission spectrometer aboard the European Space Agency's (ESA's) Envisat, which provided nearly 10 years of measurements from July 2002 to April 2012. MIPAS spectral measurements cover the wavelength range from 4.15 to 14.6 microns. The vertical coverage of MIPAS nominal measurement mode during the optimized resolution phase from January 2005 to April 2012 was 7–72 km. The field of view of MIPAS was about 3 km×30 km (vertically×horizontally) at the tangent point. The extent of the measurement volume along the line of sight was about 300 km, and the horizontal distance between two adjacent limb scans was about 500 km. On each day, ~14 orbits with ~90 profiles per orbit were measured. From January 2005 to April 2012, the vertical sampling grid spacing between the tangent altitudes was 1.5 km in the UTLS and 3 km at altitudes above~~The vertical sampling was 1.5 km in the UTLS and 3 km above the UTLS~~. In 2010 and 2011, MIPAS measured for 4 days in nominal mode followed alternately by one day in middle

atmosphere mode or upper atmosphere mode. In this study, we focussed on measurements in the nominal mode.

For the aerosol detections, we used the MIPAS altitude-resolved aerosol-cloud-index (ACI) as introduced by Griessbach et al. (2016) to compare with the MPTRAC model simulations and to analyze the poleward transport of the Merapi volcanic plume.

ACI is the maximum value of the cloud index (CI) and aerosol index (AI):

$$\mathrm{ACI} = \max(\mathrm{CI}; \mathrm{AI}), \qquad (1)$$

The CI is an established method to detect clouds and aerosol with MIPAS. The CI is the ratio between the mean radiances around the 792 cm^{-1}, where a CO_2 line is located and the atmospheric window region around 833 cm^{-1} (Spang et al., 2001):

$$\mathrm{CI} = \frac{\bar{I}_1([788.25,796.25\ \mathrm{cm}^{-1}])}{\bar{I}_2([832.31,834.37\ \mathrm{cm}^{-1}])}, \qquad (2)$$

where $\bar{I}_1$ and $\bar{I}_2$ are the mean radiances of each window. The AI is defined as the ratio between the mean radiance around the 792 cm^{-1} CO_2 band and the atmospheric window region between 960 and 961 cm^{-1}:

$$\mathrm{AI} = \frac{\bar{I}_1([788.25,796.25\ \mathrm{cm}^{-1}])}{\bar{I}_3([960.00,961.00\ \mathrm{cm}^{-1}])}, \qquad (3)$$

where $\bar{I}_1$ and $\bar{I}_3$ are the mean radiance of each window.

The ACI is a continuous unitless value. Small ACI values indicate a high cloud or aerosol particle load and large values indicate a smaller cloud or aerosol particle load. For the CI, Sembhi et al. (2012) defined a set of variable (latitude, altitude and season) thresholds to discriminate between clear and cloudy air. The most advanced set of altitude and latitude dependent thresholds allows for the detection of aerosol and clouds with infrared extinction coefficients larger than 10^{-5} km^{-1}. For the ACI, a comparable sensitivity is achieved when using a fixed threshold value of 7 (Griessbach et al. 2016). Variations in the background aerosol are also visible with larger ACI values.

To remove ice clouds and volcanic ash from the MIPAS aerosol measurements, we first separated the data into clear air (ACI>7) and cloudy air (ACI<=7). Then we applied the ice cloud filter (Griessbach et al., 2016) and the volcanic ash and mineral dust filter (Griessbach et al., 2014) to the cloudy part and removed all ice or ash detections. However, since the ice and ash cloud filters are not sensitive to non-ice PSCs, the resulting aerosol retrieval results still contain non-ice PSCs (supercooled ternary solutions and nitric acid trihydrate). We keep the non-ice PSCs in the MIPAS retrieval results in this study to show the temporal and spatial extent of the PSCs, when and where the identification of volcanic is not possible.

~~Small ACI values indicate large aerosol extinction coefficients and vice versa. As ice clouds usually have extinction coefficients larger than 1×10^{-4} km^{-1}, we applied a brightness temperature correlation method, that serves as an ice cloud filter, to all MIPAS spectra with ACI<7 (Griessbach et al., 2016) to remove the ice clouds from the data set. The resulting aerosol product is be sensitive to different types of aerosol, in particular, volcanic ash, sulfate aerosol, mineral dust, as well as non-ice PSCs.~~

2.2 AIRS

AIRS (Aumann et al., 2003) is an infrared nadir sounder with across-track scanning capabilities aboard the National Aeronautics and Space Administration's (NASA's) Aqua satellite. Aqua was launched in 2002 and operates in a nearly polar Sun-synchronous orbit at about 710 km with a period of 98 min. AIRS provides nearly continuous measurement coverage with 14.5 orbits per day and with a swath width of 1780 km it covers the globe almost twice a day. The AIRS footprint size is 13.5 km × 13.5 km at nadir and 41 km × 21.4 km for the outermost scan angles respectively. The along-track distance between two adjacent scans is 18 km. The AIRS measurements provide good horizontal resolution and make it ideal for observing the fine filamentary structures of volcanic SO_2 plumes.

In this study, we use an optimized SO_2 index (SI, unit: K) to estimate the amount of SO_2 injected into the atmosphere by the Merapi eruption in 2010. The SI is defined as the brightness temperature differences in the 7.3 μm SO_2 waveband.

$$SI = BT\left(1412.87 cm^{-1}\right) - BT\left(1371.52\ cm^{-1}\right), \quad (1)$$

where BT is the brightness temperature measured at wavenumber ν. This SI is more sensitive to low concentrations and performs better on suppressing background interfering signals than the SI provided in the AIRS operational data products. It is an improvement of the SI definition given by Hoffmann et al. (2014) by means of a better choice of the background channel (selecting 1412.87 cm^{-1} rather than 1407.2 cm^{-1}). The SI increases with increasing SO_2 column density and it is most sensitive to SO_2 at altitudes above 3-5 km. SO_2 injections into the lower troposphere are usually not detectable in the infrared spectral region because the atmosphere gets opaque due to the water vapor continuum. A detection threshold of 1 K was used in this study to identify the Merapi SO_2 injections. AIRS detected the Merapi SO_2 cloud from 3 November to 15 November 2010.

2.3 MPTRAC model and reconstruction of the volcanic SO_2 injection time series of the Merapi eruption

In this study, we use the highly scalable Massive-Parallel Trajectory Calculations (MPTRAC) ~~MPTRAC model~~ to investigate the volcanic eruption event. In the MPTRAC model, air parcel trajectories are calculated based on numerical integration using wind fields from global meteorological reanalyses (Hoffmann et al., 2016; Rößler et al., 2018). The MPTRAC model can be driven by reanalyses, e.g., ERA-Interim, Modern-Era Retrospective Analysis for Research and Applications (MERRA) and National Centers for Environmental Prediction (NCEP)/National Center for Atmospheric Research (NCAR). Hoffmann et al. (2016) showed that ERA-interim data provides the best trade-off between accuracy and computing time. So in this study, our calculations are based on ERA-interim data.

Diffusion is modeled by uncorrelated Gaussian random displacements of the air parcels with zero mean and standard deviations $\sigma_x = \sqrt{D_x \Delta t}$ (horizontally) and $\sigma_z = \sqrt{D_z \Delta t}$ (vertically). D_x and D_z are the horizontal and vertical diffusivities respectively, and Δt is the time step for the trajectory calculations. For the Merapi simulation, D_x and D_z were set to 50 $m^2 s^{-1}$ and 0 $m^2 s^{-1}$ in the troposphere and 0 $m^2 s^{-1}$ and 0.1 $m^2 s^{-1}$ in the stratosphere, respectively. In addition, sub-grid scale wind fluctuations, which are particularly important for long-range simulations, are simulated by a Markov model (Stohl et al., 2005; Hoffmann et al., 2016). Loss processes of chemical species, SO_2 in our case, are simulated based on an exponential decay of the mass assigned to each air parcel. In the stratosphere, a constant half lifetime of 7 days was assumed for SO_2. Considering that the Merapi eruption occurred in the humid tropics with a high concentration of hydroxyl radical, a half lifetime of 2.5 days was assumed for the troposphere.

To estimate the time- and altitude-resolved SO_2 injections, we follow the approach of Hoffmann et al. (2016) and Wu et al. (2017) and use backward trajectories calculated with the MPTRAC model together with AIRS SO_2 measurements. Measurements from 3 to 7 November 2010 were used to estimate the SO_2 injection during the explosive eruption. Since the AIRS measurements do not provide altitude information, we established a column of air parcels at each AIRS SO_2 detection. The vertical range of the column was set to 0–25 km, covering the possible vertical dispersion range of the SO_2 plume in the first few days. The AIRS footprint size varies between 14 and 41 km, hence in the horizontal direction, we chose an average of 30 km as the full width at half maximum ~~(FWHM)~~ for the Gaussian scatter of the air parcels. In our simulations, a fixed total number of 100,000 air parcels was assigned to all air columns and the number of air parcels in each column was scaled linearly proportional to the SO_2 index.

Then backward trajectories were calculated for all air parcels, and trajectories that were at least 2 days but no more than 5 days long and that passed the volcano domain were recorded as emissions of Merapi. The volcano domain was defined by means of a search radius of 75 km around the location of the Merapi and 0–20 km in the vertical direction, covering all possible injection heights. Sensitivity experiments have been conducted to optimize these pre-assigned parameters to obtain the best simulation results. Our estimates of the Merapi SO_2 injection are shown in Sect. 3.

Starting with the reconstructed altitude-resolved SO_2 injection time series, the transport of the Merapi plume is simulated for 6 months. The trajectory calculations are driven by the ERA–Interim data (Dee et al., 2011) interpolated on a $1° \times 1°$ horizontal grid on 60 model levels with the vertical range extending from the surface to 0.1 hPa. The ERA–Interim data are provided at 00, 06, 12 and 18 UTC. Outputs of model simulations are given every 3 hours at 00, 03, 06, 09, 12, 15, 18 and 21 UTC. The impact of different meteorological analyses on MPTRAC simulations was assessed by Hoffmann et al. (2016, 2017). In both studies the ERA–Interim data showed good performance.

3 Results

3.1 Meteorological background conditions in Antarctica

The Merapi eruption in October 2010 occurred during the seasonal transition from austral spring to summer when the polar vortex typically weakens and the ozone hole shrinks. The poleward transport from the tropics to the polar region is known to be modulated by the phase of the QBO and the state of the polar vortex. Just before the Merapi eruption in 2010, the QBO switched from the easterly phase to the westerly phase. The westerly phase of the QBO promotes meridional transport from the tropics to subtropics, especially into the winter hemisphere (O'Sullivan and Dunkerton, 1997; Shuckburgh et al., 2001; Jäger, 2005). However, it also results in zonal wind acceleration at the high latitudes (Holton and Tan, 1980; Watson and Gray, 2014) and a less dynamically disturbed polar vortex (Baldwin and Dunkerton, 1999; Anstey and Shepherd, 2014), which will make it less possible for air parcels to penetrate the polar vortex.

Figure 1 depicts the meteorological conditions at the polar lower stratosphere (150hPa, ~12km) after the eruption. ~~As depicted in Fig. 1, the meteorological conditions at the polar lower stratosphere (150hPa, ~12km) after the eruption deviated from the climatological mean.~~ The minimum temperature south of 50 °S (Fig. 1a) was much lower than the climatological mean during mid-November to mid-December but still higher than the low temperature necessary for the existence of PSCs. The polar mean

temperature in Fig. 1b, defined as the temperature averaged over latitudes south of 60 ℃S, stayed lower than the climatological mean from November 2010 until February 2011. Corresponding to the low temperatures, the average zonal wind speed at 60 ℃S (Fig. 1c) was significantly larger than the climatological mean value from November 2010 to mid-January 2011. The eddy heat flux in Fig. 1d is the product of meridional wind departures and temperature departures from the respective zonal mean values. A more negative value of the eddy heat flux indicates that wave systems are propagating into the stratosphere and are warming the polar region (Edmon et al., 1980; Newman and Nash, 2000). There is a strong anticorrelation between temperature and the 45-day average of the eddy heat flux lagged prior to the temperature. Compared with the climatological mean state, the polar vortex was more disturbed during mid-July to end of August, but from mid-October to late November, the heat flux was much smaller than the long-term average, which meant a reduction in dynamical disturbances. Considering the temperature, the subpolar wind speed and the heat flux, the polar vortex was colder and stronger in November and early December 2010 than it was at the same time in other years (see Fig. 1e). Consistent with the large wind speed and low temperature, the polar vortex was stable after the Merapi eruption until early December 2010. Afterwards, it shrunk abruptly and was destructed in by mid-January 2011. In accordance with the strength of the polar vortex, in November and early December 2010 the ozone hole area in Fig. 1f, defined as the region of ozone values below 220 Dobson Units (DU) located south of 40 ℃S, was larger than the climatological mean. Meanwhile, the low polar mean temperature and stable polar vortex resulted in a long-lasting ozone hole, which disappeared in the last week of December. The polar vortex broke down by mid-January 2011 when the subpolar wind speed decreased below 15 m/s (Fig. 1c).

~~The poleward transport from the tropics to the polar region is known to be modulated by the phase of the quasi-biennial oscillation (QBO) and the state of the polar vortex itself: Fig. 4f shows that just before the Merapi eruption in 2010, the QBO switched from easterly phase to westerly phase. The westerly phase of the QBO promotes meridional transport from the tropics to subtropics, especially into the winter hemisphere (O'Sullivan and Dunkerton, 1997; Shuckburgh et al., 2001; Jäger, 2005). However, it also results in zonal wind acceleration at the high latitudes (Watson and Gray, 2014; Holton and Tan, 1980) and a less dynamically disturbed polar vortex (Anstey and Shepherd, 2014; Baldwin and Dunkerton, 1999), which will make it less possible for air parcels to penetrate the polar vortex.~~

3.2 Merapi eruption and SO_2 injection time series

According to the chronology of the Merapi eruption that combined satellite observations from AIRS, the Infrared Atmospheric Sounding Interferometer (IASI), the Ozone Monitoring Instrument (OMI) and a limited number of Ground-based ultra-violet Differential Optical Absorption Spectroscopy (DOAS) measurements (Surono et al., 2012), the explosive eruption first occurred between 10:00 and 12:00 UTC on 26 October and this eruption generated ~~a~~an ash plume that reached 12 km altitude. A period of relatively small explosive eruptions continued from 26 October to 31 October. ~~During the initial period of the dome growth (1–3 November), the level of SO_2 degassing was relatively low compared with the SO_2 degassing before 1 November.~~ On 3 November, the eruptive intensity increased again accompanied by much stronger degassing and a series of explosions. The intermittent explosive eruptions occurred during 4–5 November with the climactic eruption on 4 November, producing an ash column that reached up to 17 km altitude. From 6 November, explosive activity decreased slowly and the degassing declined.

Figure 2 shows the time- and altitude-resolved SO_2 injections of the Merapi eruption retrieved using the AIRS SO_2 index data and the backward-trajectory approach. It agrees well with the chronology of the Merapi eruption as outlined by Surono et al. (2012). SO_2 was injected into altitudes below 8 km during the initial explosive eruptions on 26–30 October. Starting from 31 October the plume reached up to 12 km. During 1–2 November the SO_2 injections into altitudes below 12 km continued but the mass was less than the mass at the initial phase. On 3 November the intensity increased again and peaked on 4 November. Before 3 November the reconstruction indicates a minor fraction of SO_2 right above the tropopause. The SO_2 above the tropopause is not reported in the study Surono et al. (2012), but is quite robust in our simulations. Further, CALIOP profiles from 27 October 2010 to 10 November 2010 show that some dust appeared at the height from about 14 to 18 km around Mount Merapi on 2, 3, 5 November 2010, and between 3 and 17 km on 6 November 2010. It could be a fraction of volcanic plume elevated by the updraft in the convection associated with the tropical storm Anggrek. The center of the tropical storm Anggrek was on the Indian ocean about 1000 km southwest of the Mount Merapi. The SO_2 mass above the tropopause is very small compared with the total SO_2 mass.

To study the long-range transport of the Merapi plume, we initialized 100,000 air parcels as the SO_2 injection time series shown in Fig. 2. A total SO_2 mass of 0.44 Tg is assigned to these air parcels as provided in Surono et al. (2012). Then the trajectories are calculated forward for 6 months. Here, we only considered the plume in the upper troposphere and stratosphere where the lifetime of both SO_2 and

sulfate aerosol is longer than their lifetime in the lower troposphere. Further, the SO_2 was converted into sulfate aerosol within a few weeks (von Glasow et al., 2009; also confirmed by the AIRS SO_2 and MIPAS aerosol data), and we assumed that the sulfate aerosol remained collocated with the SO_2 plume~~, i.e., the sedimentation of small sulfate aerosol particles was negligible for the timescale considered~~.

Figure 3 shows the evolution of the simulated Merapi plume and compares the plume altitudes to the aerosol top altitudes measured by MIPAS between 7 and 23 November. Immediately after the eruption, the majority of the plume moved towards the southwest and was entrained by the circulation of the tropical storm Anggrek. After ~~the~~ Anggrek weakened and dissipated, the majority of the plume parcels in the upper troposphere moved eastward and those in the lower stratosphere moved westward. In general, the altitudes of the simulated plume agree with the MIPAS measurements. The remaining discrepancies of air parcel altitudes being higher than the altitudes of MIPAS aerosol detections can be attributed to the fact that the MIPAS tends to underestimate aerosol top cloud altitudes, which is about 0.9 km in case of low extinction aerosol layers and can reach down to 4.5 km in case of broken cloud conditions (Höpfner et al., 2009).

3.3 Lagrangian simulation and satellite observation of the transport of the Merapi plume

The early plume evolution until about one month after the initial eruption is shown on the maps in Fig. 3 together with MIPAS measurements of volcanic aerosol (only aerosol detections with ACI<7 are shown). Within about one month after the initial eruption, the plume is nearly entirely transported around the globe in the tropics, moving west at altitudes of about 17 km. The lower part of the plume, below about 17 km is transported south-eastward and reaches latitudes south of 30 °S by mid-November. The simulated long-term transport of the Merapi plume is illustrated in Fig. ~~5~~4, showing the proportion of air parcels reaching a latitude-altitude bin every half a month. ~~To verify the model results, the poleward transport of aerosols as detected by MIPAS is shown in Fig. 6. For comparison, only simulation results above the minimum altitude of MIPAS aerosol detections in Fig. 6 are shown in Fig. 5. In this study, we only focus on aerosol distributions in the upper troposphere and stratosphere, where sulfate aerosol has a longer lifetime and potential climate impacts.~~

The simulation results show that during the first month after the eruption (Fig. ~~4~~5a–b), the majority of the plume was transported southward roughly along the isentropic surfaces. The most significant pathway is above the core of the subtropical jet in the Southern Hemisphere. However, because of the transport barrier of the polar jet during austral spring, the plume was confined to the north of 60 °S. In December 2010 (Fig. ~~4~~5c–d), a larger fraction of the plume was transported southward above the

subtropical jet core and deep into the polar region south of 60 ℃S as the polar jet broke down. ~~Till~~ Until the end of January 2011, the majority of the plume entered the mid- and high latitudes in the Southern Hemisphere. Substantial quasi-horizontal poleward transport from the TTL towards the extratropical lowermost stratosphere (LMS)~~LMS~~ in Antarctica was found from November 2010 to February 2011 (Fig. 4~~5~~a–h), approximately between 350 and 480 K (~10–20 km). In March 2011(Fig. 4i–j~~5i–l~~), the proportion of the plume that went across 60 ℃S stopped increasing and the maxima of the proportion descended below 380 K. Besides this transport towards Antarctica, a slow upward transport could also be seen. The top of the simulated plume was below the 480 K isentropic surface at around 18 km in Fig. 4a and then the top of the plume went up to 25 km five months later in Fig. 4j. This slow upward transport was mainly located in the tropics and can be attributed to the tropical upwelling.

MIPAS aerosol detections (ACI values) are used to compare with the simulations. Figure 5~~1~~ displays the time-latitude section of the median value of the MIPAS ACI within the vertical range of 12 and 18 km from January 2005 to April 2012, covering the ~~tropical tropopause layer (TTL)~~TTL and the ~~extratropical lowermost stratosphere (LMS)~~LMS. Only ACI values from 4 to 8 are shown in Fig.5. The MIPAS data show all the key events that contributed to the aerosol load in the UTLS, i.e., moderate volcanic eruptions from 2005 to 2012 and one large bushfire in 2009, as well as the subsequent dispersion and change of aerosol load over time. The poleward transport of aerosol from the Merapi eruption in 2010, marked by the red triangle in Fig. 5, caused the most long-lasting aerosol signals in the Southern Hemisphere mid- and high latitudes. The small ACI values in the winter months of both hemispheres are attributed to the non-ice PSCs.

~~The poleward transport in the MPTRAC simulations was confirmed by MIPAS aerosol detections. MIPAS ACI zonal median values are shown in Fig. 6 for all MIPAS measurements after filtering out ice clouds. Small ACI values indicate a large aerosol load and large ACI values indicate clear air. As seen in Fig. 6, the locally confined aerosol plume from the Merapi eruption did not dominate the zonal median during the first half month after the eruption (Fig. 6a), but became evident between 350 and 380 K around the latitude of 7.5 ℃S by the end of November (Fig. 6b) as the plume was transported around the globe in the tropics. As shown in the MPTRAC simulations, the transport towards the northern mid- and high latitudes was suppressed by the strong subtropical jets. The transport of the volcanic plume towards Antarctica in the UTLS region was observed from December 2010 to February 2011 (Figs. 6c–h) consistent with the simulations. The MIPAS aerosol data also demonstrated the upward transport from the tropical upper troposphere to the stratosphere, which was observed after late January 2010.~~

~~The aerosol transported upward had increased the aerosol load in the tropical stratosphere reservoir compared to the aerosol load before the Merapi eruption.~~

~~Fig. 6 verified aerosol transport from the tropics to Antarctica and upward into the tropical stratosphere. However, before the eruption of Merapi, the aerosol load in the tropical stratosphere was already elevated by several small and moderate-size volcanic eruptions, namely the Sarychev Peak (12 Jun 2009), Nyamuragira (20 Jan 2010), Soufriere Hills (11 Feb 2010) and Pacaya (28 May 2010). In order to infer the increase of the aerosol load due to the eruption of Merapi from the MIPAS data, we calculated the median ACI in 1–4 November 2010 when there was no aerosol from the Merapi eruption, to define the "background" aerosol load and then remove this "background" from the median ACI in Fig. 6. The results shown in Fig.7 demonstrate the change of median ACIs in the tropics and southern hemisphere corresponding to the same time period as Fig. 6positive/negative values indicating an increase/decrease of aerosol load. No significant change was observed during the first half month after the eruption due to the zonal averaging degrading the aerosol signal (Fig. 7a). The largest increase first appeared in the upper troposphere directly above Mount Merapi (Fig. 7b) and then moved quasi-horizontally southward into the UTLS region to ~40 °S (Figs. 7c–f), consistent with what Figs. 5 and 6 showed. A relatively small but still significant increase of aerosol south of 60 °S in the tropopause region was found from January 2011 (Fig. 7e) and it lasted until mid- April 2011 (Fig. 7j). Six months after the eruption, the aerosol levels were still slightly elevated in the tropical upper troposphere above 350 K.~~ To show the change of aerosol load in the Southern Hemisphere due to the Merapi eruption, we first removed the seasonal cycle from the MIPAS aerosol data. Therefore, we selected a time period from November 2007 to March 2008 with no major SO_2 emission in the Southern Hemisphere UTLS (as shown in Fig. 5) as a "reference state". We calculated the biweekly median ACI between November 2010 and March 2011 and subtracted it from the biweekly ACI median of the "reference state". The results are shown in Fig. 6. Since in the MIPAS retrievals, small ACI values represent large aerosol extinction coefficients and large ACI values represent small aerosol extinction coefficients, in Fig. 6 the positive values indicate an increase of the aerosol load and negative values indicate a decrease of the aerosol load. Reference time periods from November 2003 to March 2004 and November 2005 to March 2006 were also tested and they all showed qualitatively comparable results.

In the first half of November, the zonal median (Fig. 6a) does not show a signal of the Merapi eruption, because during the initial time period, the plume was confined to longitudes around the volcano (see Fig. 3), and the MIPAS tracks did not always sample the maximum concentration, so the median ACI values are large (low concentration or clear air). In the second half of November, the plume was transported

zonally around the globe, and hence the largest aerosol increase appeared in the upper troposphere at the latitude of the Mount Merapi (Fig. 6b) and then moved quasi-horizontally southward into the UTLS region at ~30–40 °S (Figs. 6c–d), confirming the simulation result in Fig. 4c–d. The increase of the aerosol load south of 60 °S started to become prominent after December 2010, and the poleward movement is most obvious above the 350 K isentropic surface (Figs. 6e–h). The observations confirm the temporal and spatial characteristics of poleward movement of the aerosol in the simulation in Fig. 4. Later in March 2011, the enhanced aerosol load in the tropics phased out and the aerosol load maxima descended to around the 350 K isentropic surface.

However, the background aerosol level in the tropical upper troposphere and stratosphere is constantly disturbed by tropical and extratropical volcanic eruptions. The reference time period we chose (November 2007 to March 2008) is relatively free of large aerosol sources in the Southern Hemisphere, but the aerosol load in the tropical stratosphere is already elevated by previous volcanic eruptions, e.g., Soufriere Hills (May 2006), Tavurvur (October 2006), Piton de la Fournaise (April 2007), Jebel at Tair (September 2007). So the change of the aerosol load in Fig.6 underestimates the increase of aerosol load in the tropical stratosphere after the Merapi eruption. The slow upward transport in the tropics shown in Fig. 4 is about 7 km in five months. It is not visible in Fig. 6, but time series of the MIPAS measurements in the tropical stratosphere reveals a similar upward transport trend (see Fig. A1 in the appendix).

3.4 Quasi-horizontal transport from the tropics to Antarctica

~~As the results of the Lagrangian transport simulations with the MPTRAC model were comparable to the MIPAS observations (Sect. 3.3), it was possible not only to demonstrate the transport pathways but also to estimate the efficiency of the transport.~~ The MPTRAC simulations and the MIPAS measurements show the transport in~~on~~ the “surf zone” that reaches from the subtropics to high latitudes (Holton et al., 1995), where air masses are affected by both fast meridional transport and the slow BDC. The reconstructed emission time series in Fig. 2 and the MIPAS aerosol measurements in Figs. 3 and 6 show that the volcanic plume was injected into the TTL. Hence, the main transport pathway towards Antarctica is the quasi-horizontal mixing in the lower extratropical stratosphere between 350 and 480 K (see Fig. 4 and Fig. 6). Figure 7~~8~~ illustrates how the volcanic plume between 350 and 480 K approached Antarctica over time. Kunz et al. (2015) derived a climatology of potential vorticity (PV) streamer boundaries on isentropic surfaces between 320 and 500K using ERA-Interim reanalyses for the time

period from 1979 to 2011. This boundary is derived from the maximum product of the meridional PV gradient and zonal wind speed on isentropic surfaces, which identifies a PV contour that best represents the dynamical discontinuity on each isentropic surface. It can be used as an isentropic transport barrier and to determine the isentropic cross-barrier transport related to Rossby wave breaking (Haynes and Shuckburgh, 2000; Kunz et al., 2011a,b). In Fig. 7, gray dashed ~~and solid~~ lines mark PV boundaries on the 350 K isentropic surface. ~~These dynamically relevant PV contours represent horizontal transport barriers for air masses on the respective isentropic surface.~~ On isentropic surfaces below 380 K, the PV boundaries represent the dynamical discontinuity near the core of the subtropical jet stream. ~~and thus represent a transport barrier between the tropics and midlatitudes (Haynes and Shuckburgh, 2000; Kunz et al., 2011a,b).~~ Isentropic transport of air masses across these boundaries indicates exchange between the tropics and extratropics due to Rossby wave breaking. On isentropic surfaces above 400 K, PV boundaries represent a transport barrier in the lower stratosphere, in particular, due to the polar vortices in winter (Kunz et al., 2015). For comparison, we also show the 220 DU contour lines of ozone column density (black isolines in Fig. 7~~8~~), obtained from OMI on satellite Aura, indicating the ~~location~~ boundary and size of the ozone hole. The PV boundary on 480 K is in most cases collocated with the area of the ozone hole, showing that both quantities provide a consistent representation of the area of the polar vortex.

The Merapi volcanic plume first reached the ~~350 K~~ transport barrier on the 350 K isentropic surface in mid-November and went close to the ~~480 K~~ transport barrier on the 480 K isentropic surface in December. The long-lasting polar vortex prevented the volcanic plume from crossing the transport barrier at 480 K in early December. ~~, but~~But from mid-December, the polar vortex became more disturbed and displaced from the ~~south pole~~South Pole, resulting in a shrinking ozone hole. As mentioned in Sect.~~3.2~~3.1, the ozone hole broke down at the end of December 2010 and the polar vortex broke down by mid-January 2011.

The fraction of the volcanic plume that crosses the individual transport barriers or the latitude of 60 °S on each isentropic surface are shown in Fig. 8~~9~~. In both cases, the proportion increased from November 2010 to January 2011. In November and December 2010 the largest plume transport across the transport barriers occurred between the 360 and 430 K isentropic surface (Fig. 8~~9~~a), with a peak at 380–390 K. In January and February 2011 the peak was slightly elevated to 390–400 K. In November 2010, the volcanic plume did not cross the 480 K transport barrier of the polar vortex at high altitudes, especially above about 450 K. The high-latitude fraction increased from December 2010 to February 2011 as the weakening of the polar vortex made the transport barrier more permeable. In March and April 2011, the

total proportion decreased and the peak descended to 370 K in March and further to 360 K in April. The proportion of the volcanic plume south of 60 °S (Fig. 89b) increased slightly from November to December 2010, and then increased significantly from December 2010 to January and February 2011 at all altitudes as the polar vortex displaced and broke down. Finally, the transport to the south of 60 °S started to decrease in March 2011. From November 2010 to February 2011 the peak was around 370–400 K, but in March and April 2011 the peak resided around 350–370 K.

Figure 9a10 summarizes the simulated poleward transport of the volcanic plume between the isentropic surfaces of 350 and 480 K from November 2010 to March 2011 and the percentage of air parcels south of 60 °S. The percentage was calculated by dividing the number of SO_2 parcels between 350 and 480 K south of 60 °S by the total number of SO_2 parcels released for the forward trajectory simulation. Figure 9b demonstrates the change of aerosol load in the same vertical range for MIPAS aerosol detections. As in Sect. 3.3, we calculated the median ACI between November 2010 and March 2011 and subtracted it from the ACI median of the "reference state" between November 2007 and March 2008. ~~The zonally resolved fractions derived from the Lagrangian MPTRAC simulations and the fraction of air parcels south of 60 °S are shown in Fig. 10a. Figure 10b demonstrates the increasing and decreasing aerosol load in this vertical range for MIPAS aerosol detections relative to 1–4 November median (see Sect.3.3). The poleward transport trend in Fig. 10a is comparable to the poleward migration of the enhanced aerosol in Fig. 10b.~~ The simulations show that the plume reached 60 °S in December 2010. Correspondingly, the aerosol load south of 60 °S was elevated. The percentage fluctuated, but increased until the end of February 2011, with a maximum percentage of about 4%. A steep increase occurred from mid-December 2010 to end of January 2011, following the displacement and breakdown of the polar vortex. The elevated aerosol load south of 60 °S decreased from March 2011, and part of the plume descended to altitudes below 350 K as shown by Fig. 89b. The MIPAS aerosol measurements in Fig. 9b where a positive ACI difference indicates an increase in the aerosol load, confirm the simulated transport pattern in Fig. 9a. Overall, simulations and observations indicate the largest increase of the aerosol load in the tropics and mid-latitudes, but also show a significant enhancement over the south polar region after December 2010.

4 Discussion

The results presented in Sect. 3 show that the main transport pathway for the poleward transport of the Merapi volcanic plume to Antarctica was between the isentropic surfaces of 350 and 480 K (about 10 to

20 km), covering the TTL and the lower stratosphere at mid- and high latitudes. For this long-range transport on timescales of a few months, fast isentropic transport associated with quasi-horizontal mixing played the main role in transporting the volcanic aerosol from the TTL to the Antarctic lower stratosphere. ~~was found to be the most efficient pathway. The phase of QBO, subtropical Rossby wave breaking and the strength and stability of the polar vortex all have an impact on the transport efficiency.~~ The Merapi eruption occurred in austral spring and fast poleward transport was facilitated by the weakening of the subtropical jet and active Rossby wave breaking events. ~~The westerly QBO enhanced transport and mixing in the subtropics with implications on the position of the subtropical barrier (Shuckburgh et al., 2001; Palazzi et al., 2011). The QBO also modulated the ability of upward propagating planetary waves to influence the strength of the polar vortex.~~ The polar vortex was relatively stable when the Merapi erupted, but by the time the volcanic plume reached the south polar region, the polar vortex was displaced from the ~~south pole~~South Pole and distorted because more wave systems propagated into the polar stratosphere and warmed the polar region, so that the volcanic plume was transported from the tropics deep into Antarctica.

~~The phase of the QBO influences the amount of volcanic emissions transported out of tropics, while the heating effect of a large amount of sulfur injected by volcanic eruptions can change the pattern of the QBO (Niemeier and Schmidt, 2017). With increasing emission rates the velocity of the equatorial jet streams increases and less sulfate is transported out of the tropics. The amount of SO_2 injected during the Merapi eruption 2010 was 0.44 Tg, far less than the 8 TgS/yr required to shut down or reverse the QBO pattern (Niemeier and Schmidt, 2017), so that the westerly phase of the QBO that promote meridional transport was under minor influence of the heating effect of sulfur in this case.~~

Based on the simulation results in Sect. 3.4, up to 4% of the volcanic plume air parcels was transported from the TTL to the lower stratosphere in the south polar region till the end of February 2011~~,~~. Based on previous research on the Merapi case, we assigned a total mass of 0.44 Tg to all SO_2 parcel released, which means the Merapi eruption contributed about 8800 tons of sulfur to the polar lower stratosphere within 4 months after the eruption, assuming that the sulfate aerosol converted from the SO_2 remained in the plume. Although the MPTRAC model we used to simulate the 3D movement of air parcels in the volcanic plumes can estimate the conversion of SO_2 to sulf~~ph~~ate aerosol during the transport process, however, it does not resolve the chemical processes of aerosol formation. Hence, the estimated 8800 tons of sulfur are the maximum value since processes as e.g. wet deposition remove sulfur from the atmosphere. But in~~In~~ the lower stratosphere, the atmosphere is relatively dry and clean compared with the lower troposphere, so the sulfate ~~aerosols~~aerosol has a lower posibility to interact with clouds or to be

washed out. In fact, in the polar lower stratosphere usually sedimentation and downward transport by the BDC are the main removal processes. Clouds and washout processes usually cannot be expected in the lower stratosphere. However, the amount of sulfate ~~aerosols~~aerosol in the plume could also be affected by other mechanisms that speed up the loss of sulfur, for example, coagulation in the volcanic plume, or the absorption of sulfur onto fine ash particles. But for the moderate eruption Merapi in 2010, sulfuric~~sulphuric~~ particle growth may not be as significant as it is in a large volcanic eruption, so the scavenging efficiency of sulfur will be low. So generally, our estimation may be larger than the actual value, but this number may be considered as the upper limit of the contribution of the Merapi eruption.

Besides, a kinematic trajectory model like MPTRAC, in which reanalysis vertical wind is used as vertical velocity, typically shows higher vertical dispersion in the equatorial lower stratosphere compared with a diabatic trajectory model (Schoeberl et al., 2003; Wohltmann and Rex, 2008; Liu et al., 2010; Ploeger et al., 2010, 2011). However, the ERA–Interim reanalysis data used in this study to drive the model may constrain the vertical dispersion much better than older reanalyses (Liu et al., 2010; Hoffmann et al., 2017). The meridional transport in this study was mainly quasi-horizontal transport in the mid- and high latitude UTLS region, so the effect of the vertical speed scheme is limited.

The aerosol transported to the polar lower stratosphere will finally descend with the downward flow and have a chance to become a nonlocal source of sulfur for Antarctica by dry and wet deposition, following the general precipitation patterns. Quantifying the sulfur deposition flux onto Antarctica is beyond the scope of this study, though. Model results of Solomon et al. (2016) suggest that the Merapi eruption made a small but significant contribution to the ozone depletion over Antarctica in the vertical range of 100–200 hPa, roughly between 10 and 14 km. This altitude range is in agreement with our results, where we found transport into the Antarctic stratosphere between 10 and 20 km. When the volcanic plume was transported to Antarctica in December 2010, the polar synoptic temperature at these low height levels was already too high for the formation of PSCs. The additional ozone depletion found by Solomon et al. (2016) together with the fact that sulfate aerosol was transported from the Merapi into the Antarctic stratosphere between November and February where no PSCs are present during polar summer, may support the study that suggested that significant ozone depletion can also occur on cold binary aerosol (Drdla and Müller, 2012). The Merapi eruption in 2010 could be an interesting case study for more sophisticated geophysical models to study the aftermath of volcanic eruptions on polar processes.

5 Summary and conclusion

In this study, we analyzed the poleward transport of volcanic aerosol released by the Merapi eruption in 2010 from the tropics to the Antarctic lower stratosphere. The analysis was based on AIRS SO_2 measurements, MIPAS sulfate aerosol detections and MPTRAC transport simulations. First, we estimated altitude-resolved SO_2 injection time series during the explosive eruption period using AIRS data together with a backward trajectory approach. Second, the long-range transport of the volcanic plume from the initial eruption to April 2011~~0~~ was simulated based on the derived SO_2 injection time series. Then the evolution and the poleward migration of the volcanic plume were analyzed using the forward trajectory simulations and MIPAS aerosol measurements. The simulations are compared with and verified by the MIPAS aerosol measurements.

Results of this study suggest that the volcanic plume from the Merapi eruption was transported from the tropics to the south of 60 ℃S within a time scale of one month. Later on, in the UTLS region a fraction of the volcanic plume (~4%) crossed 60 ℃S, even further to Antarctica until the end of February 2011. As a result, the aerosol load in the Antarctic lower stratosphere was significantly elevated. This relatively fast meridional transport of volcanic aerosol was mainly carried out by quasi-horizontal mixing from the TTL to the extratropical lower stratosphere. Based on the simulations, most of the quasi-horizontal mixing occurred between the isentropic surfaces of 360 to 430 K. This transport was in turn facilitated by the weakening of the subtropical jet and the breakdown of the polar vortex in the seasonal transition from austral spring to summer. The polar vortex in late austral spring 2010 was relatively strong compared to the climatological mean state. However, in December 2010 the polar vortex was displaced off the South Pole and later on broke down when the plume went to the ~~south polar region~~high latitudes, so the volcanic plume did not penetrate the polar vortex but entered the South Pole with the breakdown of the polar vortex.

Overall, after the Merapi eruption, the largest increase of aerosol load occurred in the Southern Hemisphere midlatitudes and a relatively small but significant fraction of the volcanic plume (4%) was further transported to the Antarctic lower stratosphere within 4 months after the eruption. As a maximum estimation, it contributed up to 8800 tons of sulfur to the Antarctic stratosphere, which indicates that long-range transport under favorable meteorological conditions can make moderate tropical volcanic eruptions an important remote source of sulfur to Antarctica.

Code and data availability. AIRS data are distributed by the NASA Goddard Earth Sciences Data Information and Services Center. The SO_2 index data used in this study (Hoffmann et al., 2014) are available for download at https://datapub.fz-juelich.de/slcs/airs/volcanoes/ (last access: 26 March 2018). Envisat MIPAS Level-1B data are distributed by the European Space Agency. The ERA–Interim reanalysis data (Dee et al., 2011) were obtained from the European Centre for Medium-Range Weather Forecasts. The code of the Massive-Parallel Trajectory Calculations (MPTRAC) model is available under the terms and conditions of the GNU General Public License, Version 3 from the repository at https://github.com/slcs-jsc/mptrac (last access: 31 January 2018).

Appendix

Figure A1 shows the 9-day running median values of the MIPAS ACI between 10 °N and 10 °S. During the time period of the reference state (November 2007 to March 2008), the aerosol load in the tropical stratosphere from 20 to 25 km is elevated by a couple of previous volcanic eruptions. The aerosol load at this vertical range after the Merapi eruption in 2010 is apparently smaller compared with the reference state.

It should be noted that there are semiannual data oscillations in the MIPAS ACI aerosol detections. This periodic pattern is caused by the aerosol index that uses the atmospheric window region between 960 and 961 cm^{-1}. Around this window region, there are CO_2 laser bands. Due to the semiannual temperature changes at about 50 km (semiannual oscillation), the CO_2 radiance contribution to this window region also oscillates. As this window is generally very clear of other trace gases, this oscillation is not only visible at higher altitudes but also in the lower stratosphere, because the satellite line of sight looks through the whole layer (Wu et al., 2017). But even though with the semiannual data oscillations, the upward transport of the aerosol from the Merapi eruption in the tropical stratosphere is still visible and the vertical speed is estimated to about 7–8 km in five months (November 2010 to March 2011).

Competing interests. The authors declare that they have no conflict of interest.

Acknowledgments. This work was supported by National Natural Science Foundation of China under grant no. 41605023, China Postdoctoral Science Foundation under grant no. 2018T110131 and International Postdoctoral Exchange Fellowship Program 2015 under grant no. 20151006.

Reference

Anstey, J. A., and Shepherd, T. G.: High-latitude influence of the quasi-biennial oscillation, Q. J. R. Meteorol. Soc., 140, 1-21, doi: 10.1002/qj.2132, 2014.

~~Aquila, V., C. I. Garfinkel,P.A.Newman, L. D. Oman, and D. W. Waugh, Modifications of the quasi-biennial oscillation by a geoengineering perturbation of the stratospheric aerosol layer, Geophys. Res. Lett., 41, 1738-1744, doi: 10.1002/2013GL058818, 2014.~~

Aumann, H. H., Chahine, M. T., Gautier, C., Goldberg, M. D., Kalnay, E., McMillin, L. M., Revercomb, H., Rosenkranz, P. W., Smith, W. L., Staelin, D. H., Strow, L. L., and Susskind, J.: AIRS/AMSU/HSB on the Aqua mission: design, science objectives, data products, and processing systems, IEEE Trans. Geosci. Remote Sens., 41, 253-264, doi: 10.1109/TGRS.2002.808356, 2003.

Baldwin, M. P., and Dunkerton, T. J.: Propagation of the Arctic Oscillation from the stratosphere to the troposphere, J. Geophys. Res. Atmos., 104, 30937-30946, doi: 10.1029/1999JD900445, 1999.

Bosilovich, M., Akella, S., Coy, L., Cullather, R., Draper, C., Gelaro, R., Kovach, R., Liu, Q., Molod, A., Norris, P., Wargan, K., Chao, W., Reichle, R., Takacs, L., Vikhliaev, Y., Bloom, S., Collow, A., Firth, S., Labow, G., Partyka, G., Pawson, S., Reale, O., Schubert, S. D., and Suarez, M.: MERRA-2: Initial evaluation of the climate, Tech. rep., NASA, series on Global Modeling and Data Assimilation, NASA/TM–2015-104606, Vol. 43, 2015.

Dee, D. P., Uppala, S. M., Simmons, A. J., Berrisford, P., Poli, P., Kobayashi, S., Andrae, U., Balmaseda, M. A., Balsamo, G., Bauer, P., Bechtold, P., Beljaars, A. C. M., van de Berg, L., Bidlot, J., Bormann, N., Delsol, C., Dragani, R., Fuentes, M., Geer, A. J., Haimberger, L., Healy, S. B., Hersbach, H., Holm, E. V., Isaksen, L., Kallberg, P., Kohler, M., Matricardi, M., McNally, A. P., Monge-Sanz, B. M., Morcrette, J. J., Park, B. K., Peubey, C., de Rosnay, P., Tavolato, C., Thepaut, J. N., and Vitart, F.: The ERA-Interim reanalysis: configuration and performance of the data assimilation system, Q. J. R. Meteorol. Soc., 137, 553-597, doi: 10.1002/qj.828, 2011.

Drdla, K., and Müller, R.: Temperature thresholds for chlorine activation and ozone loss in the polar stratosphere, Ann. Geophys., 30, 1055-1073, doi: 10.5194/angeo-30-1055-2012, 2012.

Edmon, H. J. J., Hoskins, B. J., and McIntyre, M. E.: Eliassen-Palm Cross Sections for the Troposphere, J. Atmos. Sci., 37, 2600-2616, doi: 10.1175/1520-0469(1980)037<2600:epcsft>2.0.co;2, 1980.

Fischer, H., Birk, M., Blom, C., Carli, B., Carlotti, M., von Clarmann, T., Delbouille, L., Dudhia, A., Ehhalt, D., Endemann, M., Flaud, J. M., Gessner, R., Kleinert, A., Koopman, R., Langen, J., López-Puertas, M., Mosner, P., Nett, H., Oelhaf, H., Perron, G., Remedios, J., Ridolfi, M., Stiller, G., and Zander, R.: MIPAS: an instrument for atmospheric and climate research, Atmos. Chem. Phys., 8, 2151-2188, doi: 10.5194/acp-8-2151-2008, 2008.

Friberg, J., Martinsson, B. G., Andersson, S. M., and Sandvik, O. S.: Volcanic impact on the climate – the stratospheric aerosol load in the period 2006–2015, Atmos. Chem. Phys., 18, 11149-11169, doi: 10.5194/acp-18-11149-2018, 2018.

Gao, C., Oman, L., Robock, A., and Stenchikov, G. L.: Atmospheric volcanic loading derived from bipolar ice cores: Accounting for the spatial distribution of volcanic deposition, J. Geophys. Res. Atmos., 112, D09109, doi: 10.1029/2006JD007461, 2007.

Griessbach, S., L. Hoffmann, R. Spang and M. Riese: Volcanic ash detection with infrared limb sounding: MIPAS observations and radiative transfer simulations, Atmos. Meas. Tech. 7, 1487-1507, doi: 10.5194/amt-7-1487-2014, 2014.

Griessbach, S., Hoffmann, L., Spang, R., von Hobe, M., Müller, R., and Riese, M.: Infrared limb emission measurements of aerosol in the troposphere and stratosphere, Atmos. Meas. Tech., 9, 4399-4423, doi:10.5194/amt-9-4399-2016, 2016.

Günther, A., Höpfner, M., Sinnhuber, B. M., Griessbach, S., Deshler, T., von Clarmann, T., and Stiller, G.: MIPAS observations of volcanic sulphate aerosol and sulphur dioxide in the stratosphere, Atmos. Chem. Phys., 2017, 1-32, doi: 10.5194/acp-18-1217-2018, 2018.

Haynes, P., and Shuckburgh, E.: Effective diffusivity as a diagnostic of atmospheric transport: 2. Troposphere and lower stratosphere, J. Geophys. Res. Atmos., 105, 22795-22810, doi: 10.1029/2000JD900092, 2000.

Heng, Y., Hoffmann, L., Griessbach, S., Rößler, T., and Stein, O.: Inverse transport modeling of volcanic sulfur dioxide emissions using large-scale simulations, Geosci. Model Dev., 9, 1627-1645, doi:10.5194/gmd-9-1627-2016, 2016.

Hoffmann, L., Griessbach, S., and Meyer, C. I.: Volcanic emissions from AIRS observations: detection methods, case study, and statistical analysis, in: Remote Sensing of Clouds and the Atmosphere XIX and Optics in Atmospheric Propagation and Adaptive Systems XVII, edited by: Comeron, A., Kassianov, E. I., Schafer, K., Picard, R. H., Stein, K., and Gonglewski, J. D., Proceedings of SPIE, Spie-Int Soc Optical Engineering, Bellingham, doi: 92421410.1117/12.2066326, 2014.

Hoffmann, L., Hertzog, A., Rößler, T., Stein, O., and Wu, X.: Intercomparison of meteorological analyses and trajectories in the Antarctic lower stratosphere with Concordiasi superpressure balloon observations, Atmos. Chem. Phys., 17, 8045-8061, doi: 10.5194/acp-17-8045-2017, 2017.

Hoffmann, L., Rößler, T., Griessbach, S., Heng, Y., and Stein, O.: Lagrangian transport simulations of volcanic sulfur dioxide emissions: Impact of meteorological data products, J. Geophys. Res. Atmos., 121, 4651-4673, doi: 10.1002/2015JD023749, 2016.

Hofmann, D. J., Rosen, J. M., and Gringel, W.: Delayed production of sulfuric acid condensation nuclei in the polar stratosphere from El Chichon volcanic vapors, J. Geophys. Res. Atmos., 90, 2341-2354, doi:10.1029/JD090iD01p02341, 1985.

Hofmann, D. J., Rosen, J. M., and Harder, J. W.: Aerosol measurements in the winter/spring Antarctic stratosphere: 1. Correlative measurements with ozone, J. Geophys. Res. Atmos., 93, 665-676, doi:10.1029/JD093iD01p00665, 1988.

Holton, J. R., Haynes, P. H., McIntyre, M. E., Douglass, A. R., Rood, R. B., and Pfister, L.: Stratosphere-troposphere exchange, Rev. Geophys., 33, 403-439, doi: 10.1029/95RG02097, 1995.

Holton, J. R., and Tan, H. C.: The Influence of the Equatorial Quasi-Biennial Oscillation on the Global Circulation at 50 mb, J. Atmos. Sci., 37, 2200-2208, doi: 10.1175/1520-0469(1980)037<2200:tioteq>2.0.co;2, 1980.

Höpfner, M., Pitts, M. C., and Poole, L. R.: Comparison between CALIPSO and MIPAS observations of polar stratospheric clouds, J. Geophys. Res. Atmos., 114, doi:10.1029/2009JD012114, 2009.

Ivy, D. J., Solomon, S., Kinnison, D., Mills, M. J., Schmidt, A., and Neely, R. R.: The influence of the Calbuco eruption on the 2015 Antarctic ozone hole in a fully coupled chemistry-climate model, Geophys. Res. Lett., 44, 2556-2561, doi: 10.1002/2016GL071925, 2017.

Jäger, H.: Long-term record of lidar observations of the stratospheric aerosol layer at Garmisch-Partenkirchen, J. Geophys. Res. Atmos., 110, D08106, doi: 10.1029/2004JD005506, 2005.

Jäger, H., and Wege, K.: Stratospheric ozone depletion at northern midlatitudes after major volcanic eruptions, J. Atmos. Chem., 10, 273-287, doi: 10.1007/bf00053863, 1990.

Kalnay, E., Kanamitsu, M., Kistler, R., Collins, W., Deaven, D., Gandin, L., Iredell, M., Saha, S., White, G., Woollen, J., Zhu, Y., Chelliah, M., Ebisuzaki, W., Higgins, W., Janowiak, J., Mo, K. C., Ropelewski, C., Wang, J., Leetmaa, A., Reynolds, R., Jenne, R., and Joseph, D.: The NCEP/NCAR 40-Year Reanalysis Project, Bull. Am. Meteorol. Soc. 77, 437-472, doi: 10.1175/1520-0477(1996)077<0437:tnyrp>2.0.co;2, 1996.

Khaykin, S. M., Godin-Beekmann, S., Keckhut, P., Hauchecorne, A., Jumelet, J., Vernier, J. P., Bourassa, A., Degenstein, D. A., Rieger, L. A., Bingen, C., Vanhellemont, F., Robert, C., DeLand,

M., and Bhartia, P. K.: Variability and evolution of the midlatitude stratospheric aerosol budget from 22 years of ground-based lidar and satellite observations, Atmos. Chem. Phys., 17, 1829-1845, doi: 10.5194/acp-17-1829-2017, 2017.

~~Kravitz, B., and Robock, A.: Climate effects of high-latitude volcanic eruptions: Role of the time of year, J. Geophys. Res. Atmos., 116, D01105, 10.1029/2010JD014448, 2011.~~

Kunz, A., Konopka, P., Müller, R., and Pan, L. L.: Dynamical tropopause based on isentropic potential vorticity gradients, J. Geophys. Res. Atmos., 116, D01110, doi: 10.1029/2010JD014343, 2011a.

Kunz, A., Pan, L. L., Konopka, P., Kinnison, D. E., and Tilmes, S.: Chemical and dynamical discontinuity at the extratropical tropopause based on START08 and WACCM analyses, J. Geophys. Res. Atmos., 116, D24302, doi: 10.1029/2011JD016686, 2011b.

Kunz, A., Sprenger, M., and Wernli, H.: Climatology of potential vorticity streamers and associated isentropic transport pathways across PV gradient barriers, J. Geophys. Res. Atmos., 120, 3802-3821, doi: 10.1002/2014jd022615, 2015.

Levelt, P. F., Oord, G. H. J. v. d., Dobber, M. R., Malkki, A., Huib, V., Johan de, V., Stammes, P., Lundell, J. O. V., and Saari, H.: The ozone monitoring instrument, IEEE Trans. Geosci. Remote Sens., 44, 1093-1101, doi: 10.1109/TGRS.2006.872333, 2006.

Liu, Y. S., Fueglistaler, S., and Haynes, P. H.: Advection-condensation paradigm for stratospheric water vapor, J. Geophys. Res. Atmos., 115,D24307, doi: 10.1029/2010JD014352, 2010.

Mazzera, D. M., Lowenthal, D. H., Chow, J. C., and Watson, J. G.: Sources of PM10 and sulfate aerosol at McMurdo station, Antarctica, Chemosphere, 45, 347-356, doi: https://doi.org/10.1016/S0045-6535(00)00591-9, 2001.

McCormick, M. P., Steele, H. M., Hamill, P., Chu, W. P., and Swissler, T. J.: Polar Stratospheric Cloud Sightings by SAM II, J. Atmos. Sci., 39, 1387-1397, doi: 10.1175/1520-0469(1982)039<1387:pscsbs>2.0.co;2, 1982.

Newman, P. A., and Nash, E. R.: Quantifying the wave driving of the stratosphere, J. Geophys. Res. Atmos.,105, 12485-12497, doi: 10.1029/1999JD901191, 2000.

~~Niemeier, U., and Schmidt, H.: Changing transport processes in the stratosphere by radiative heating of sulfate aerosols, Atmos. Chem. Phys., 17, 14871-14886, doi: 10.5194/acp-17-14871-2017, 2017.~~

Olsen, M. A., Douglass, A. R., Schoeberl, M. R., Rodriquez, J. M., and Yoshida, Y.: Interannual variability of ozone in the winter lower stratosphere and the relationship to lamina and irreversible transport, J. Geophys. Res. Atmos., 115, 10.1029/2009jd013004, 2010.

O'Sullivan, D., and Dunkerton, T. J.: The influence of the quasi-biennial oscillation on global constituent distributions, J. Geophys. Res. Atmos., 102, 21731-21743, doi: 10.1029/97JD01689, 1997.

~~Palazzi, E., Fierli, F., Stiller, G. P., and Urban, J.: Probability density functions of long-lived tracer observations from satellite in the subtropical barrier region: data intercomparison, Atmos. Chem. Phys., 11, 10579-10598, doi: 10.5194/acp-11-10579-2011, 2011.~~

Pallister, J. S., Schneider, D. J., Griswold, J. P., Keeler, R. H., Burton, W. C., Noyles, C., Newhall, C. G., and Ratdomopurbo, A.: Merapi 2010 eruption—Chronology and extrusion rates monitored with satellite radar and used in eruption forecasting, J. Volcanol. Geotherm. Res., 261, 144-152, doi: http://dx.doi.org/10.1016/j.jvolgeores.2012.07.012, 2013.

~~Pausata, F. S. R., Chafik, L., Caballero, R., and Battisti, D. S.: Impacts of high-latitude volcanic eruptions on ENSO and Asian monsoon, Proc. Natl. Acad. Sci. U.S.A., 112, 13784-13788, doi: 10.1073/pnas.1509153112, 2015.~~

Ploeger, F., Konopka, P., Gunther, G., Grooss, J. U., and Muller, R.: Impact of the vertical velocity scheme on modeling transport in the tropical tropopause layer, J. Geophys. Res. Atmos., 115, 14, doi: 10.1029/2009jd012023, 2010.

Ploeger, F., Fueglistaler, S., Grooss, J. U., Gunther, G., Konopka, P., Liu, Y. S., Muller, R., Ravegnani, F., Schiller, C., Ulanovski, A., and Riese, M.: Insight from ozone and water vapour on transport in the tropical tropopause layer (TTL), Atmos. Chem. Phys., 11, 407-419, doi: 10.5194/acp-11-407-2011, 2011.

Portmann, R. W., Solomon, S., Garcia, R. R., Thomason, L. W., Poole, L. R., and McCormick, M. P.: Role of aerosol variations in anthropogenic ozone depletion in the polar regions, J. Geophys. Res. Atmos., doi: 101, 22991-23006, doi:10.1029/96JD02608, 1996.

Rößler, T., Stein, O., Heng, Y., Baumeister, P., and Hoffmann, L.: Trajectory errors of different numerical integration schemes diagnosed with the MPTRAC advection module driven by ECMWF operational analyses, Geosci. Model Dev., 11, 575-592, doi: 10.5194/gmd-11-575-2018, 2018.

Sand, M., Samset, B. H., Balkanski, Y., Bauer, S., Bellouin, N., Berntsen, T. K., Bian, H., Chin, M., Diehl, T., Easter, R., Ghan, S. J., Iversen, T., Kirkevåg, A., Lamarque, J. F., Lin, G., Liu, X., Luo, G., Myhre, G., Noije, T. V., Penner, J. E., Schulz, M., Seland, Ø., Skeie, R. B., Stier, P., Takemura, T., Tsigaridis, K., Yu, F., Zhang, K., and Zhang, H.: Aerosols at the poles: an AeroCom Phase II multi-model evaluation, Atmos. Chem. Phys., 17, 12197-12218, doi: 10.5194/acp-17-12197-2017, 2017.

Schoeberl, M. R., Douglass, A. R., Zhu, Z. X., and Pawson, S.: A comparison of the lower stratospheric age spectra derived from a general circulation model and two data assimilation systems, J. Geophys. Res. Atmos., 108, 16, doi: 10.1029/2002jd002652, 2003.

Sembhi, H., Remedios, J., Trent, T., Moore, D. P., Spang, R., Massie, S., and Vernier, J. P.: MIPAS detection of cloud and aerosol particle occurrence in the UTLS with comparison to HIRDLS and CALIOP, Atmos. Meas. Tech., 5, 2537-2553, doi: 10.5194/amt-5-2537-2012, 2012.

Shuckburgh, E., Norton, W., Iwi, A., and Haynes, P.: Influence of the quasi-biennial oscillation on isentropic transport and mixing in the tropics and subtropics, J. Geophys. Res. Atmos., 106, 14327-14337, doi: 10.1029/2000JD900664, 2001.

Sigl, M., Winstrup, M., McConnell, J. R., Welten, K. C., Plunkett, G., Ludlow, F., Buntgen, U., Caffee, M., Chellman, N., Dahl-Jensen, D., Fischer, H., Kipfstuhl, S., Kostick, C., Maselli, O. J., Mekhaldi, F., Mulvaney, R., Muscheler, R., Pasteris, D. R., Pilcher, J. R., Salzer, M., Schupbach, S., Steffensen, J. P., Vinther, B. M., and Woodruff, T. E.: Timing and climate forcing of volcanic eruptions for the past 2,500 years, Nature, 523, 543-549, doi: 10.1038/nature14565http://www.nature.com/nature/journal/v523/n7562/abs/nature14565.html#supplementary-information, 2015.

Solomon, S.: Stratospheric ozone depletion: A review of concepts and history, Rev. Geophys., 37, 275-316, doi: 10.1029/1999RG900008, 1999.

Solomon, S., Daniel, J. S., Neely, R. R., Vernier, J.-P., Dutton, E. G., and Thomason, L. W.: The Persistently Variable "Background" Stratospheric Aerosol Layer and Global Climate Change, Science, 333, 866-870, doi: 10.1126/science.1206027, 2011.

Solomon, S., Garcia, R. R., Rowland, F. S., and Wuebbles, D. J.: On the depletion of Antarctic ozone, Nature, 321, 755, doi: 10.1038/321755a0, 1986.

Solomon, S., Ivy, D. J., Kinnison, D., Mills, M. J., Neely, R. R., and Schmidt, A.: Emergence of healing in the Antarctic ozone layer, Science, doi: 10.1126/science.aae0061, 2016.

Solomon, S., Sanders, R. W., Garcia, R. R., and Keys, J. G.: Increased chlorine dioxide over Antarctica caused by volcanic aerosols from Mount-Pinatubo, Nature, 363, 245–248, doi: https://doi.org/10.1038/363245a0, 1993.

Spang, R., Riese, M., and Offermann, D.: CRISTA-2 observations of the south polar vortex in winter 1997: A new dataset for polar process studies, Geophys. Res. Lett., 28, 3159–3162, doi: 10.1029/2000GL012374, 2001.

Stohl, A., Forster, C., Frank, A., Seibert, P., and Wotawa, G.: Technical note: The Lagrangian particle dispersion model FLEXPART version 6.2, Atmos. Chem. Phys., 5, 2461-2474, doi:10.5194/acp-5-2461-2005, 2005.

Stone, K. A., Solomon, S., Kinnison, D. E., Pitts, M. C., Poole, L. R., Mills, M. J., Schmidt, A., Neely, R. R., Ivy, D., Schwartz, M. J., Vernier, J.-P., Johnson, B. J., Tully, M. B., Klekociuk, A. R., König-Langlo, G., and Hagiya, S.: Observing the Impact of Calbuco Volcanic Aerosols on South Polar Ozone Depletion in 2015, J. Geophys. Res. Atmos., 122, 11,862-811,879, doi: 10.1002/2017JD026987, 2017.

Surono, Jousset, P., Pallister, J., Boichu, M., Buongiorno, M. F., Budisantoso, A., Costa, F., Andreastuti, S., Prata, F., Schneider, D., Clarisse, L., Humaida, H., Sumarti, S., Bignami, C., Griswold, J., Carn, S., Oppenheimer, C., and Lavigne, F.: The 2010 explosive eruption of Java's Merapi volcano—A '100-year' event, J. Volcanol. Geotherm. Res., 241, 121-135, doi: http://dx.doi.org/10.1016/j.jvolgeores.2012.06.018, 2012.

Tilmes, S., Muller, R., and Salawitch, R.: The sensitivity of polar ozone depletion to proposed geoengineering schemes, Science, 320, 1201-1204, doi: 10.1126/science.1153966, 2008.

Toohey, M., Krüger, K., Niemeier, U., and Timmreck, C.: The influence of eruption season on the global aerosol evolution and radiative impact of tropical volcanic eruptions, Atmos. Chem. Phys., 11, doi: 12351-12367, 10.5194/acp-11-12351-2011, 2011.

Vernier, J. P., Thomason, L. W., Pommereau, J. P., Bourassa, A., Pelon, J., Garnier, A., Hauchecorne, A., Blanot, L., Trepte, C., Degenstein, D., and Vargas, F.: Major influence of tropical volcanic eruptions on the stratospheric aerosol layer during the last decade, Geophys. Res. Lett., 38, L12807, doi: 10.1029/2011GL047563, 2011.

Vogel, B., Pan, L. L., Konopka, P., Gunther, G., Muller, R., Hall, W., Campos, T., Pollack, I., Weinheimer, A., Wei, J., Atlas, E. L., and Bowman, K. P.: Transport pathways and signatures of mixing in the extratropical tropopause region derived from Lagrangian model simulations, J. Geophys. Res. Atmos., 116, 16, doi: 10.1029/2010jd014876, 2011.

von Glasow, R., Bobrowski, N., and Kern, C.: The effects of volcanic eruptions on atmospheric chemistry, Chem. Geol., 263, 131-142, doi: http://dx.doi.org/10.1016/j.chemgeo.2008.08.020, 2009.

Watson, P. A. G., and Gray, L. J.: How Does the Quasi-Biennial Oscillation Affect the Stratospheric Polar Vortex?, J. Atmos. Sci., 71, 391-409, doi: 10.1175/jas-d-13-096.1, 2014.

Wohltmann, I., and Rex, M.: Improvement of vertical and residual velocities in pressure or hybrid sigma-pressure coordinates in analysis data in the stratosphere, Atmos. Chem. Phys., 8, 265-272, doi: 10.5194/acp-8-265-2008, 2008.

Wu, X., Griessbach, S., and Hoffmann, L.: Equatorward dispersion of a high-latitude volcanic plume and its relation to the Asian summer monsoon: a case study of the Sarychev eruption in 2009, Atmos. Chem. Phys., 17, 13439-13455, doi: 10.5194/acp-17-13439-2017, 2017.

Zuev, V. V., Zueva, N. E., Savelieva, E. S., and Gerasimov, V. V.: The Antarctic ozone depletion caused by Erebus volcano gas emissions, Atmos. Environ., 122, 393-399, doi: https://doi.org/10.1016/j.atmosenv.2015.10.005, 2015.

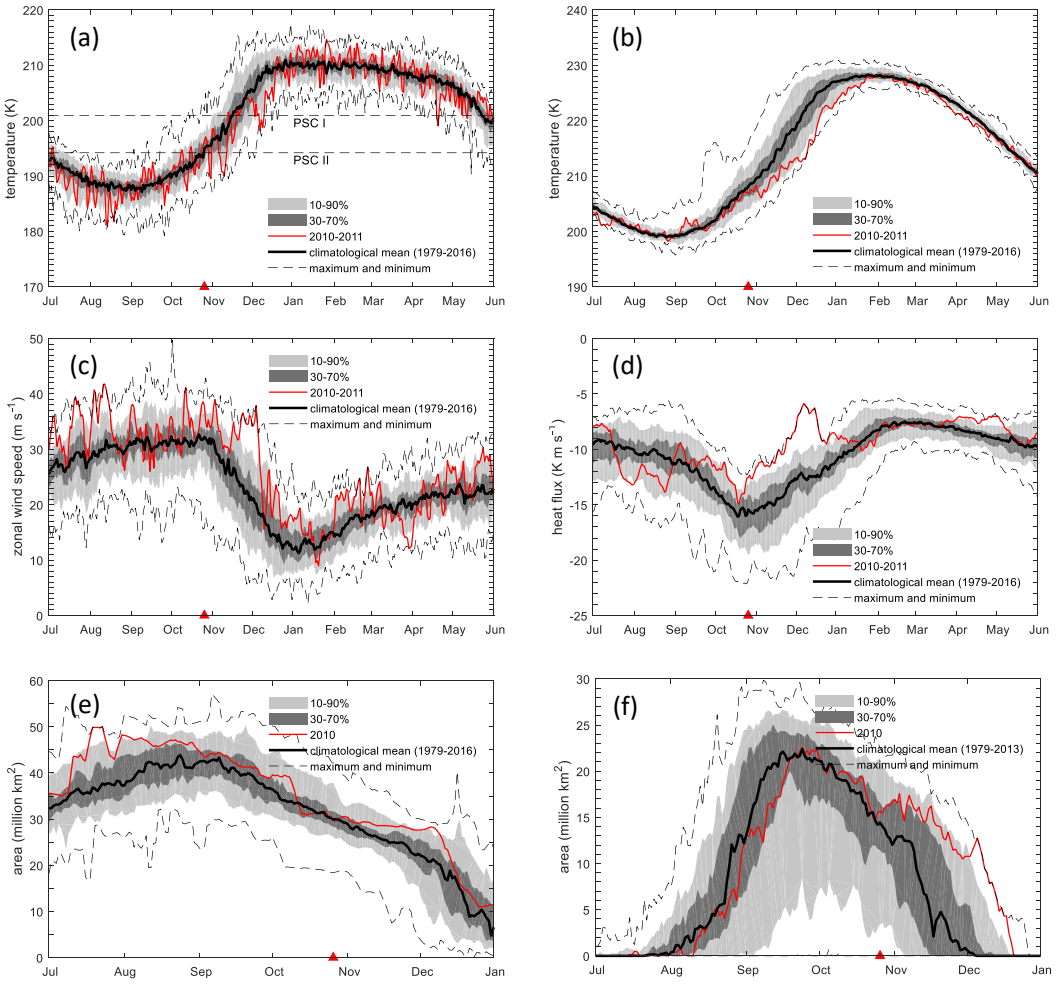

Figure 1: (a) Minimum temperature south of 50 ℃S at 150 hPa; (b) temperature averaged over the polar cap for latitudes south of 60 ℃S at 150 hPa; (c) zonal wind speed at 60 ℃S at 150 hPa; (d) eddy heat flux averaged between 45 ℃S and 75 ℃S for the 45-day period prior to the date indicated at 150 hPa; (e) the area of the polar vortex for 1 July–31 December 2010 on the 460 K isentropic surface; (f) ozone hole area for 1 July 2010–31 December 2010. Temperatures for PSC existence in (a) are determined by assuming a nitric acid concentration of 6 ppbv and a water vapor concentration of 4.5 ppmv. (a)–(f) are based on Modern-Era Retrospective analysis for Research and Applications reanalysis version 2 (MERRA2) data (Bosilovich et al., 2015). The ozone hole area in (f) is determined from OMI ozone satellite measurements (Levelt et al., 2006). The red triangles indicate the time of the Merapi eruption.

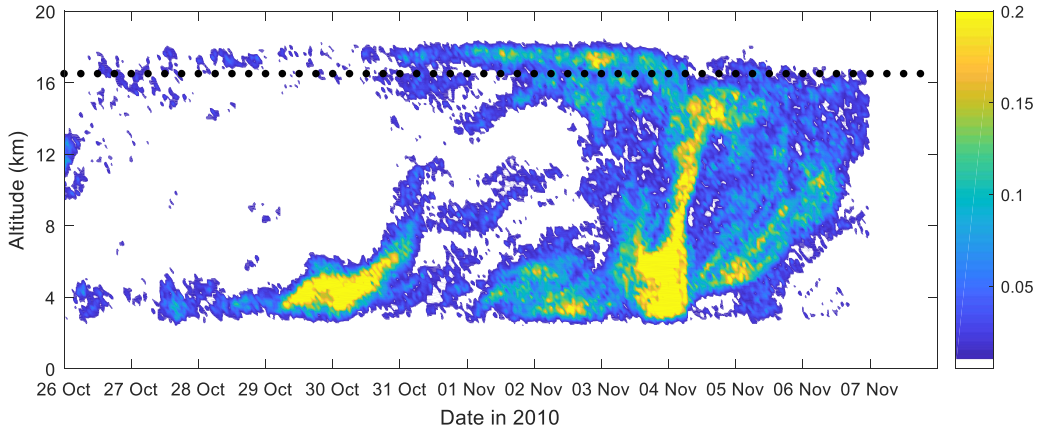

Figure 2: Merapi SO_2 emission time series (unit: kg m^{-1} s^{-1}) derived from AIRS measurements using a backward trajectory approach (see text for details). The emission data are binned every 1 h and 0.2 km. The ticks for the horizontal axis mark 0 UTC on each day. Black dots denote the height of the thermal tropopause (based on the ERA–Interim reanalysis).

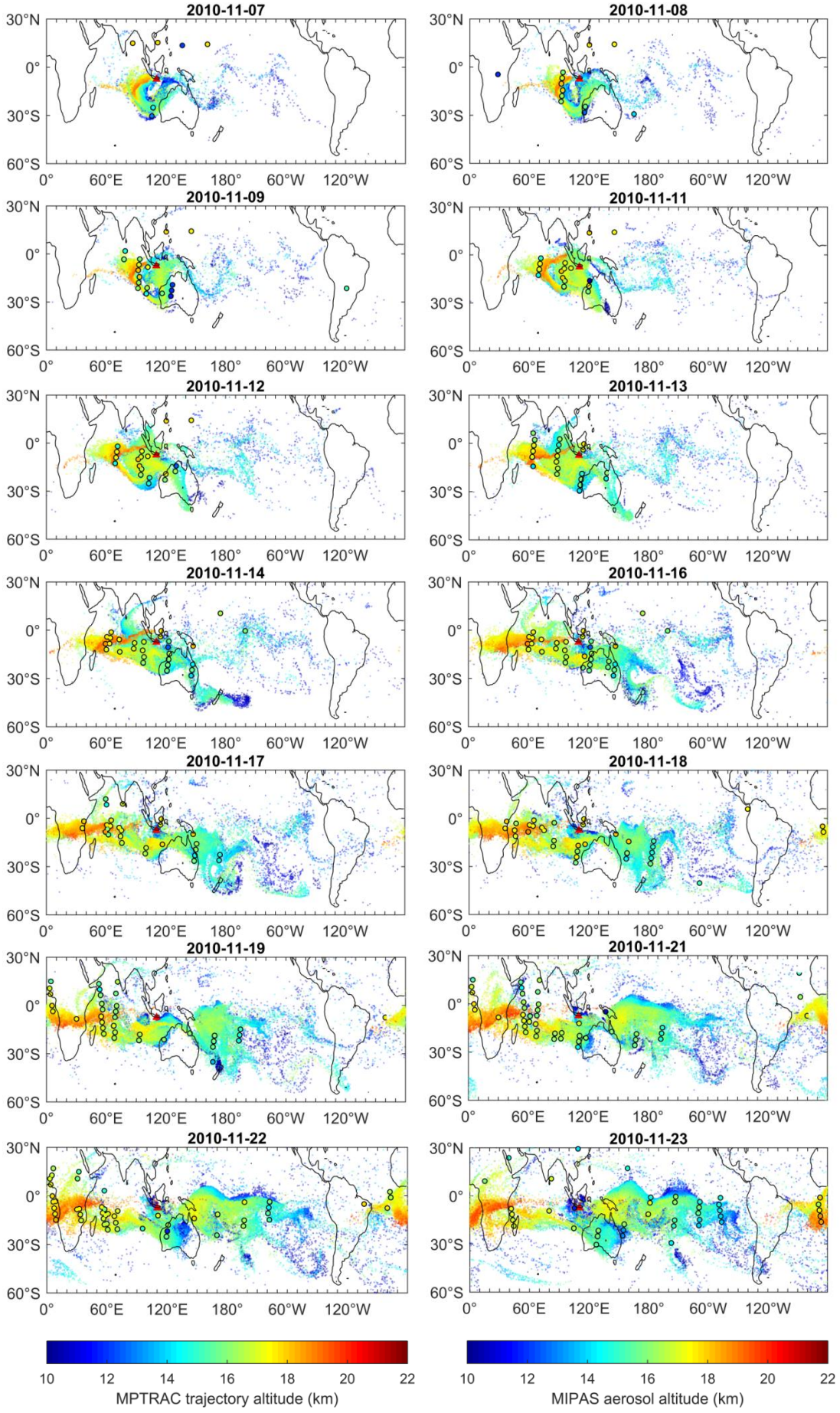

Figure 3: Distribution of the volcanic plume (showing only air parcels higher than 10 km, shading) from MPTRAC simulations (shown for 00:00UTC on selected days) and MIPAS aerosol detections (ACI < 7) within ±6 h (color-filled circles). The altitudes of all

air parcels, regardless of their SO_2 values, are shown. The red triangle denotes the location of Mount Merapi.

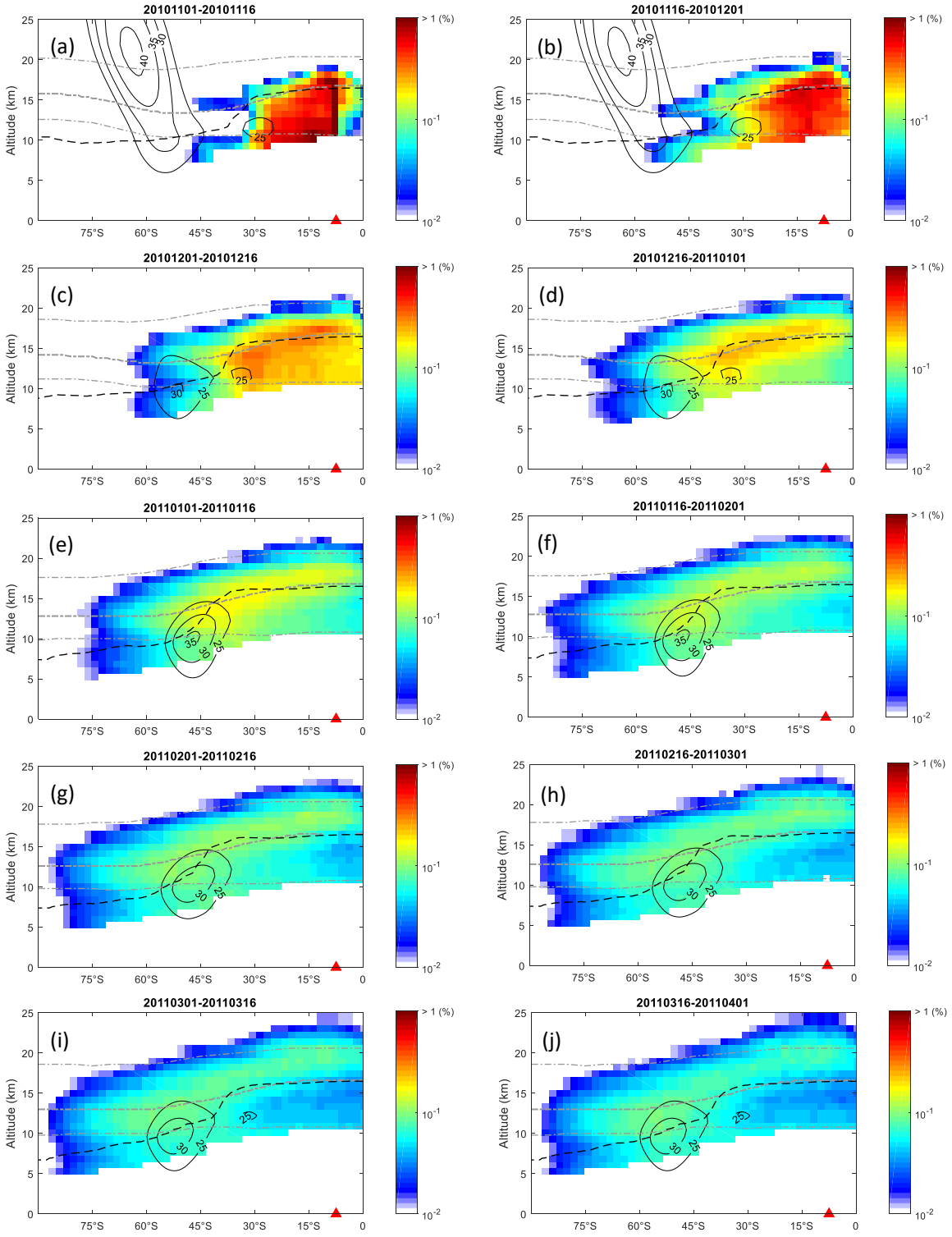

Figure 4: Percentage (%) of air parcels in proportion to the total number of air parcels released in the Lagrangian forward simulation, overlaid with monthly mean zonal winds (black contours), the thermal tropopause (black dashed line), the 380 K potential temperature isoline (thick gray dashed line) and 350 and 480 K potential temperature isolines (thin gray dashed lines). Results are binned every 2 °in latitude and 1 km in altitude. The red triangle denotes the latitude of the Mount Merapi. Please see title of each figure for the time period covered.

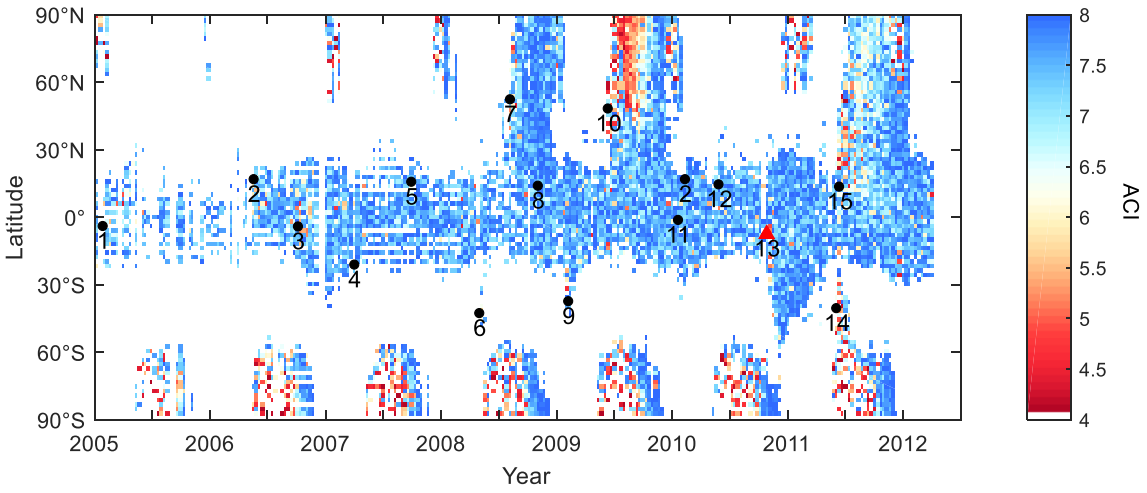

Figure 5: Median value of MIPAS ACI detections between 12–18 km (bin size: 10 days and 2 °in latitude) from January 2005 to April 2012. Only ACI values from 4 to 8 are shown. The red triangle indicates the eruption of Mount Merapi (No. 13). The black filled circles indicate 1 Manam, 2 Soufriere Hills, 3 Tavurvur (Rabaul), 4 Piton de la Fournaise, 5 Jebel at Tair, 6 Chaitén, 7 Kasatochi, 8 Dalaffilla, 9 Australian bushfire, 10 Sarychev Peak, 11 Nyamuragira, 12 Pacaya, 14 Puyehue-Cordón Caulle, 15 Nabro.

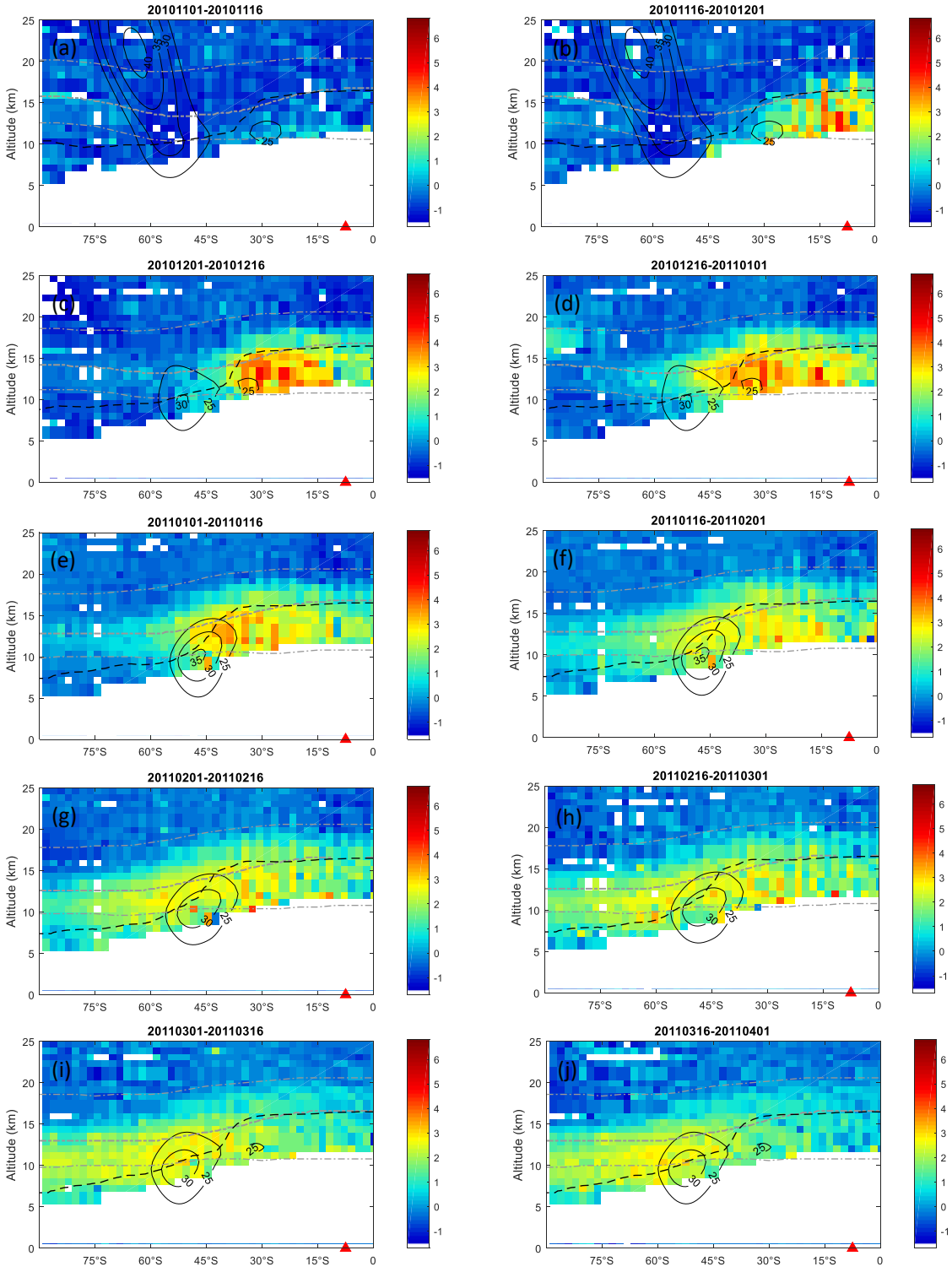

Figure 6: The change of ~~aerosol load~~MIPAS ACI values after the eruption of Merapi in 2010, overlaid with monthly mean zonal winds (black contours), the thermal tropopause (black dashed line), the 380 K potential temperature isoline (thick gray dashed line) and 350 and 480 K potential temperature isolines (thin gray dashed lines). Positive values indicate an increase of the aerosol load and negative values indicate a decrease of the aerosol load. Results are binned every 2 °in latitude and 1 km in altitude. The red triangle denotes the latitude of the Mount Merapi. Please see title of each figure for the time period covered.

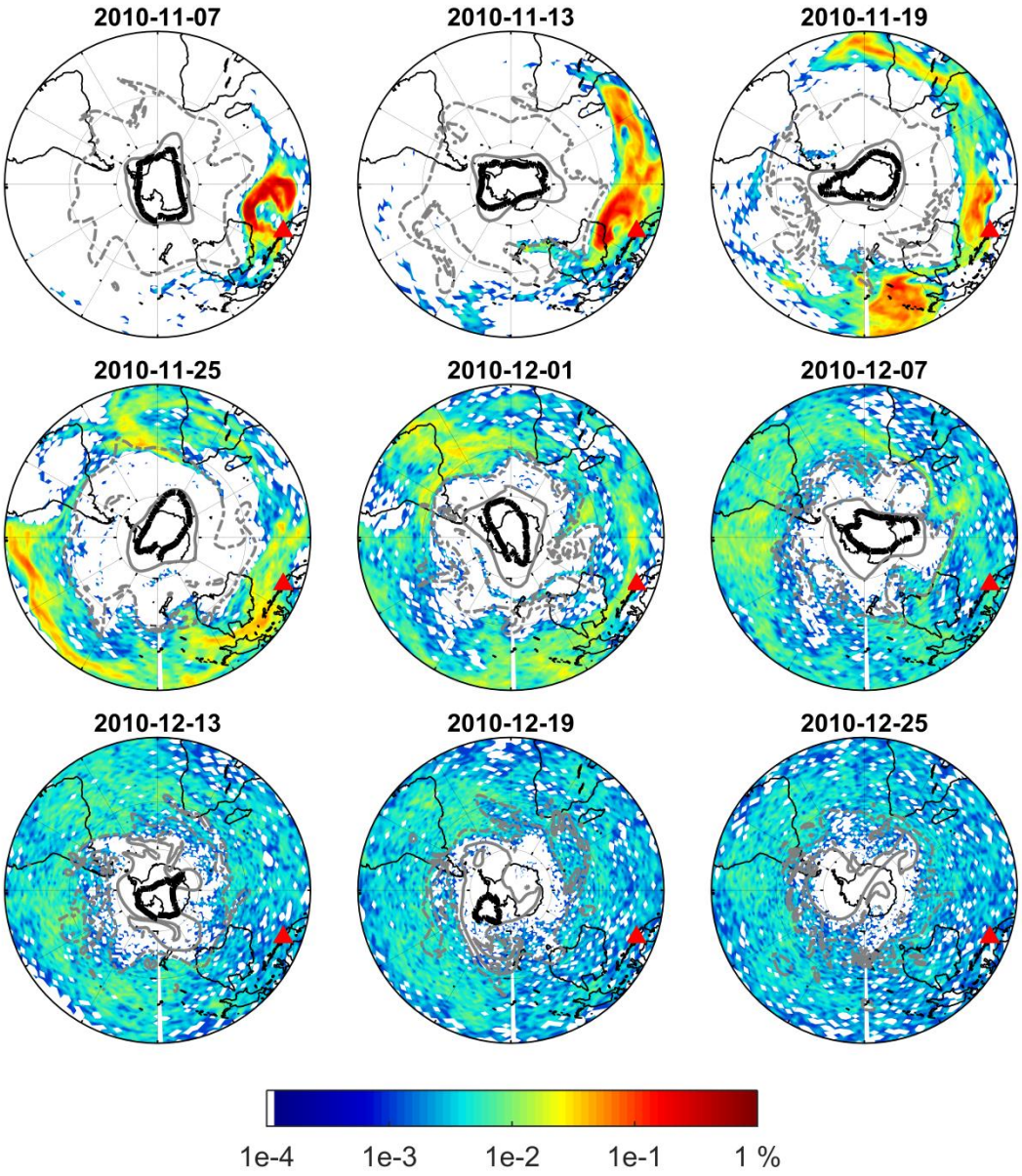

Figure 7: Percentage (%) of air parcels between the isentropic surfaces of 350 and 480 K in proportion to the total number of air parcels released in the Lagrangian forward simulation. All results are at 12:00 UTC on selected dates and binned every 2 ° in longitude and 1 ° in latitude. The black contours indicate the 220 DU contour lines of daily mean ozone column density provided by OMI. PV contours marked with gray dashed and solid lines show PV boundaries on the 350 and 480 K isentropic surfaces respectively (Kunz et al., 2015). The red triangle denotes the location of Mount Merapi.

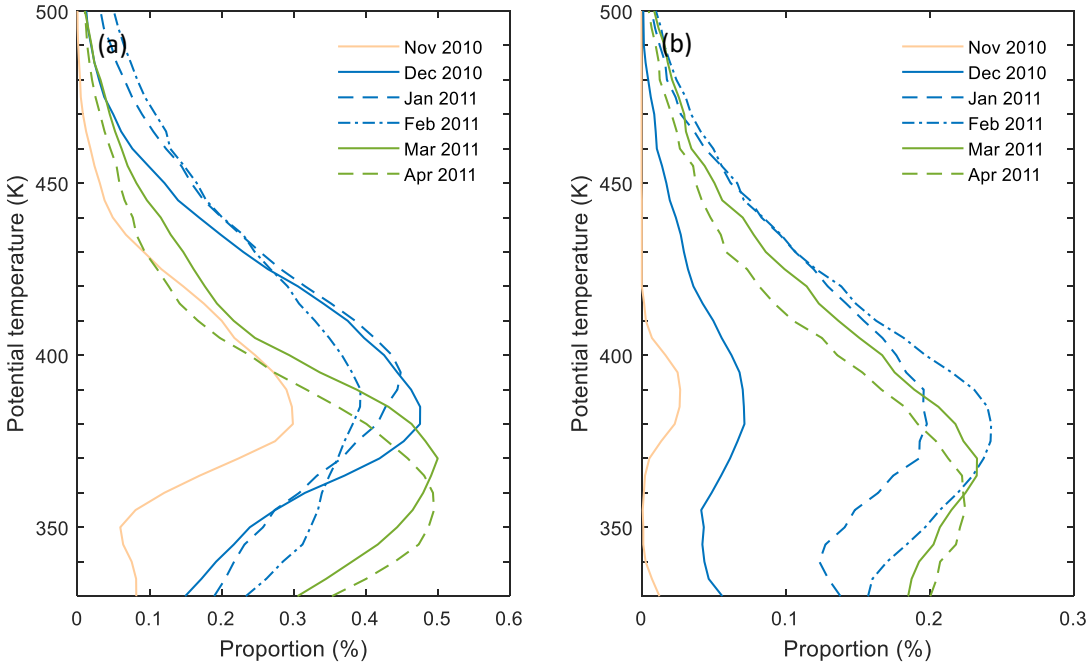

Figure 8: (a) Proportion (%) of the air parcels poleward of the PV-based transport boundaries at the end of each month; (b) proportion (%) of the air parcels south of 60 ℃S.

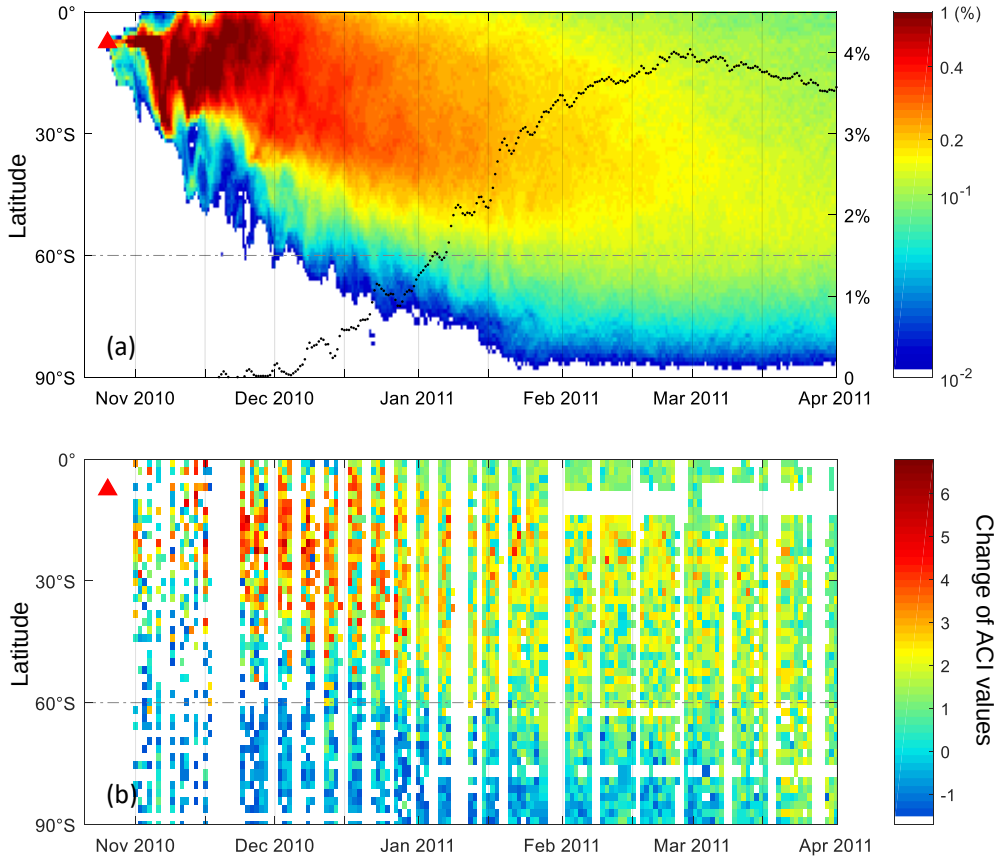

Figure 9: Time and latitude evolution of the (a) percentage (%) of air parcels between the isentropic surfaces of 350 and 480 K from the Lagrangian simulations (shading, only percentages larger than 0.05% are shown; bin size: 12h and 1 ° in latitude) and the proportion (%) of air parcels south of 60 °S (black dots); (b) the change of MIPAS ~~measured aerosol load~~ACI values after the eruption of Merapi in 2010 between 350 and 480 K. Positive values indicate an increase and negative values indicate a decrease of the aerosol load (bin size: 24h and 2 ° in latitude). The red triangle denotes the time and latitude of the Merapi eruption.

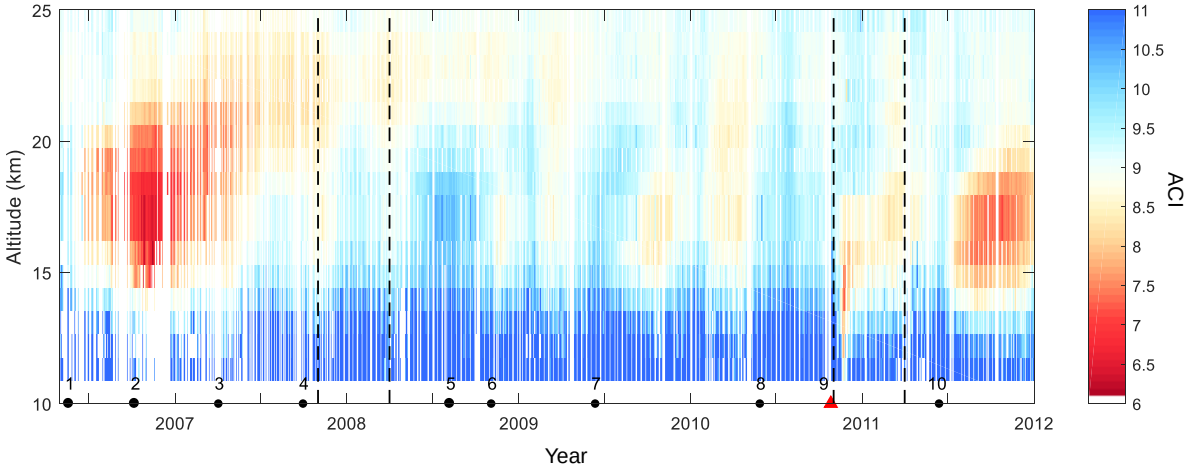

Figure A1: MIPAS 9-day running median of ACI between 10 ℕ and 10 ℚ from May 2006 to December 2011.The dashed vertical lines indicate the reference state from November 2007 to March 2008, and the investigation period for the Merapi eruption from November 2010 to March 2011. The red triangle indicates the time of the Merapi eruption (No. 9). The black dots indicate 1 Soufriere Hills, 2 Tavurvur (Rabaul), 3 Piton de la Fournaise, 4 Jebel at Tair, 5 Kasatochi, 6 Dalaffilla, 7 Sarychev, 8 Pacaya, 10 Nabro.

Long-range transport of volcanic aerosol from the 2010 Merapi tropical eruption to Antarctica

Xue Wu[1,2], Sabine Griessbach[1], Lars Hoffmann[1]

[1]Jülich Supercomputing Centre, Forschungszentrum Jülich, Jülich, Germany
[2]Key Laboratory of Middle Atmosphere and Global Environment Observation, Institute of Atmospheric Physics, Chinese Academy of Sciences, Beijing, China

Correspondence to: Xue Wu (xu.wu@fz-juelich.de)

Abstract

Volcanic sulfate aerosol is an important source of sulfur for Antarctica where other local sources of sulfur are rare. Mid- and high latitude volcanic eruptions can directly influence the aerosol budget of the polar stratosphere. However, tropical eruptions can also enhance polar aerosol load following long-range transport. In the present work, we analyze the volcanic plume of a tropical eruption, Mount Merapi in October 2010, and investigate the transport pathway of the volcanic aerosol from the tropical tropopause layer (TTL) to the lower stratosphere over Antarctica. We use the Lagrangian particle dispersion model Massive-Parallel Trajectory Calculations (MPTRAC) and Atmospheric Infrared Sounder (AIRS) SO_2 measurements to reconstruct the altitude-resolved SO_2 injection time series during the explosive eruption period and simulate the transport of the volcanic plume using the MPTRAC model. AIRS SO_2 and aerosol measurements, the aerosol-cloud-index values provided by Michelson Interferometer for Passive Atmospheric Sounding (MIPAS) are used to verify and complement the simulations. The Lagrangian transport simulation of the volcanic plume is compared with MIPAS aerosol measurements and shows good agreement. Both the simulations and the observations presented in this study suggest that volcanic plumes from the Merapi eruption was transported to the south of 60 °S one month after the eruption and even further to Antarctica in the following months. This relatively fast meridional transport of volcanic aerosol was mainly driven by quasi-horizontal mixing from the TTL to the extratropical lower stratosphere and the most of the quasi-horizontal mixing occurred between the isentropic surfaces of 360 to 430 K. When the plume went to Southern Hemisphere high latitudes, the polar vortex was displaced from the South Pole, so that the volcanic plume was carried to the South Pole without penetrating the polar vortex. Although only 4% of the sulfur injected by the Merapi eruption was transported into the lower stratosphere south of 60 °S, the Merapi eruption contributed up to 8800 tons of sulfur to the Antarctic lower stratosphere. This indicates

that the long-range transport under favorable meteorological conditions enables a moderate tropical volcanic eruption to be an important remote source of sulfur for the Antarctic stratosphere.

1 Introduction

Over the past two decades, multiple volcanic eruptions injected sulfur into the upper troposphere and lower stratosphere, which has been the dominant source of the stratospheric sulfate aerosol load (Vernier et al., 2011), preventing the background level from other sources ever being seen (Solomon et al., 2011). Stratospheric sulfate aerosol mainly reflects solar radiation and absorbs infrared radiation, causing cooling of the troposphere and heating of the stratosphere. Stratospheric sulfate aerosol also has an impact on chemical processes in the lower stratosphere (Jäger and Wege, 1990; Solomon et al., 1993), in particular on polar ozone depletion (e.g. McCormick et al., 1982; Solomon et al., 1986, 1999, 2016; Portmann et al., 1996; Tilmes et al., 2008; Drdla and Müller, 2012). The presence of H_2SO_4 in the polar stratosphere in combination with cold temperatures facilitates the formation of polar stratospheric clouds (PSCs), which increase heterogeneous ozone depletion chemistry (Solomon et al., 1999; Zuev et al., 2015). Recent healing of Antarctic ozone depletion was constantly disturbed by moderate volcanic eruptions (Solomon et al., 2016). Mid- and high latitude explosive volcanic eruptions may directly influence the polar stratosphere and may have an effect on ozone depletion in the next austral spring. For example, the aerosol plume from the Calbuco eruption in 2015, including various volcanic gases, penetrated the polar vortex and caused an Antarctic ozone hole with the largest daily averaged size on record in October 2015 (Solomon et al., 2016; Ivy et al., 2017; Stone et al., 2017).

Usually, Antarctica is relatively free of local aerosol sources, but aerosol from low latitudes can reach Antarctica through long-range transport (Sand et al., 2017). Most of the sulfate found in ice cores can be attributed to volcanic eruptions (Mazzera et al., 2001; Gao et al., 2007; Sigl et al., 2015). Measurements of enhanced aerosol in the lower Antarctic stratosphere right above the tropopause were made in October/November 1983, 1984 and 1985. These enhanced aerosol number concentrations were attributed to aerosol transported to Antarctica from the eruption of the tropical volcano El Chichón in 1982 (Hofman and Rosen, 1985; Hofmann et al., 1988). Model results indicated that numerous moderate eruptions affected ozone distributions over Antarctica, including the Merapi tropical eruption in October 2010 (Solomon et al., 2016). However, due to the limit of spatial and temporal resolution of satellite data and in-situ observations, it is difficult to investigate transport process as well as the influence of the location of the eruption, the plume height and the background meteorological

conditions. Thus the transport mechanism is not well represented in present global climate models and the uncertainties of the modeled AOD in polar regions are large (Sand et al., 2017).

Mount Merapi (7.5 °S, 110.4 °E, elevation: 2930 m) is an active stratovolcano located in Central Java, Indonesia. Merapi has a long record of eruptive activities. The most recent large eruption with a volcanic explosivity index of 4 occurred between 26 October and 7 November 2010 (Pallister et al., 2013), with SO_2 emission rates being a few orders of magnitude higher than previous eruptions. Following the Merapi eruption in 2010, evidence of poleward transport of sulfate aerosol towards the Southern Hemisphere high latitudes was found in time series of aerosol measurements by the Michelson Interferometer for Passive Atmospheric Sounding (MIPAS) (Günther et al., 2018) and Cloud-Aerosol Lidar with Orthogonal Polarization (CALIOP) (Khaykin et al., 2017; Friberg et al., 2018) .

There are three main ways for transport out of the tropical tropopause layer (TTL): the deep and shallow branches of the Brewer-Dobson circulation (BDC) and horizontal mixing (Vogel et al., 2011). There is considerable year-to-year seasonal variability in the amount of irreversible transport from the tropics to high latitudes, which is related to the phase of the quasi-biennial oscillation (QBO) and the state of the polar vortex (Olsen et al., 2010). The BDC plays a large role in determining the distributions of many constituents in the extratropical lower stratosphere. The faster quasi-horizontal transport between the tropics and polar regions also significantly contributes to determining these distributions. The efficiency of transporting constituents quasi-horizontally depends on wave breaking patterns and varies with the time of the year (Toohey et al., 2011; Wu et al., 2017). Better knowledge of the transport pathways and an accurate representation of volcanic sulfur injections into the upper troposphere and lower stratosphere (UTLS) are key elements for estimating the global stratospheric aerosol budget, the cooling effects and the ozone loss linked to volcanic activity.

The aim of the present study is to reveal the transport process and the influence of meteorological conditions by combining satellite observations with model simulations in a case study. We investigate the quasi-horizontal transport by tracing the volcanic plume of the Merapi eruption from the tropics to Antarctica and quantifying its contribution to the sulfur load in the Antarctic lower stratosphere. In Sect. 2, the new Atmospheric Infrared Sounder (AIRS) SO_2 measurements (Hoffmann et al., 2014), the MIPAS aerosol measurements (Griessbach et al., 2016) and the method for reconstructing the SO_2 injection time series of the Merapi eruption are introduced. In Sect. 3 the results are presented: first, the reconstructed time series of the Merapi eruption is discussed; second, the dispersion of the Merapi plume is investigated using long Lagrangian forward trajectories initialized with the reconstructed SO_2 time series; third, the simulation results are compared with MIPAS aerosol measurements and the plume

dispersion is investigated using MIPAS aerosol detections. In Sect.4 the results are discussed and the conclusions are given in Sect. 5.

2 Satellite data, model and method

2.1 MIPAS aerosol measurements

MIPAS (Fischer et al., 2008) is an infrared limb emission spectrometer aboard the European Space Agency's (ESA's) Envisat, which provided nearly 10 years of measurements from July 2002 to April 2012. MIPAS spectral measurements cover the wavelength range from 4.15 to 14.6 microns. The vertical coverage of MIPAS nominal measurement mode during the optimized resolution phase from January 2005 to April 2012 was 7–72 km. The field of view of MIPAS was about 3 km×30 km (vertically×horizontally) at the tangent point. The extent of the measurement volume along the line of sight was about 300 km, and the horizontal distance between two adjacent limb scans was about 500 km. On each day, ~14 orbits with ~90 profiles per orbit were measured. From January 2005 to April 2012, the vertical sampling grid spacing between the tangent altitudes was 1.5 km in the UTLS and 3 km at altitudes above. In 2010 and 2011, MIPAS measured for 4 days in nominal mode followed alternately by one day in middle atmosphere mode or upper atmosphere mode. In this study, we focussed on measurements in the nominal mode.

For the aerosol detection, we used the MIPAS altitude-resolved aerosol-cloud-index (ACI) as introduced by Griessbach et al. (2016) to compare with the model simulations and to analyze the poleward transport of the Merapi volcanic plume.

ACI is the maximum value of the cloud index (CI) and aerosol index (AI):

$$\mathrm{ACI} = \max(\mathrm{CI}; \mathrm{AI}), \qquad (1)$$

The CI is an established method to detect clouds and aerosol with MIPAS. The CI is the ratio between the mean radiances around the 792 cm^{-1}, where a CO_2 line is located and the atmospheric window region around 833 cm^{-1} (Spang et al., 2001):

$$\mathrm{CI} = \frac{\overline{I_1}([788.25,796.25\ \mathrm{cm}^{-1}])}{\overline{I_2}([832.31,834.37\ \mathrm{cm}^{-1}])}, \qquad (2)$$

where $\overline{I_1}$ and $\overline{I_2}$ are the mean radiances of each window. The AI is defined as the ratio between the mean radiance around the 792 cm^{-1} CO_2 band and the atmospheric window region between 960 and 961 cm^{-1}:

$$\mathrm{AI} = \frac{\overline{I_1}([788.25,796.25\ \mathrm{cm}^{-1}])}{\overline{I_3}([960.00,961.00\ \mathrm{cm}^{-1}])}, \qquad (3)$$

where $\overline{I_1}$ and $\overline{I_3}$ are the mean radiance of each window.

The ACI is a continuous unitless value. Small ACI values indicate a high cloud or aerosol particle load and large values indicate a smaller cloud or aerosol particle load. For the CI, Sembhi et al. (2012) defined a set of variable (latitude, altitude and season) thresholds to discriminate between clear and cloudy air. The most advanced set of altitude and latitude dependent thresholds allows for the detection of aerosol and clouds with infrared extinction coefficients larger than 10^{-5} km^{-1}. For the ACI, a comparable sensitivity is achieved when using a fixed threshold value of 7 (Griessbach et al. 2016). Variations in the background aerosol are also visible with larger ACI values.

To remove ice clouds and volcanic ash from the MIPAS aerosol measurements, we first separated the data into clear air (ACI>7) and cloudy air (ACI<=7). Then we applied the ice cloud filter (Griessbach et al., 2016) and the volcanic ash and mineral dust filter (Griessbach et al., 2014) to the cloudy part and removed all ice or ash detections. However, since the ice and ash cloud filters are not sensitive to non-ice PSCs, the resulting aerosol retrieval results still contain non-ice PSCs (supercooled ternary solutions and nitric acid trihydrate). We keep the non-ice PSCs in the MIPAS retrieval results in this study to show the temporal and spatial extent of the PSCs, when and where the identification of volcanic is not possible.

2.2 AIRS

AIRS (Aumann et al., 2003) is an infrared nadir sounder with across-track scanning capabilities aboard the National Aeronautics and Space Administration's (NASA's) Aqua satellite. Aqua was launched in 2002 and operates in a nearly polar Sun-synchronous orbit at about 710 km with a period of 98 min. AIRS provides nearly continuous measurement coverage with 14.5 orbits per day and with a swath width of 1780 km it covers the globe almost twice a day. The AIRS footprint size is 13.5 km × 13.5 km at nadir and 41 km × 21.4 km for the outermost scan angles respectively. The along-track distance between two adjacent scans is 18 km. The AIRS measurements provide good horizontal resolution and make it ideal for observing the fine filamentary structures of volcanic SO_2 plumes.

In this study, we use an optimized SO_2 index (SI, unit: K) to estimate the amount of SO_2 injected into the atmosphere by the Merapi eruption in 2010. The SI is defined as the brightness temperature differences in the 7.3 μm SO_2 waveband.

$$SI = BT\left(1412.87 cm^{-1}\right) - BT\left(1371.52\ cm^{-1}\right), \qquad (1)$$

where BT is the brightness temperature measured at wavenumber ν. This SI is more sensitive to low concentrations and performs better on suppressing background interfering signals than the SI provided in

the AIRS operational data products. It is an improvement of the SI definition given by Hoffmann et al. (2014) by means of a better choice of the background channel (selecting 1412.87 cm^{-1} rather than 1407.2 cm^{-1}). The SI increases with increasing SO_2 column density and it is most sensitive to SO_2 at altitudes above 3-5 km. SO_2 injections into the lower troposphere are usually not detectable in the infrared spectral region because the atmosphere gets opaque due to the water vapor continuum. A detection threshold of 1 K was used in this study to identify the Merapi SO_2 injections. AIRS detected the Merapi SO_2 cloud from 3 November to 15 November 2010.

2.3 MPTRAC model and reconstruction of the volcanic SO_2 injection time series of the Merapi eruption

In this study, we use the highly scalable Massive-Parallel Trajectory Calculations (MPTRAC) to investigate the volcanic eruption event. In the MPTRAC model, air parcel trajectories are calculated based on numerical integration using wind fields from global meteorological reanalyses (Hoffmann et al., 2016; Rößler et al., 2018). The MPTRAC model can be driven by reanalyses, e.g., ERA-Interim, Modern-Era Retrospective Analysis for Research and Applications (MERRA) and National Centers for Environmental Prediction (NCEP)/National Center for Atmospheric Research (NCAR). Hoffmann et al. (2016) showed that ERA-interim data provides the best trade-off between accuracy and computing time. So in this study, our calculations are based on ERA-interim data.

Diffusion is modeled by uncorrelated Gaussian random displacements of the air parcels with zero mean and standard deviations $\sigma_x = \sqrt{2D_x \Delta t}$ (horizontally) and $\sigma_z = \sqrt{2D_z \Delta t}$ (vertically). D_x and D_z are the horizontal and vertical diffusivities respectively, and Δt is the time step for the trajectory calculations. For the Merapi simulation, D_x and D_z were set to 50 $m^2 s^{-1}$ and 0 $m^2 s^{-1}$ in the troposphere and 0 $m^2 s^{-1}$ and 0.1 $m^2 s^{-1}$ in the stratosphere, respectively. In addition, sub-grid scale wind fluctuations, which are particularly important for long-range simulations, are simulated by a Markov model (Stohl et al., 2005; Hoffmann et al., 2016). Loss processes of chemical species, SO_2 in our case, are simulated based on an exponential decay of the mass assigned to each air parcel. In the stratosphere, a constant half lifetime of 7 days was assumed for SO_2. Considering that the Merapi eruption occurred in the humid tropics with a high concentration of hydroxyl radical, a half lifetime of 2.5 days was assumed for the troposphere.

To estimate the time- and altitude-resolved SO_2 injections, we follow the approach of Hoffmann et al. (2016) and Wu et al. (2017) and use backward trajectories calculated with the MPTRAC model together with AIRS SO_2 measurements. Measurements from 3 to 7 November 2010 were used to estimate the SO_2 injection during the explosive eruption. Since the AIRS measurements do not provide altitude

information, we established a column of air parcels at each AIRS SO_2 detection. The vertical range of the column was set to 0–25 km, covering the possible vertical dispersion range of the SO_2 plume in the first few days. The AIRS footprint size varies between 14 and 41 km, hence in the horizontal direction, we chose an average of 30 km as the full width at half maximum for the Gaussian scatter of the air parcels. In our simulations, a fixed total number of 100,000 air parcels was assigned to all air columns and the number of air parcels in each column was scaled linearly proportional to the SO_2 index. Then backward trajectories were calculated for all air parcels, and trajectories that were at least 2 days but no more than 5 days long and that passed the volcano domain were recorded as emissions of Merapi. The volcano domain was defined by means of a search radius of 75 km around the location of the Merapi and 0–20 km in the vertical direction, covering all possible injection heights. Sensitivity experiments have been conducted to optimize these pre-assigned parameters to obtain the best simulation results. Our estimates of the Merapi SO_2 injection are shown in Sect. 3.

Starting with the reconstructed altitude-resolved SO_2 injection time series, the transport of the Merapi plume is simulated for 6 months. The trajectory calculations are driven by the ERA–Interim data (Dee et al., 2011) interpolated on a $1° \times 1°$ horizontal grid on 60 model levels with the vertical range extending from the surface to 0.1 hPa. The ERA–Interim data are provided at 00, 06, 12 and 18 UTC. Outputs of model simulations are given every 3 hours at 00, 03, 06, 09, 12, 15, 18 and 21 UTC. The impact of different meteorological analyses on MPTRAC simulations was assessed by Hoffmann et al. (2016, 2017). In both studies the ERA–Interim data showed good performance.

3 Results

3.1 Meteorological background conditions in Antarctica

The Merapi eruption in October 2010 occurred during the seasonal transition from austral spring to summer when the polar vortex typically weakens and the ozone hole shrinks. The poleward transport from the tropics to the polar region is known to be modulated by the phase of the QBO and the state of the polar vortex. Just before the Merapi eruption in 2010, the QBO switched from the easterly phase to the westerly phase. The westerly phase of the QBO promotes meridional transport from the tropics to subtropics, especially into the winter hemisphere (O'Sullivan and Dunkerton, 1997; Shuckburgh et al., 2001; Jäger, 2005). However, it also results in zonal wind acceleration at the high latitudes (Holton and Tan, 1980; Watson and Gray, 2014) and a less dynamically disturbed polar vortex (Baldwin and

Dunkerton, 1999; Anstey and Shepherd, 2014), which will make it less possible for air parcels to penetrate the polar vortex.

Figure 1 depicts the meteorological conditions at the polar lower stratosphere (150hPa, ~12km) after the eruption. The minimum temperature south of 50 ℃ (Fig. 1a) was much lower than the climatological mean during mid-November to mid-December but still higher than the low temperature necessary for the existence of PSCs. The polar mean temperature in Fig. 1b, defined as the temperature averaged over latitudes south of 60 ℃, stayed lower than the climatological mean from November 2010 until February 2011. Corresponding to the low temperatures, the average zonal wind speed at 60 ℃ (Fig. 1c) was significantly larger than the climatological mean value from November 2010 to mid-January 2011. The eddy heat flux in Fig. 1d is the product of meridional wind departures and temperature departures from the respective zonal mean values. A more negative value of the eddy heat flux indicates that wave systems are propagating into the stratosphere and are warming the polar region (Edmon et al., 1980; Newman and Nash, 2000). There is a strong anticorrelation between temperature and the 45-day average of the eddy heat flux lagged prior to the temperature. Compared with the climatological mean state, the polar vortex was more disturbed during mid-July to end of August, but from mid-October to late November, the heat flux was much smaller than the long-term average, which meant a reduction in dynamical disturbances. Considering the temperature, the subpolar wind speed and the heat flux, the polar vortex was colder and stronger in November and early December 2010 than it was at the same time in other years (see Fig. 1e). Consistent with the large wind speed and low temperature, the polar vortex was stable after the Merapi eruption until early December 2010. Afterwards, it shrunk abruptly and was destructed in by mid-January 2011. In accordance with the strength of the polar vortex, in November and early December 2010 the ozone hole area in Fig. 1f, defined as the region of ozone values below 220 Dobson Units (DU) located south of 40 ℃, was larger than the climatological mean. Meanwhile, the low polar mean temperature and stable polar vortex resulted in a long-lasting ozone hole, which disappeared in the last week of December. The polar vortex broke down by mid-January 2011 when the subpolar wind speed decreased below 15 m/s (Fig. 1c).

3.2 Merapi eruption and SO_2 injection time series

According to the chronology of the Merapi eruption that combined satellite observations from AIRS, the Infrared Atmospheric Sounding Interferometer (IASI), the Ozone Monitoring Instrument (OMI) and a limited number of Ground-based ultra-violet Differential Optical Absorption Spectroscopy (DOAS) measurements (Surono et al., 2012), the explosive eruption first occurred between 10:00 and 12:00 UTC

on 26 October and this eruption generated an ash plume that reached 12 km altitude. A period of relatively small explosive eruptions continued from 26 October to 31 October. On 3 November, the eruptive intensity increased again accompanied by much stronger degassing and a series of explosions. The intermittent explosive eruptions occurred during 4–5 November with the climactic eruption on 4 November, producing an ash column that reached up to 17 km altitude. From 6 November, explosive activity decreased slowly and the degassing declined.

Figure 2 shows the time- and altitude-resolved SO_2 injections of the Merapi eruption retrieved using the AIRS SO_2 index data and the backward-trajectory approach. It agrees well with the chronology of the Merapi eruption as outlined by Surono et al. (2012). SO_2 was injected into altitudes below 8 km during the initial explosive eruptions on 26–30 October. Starting from 31 October the plume reached up to 12 km. During 1–2 November the SO_2 injections into altitudes below 12 km continued but the mass was less than the mass at the initial phase. On 3 November the intensity increased again and peaked on 4 November. Before 3 November the reconstruction indicates a minor fraction of SO_2 right above the tropopause. The SO_2 above the tropopause is not reported in the study Surono et al. (2012), but is quite robust in our simulations. Further, CALIOP profiles from 27 October 2010 to 10 November 2010 show that some dust appeared at the height from about 14 to 18 km around Mount Merapi on 2, 3, 5 November 2010, and between 3 and 17 km on 6 November 2010. It could be a fraction of volcanic plume elevated by the updraft in the convection associated with the tropical storm Anggrek. The center of the tropical storm Anggrek was on the Indian ocean about 1000 km southwest of the Mount Merapi. The SO_2 mass above the tropopause is very small compared with the total SO_2 mass.

To study the long-range transport of the Merapi plume, we initialized 100,000 air parcels as the SO_2 injection time series shown in Fig. 2. A total SO_2 mass of 0.44 Tg is assigned to these air parcels as provided in Surono et al. (2012). Then the trajectories are calculated forward for 6 months. Here, we only considered the plume in the upper troposphere and stratosphere where the lifetime of both SO_2 and sulfate aerosol is longer than their lifetime in the lower troposphere. Further, the SO_2 was converted into sulfate aerosol within a few weeks (von Glasow et al., 2009; also confirmed by the AIRS SO_2 and MIPAS aerosol data), and we assumed that the sulfate aerosol remained collocated with the SO_2 plume.

Figure 3 shows the evolution of the simulated Merapi plume and compares the plume altitudes to the aerosol top altitudes measured by MIPAS between 7 and 23 November. Immediately after the eruption, the majority of the plume moved towards the southwest and was entrained by the circulation of the tropical storm Anggrek. After Anggrek weakened and dissipated, the majority of the plume parcels in the upper troposphere moved eastward and those in the lower stratosphere moved westward. In general,

the altitudes of the simulated plume agree with the MIPAS measurements. The remaining discrepancies of air parcel altitudes being higher than the altitudes of MIPAS aerosol detections can be attributed to the fact that the MIPAS tends to underestimate aerosol top cloud altitudes, which is about 0.9 km in case of low extinction aerosol layers and can reach down to 4.5 km in case of broken cloud conditions (Höpfner et al., 2009).

3.3 Lagrangian simulation and satellite observation of the transport of the Merapi plume

The early plume evolution until about one month after the initial eruption is shown on the maps in Fig. 3 together with MIPAS measurements of volcanic aerosol (only aerosol detections with ACI<7 are shown). Within about one month after the initial eruption, the plume is nearly entirely transported around the globe in the tropics, moving west at altitudes of about 17 km. The lower part of the plume, below about 17 km is transported south-eastward and reaches latitudes south of 30 °S by mid-November. The simulated long-term transport of the Merapi plume is illustrated in Fig. 4, showing the proportion of air parcels reaching a latitude-altitude bin every half a month.

The simulation results show that during the first month after the eruption (Fig. 4a–b), the majority of the plume was transported southward roughly along the isentropic surfaces. The most significant pathway is above the core of the subtropical jet in the Southern Hemisphere. However, because of the transport barrier of the polar jet during austral spring, the plume was confined to the north of 60 °S. In December 2010 (Fig. 4c–d), a larger fraction of the plume was transported southward above the subtropical jet core and deep into the polar region south of 60 °S as the polar jet broke down. Until the end of January 2011, the majority of the plume entered the mid- and high latitudes in the Southern Hemisphere. Substantial quasi-horizontal poleward transport from the TTL towards the extratropical lowermost stratosphere (LMS) in Antarctica was found from November 2010 to February 2011 (Fig. 4a–h), approximately between 350 and 480 K (~10–20 km). In March 2011(Fig. 4i–j), the proportion of the plume that went across 60 °S stopped increasing and the maxima of the proportion descended below 380 K. Besides this transport towards Antarctica, a slow upward transport could also be seen. The top of the simulated plume was below the 480 K isentropic surface at around 18 km in Fig. 4a and then the top of the plume went up to 25 km five months later in Fig. 4j. This slow upward transport was mainly located in the tropics and can be attributed to the tropical upwelling.

MIPAS aerosol detections (ACI values) are used to compare with the simulations. Figure 5 displays the time-latitude section of the median value of the MIPAS ACI within the vertical range of 12 and 18 km from January 2005 to April 2012, covering the TTL and the LMS. Only ACI values from 4 to 8 are

shown in Fig.5. The MIPAS data show all the key events that contributed to the aerosol load in the UTLS, i.e., moderate volcanic eruptions from 2005 to 2012 and one large bushfire in 2009, as well as the subsequent dispersion and change of aerosol load over time. The poleward transport of aerosol from the Merapi eruption in 2010, marked by the red triangle in Fig. 5, caused the most long-lasting aerosol signals in the Southern Hemisphere mid- and high latitudes. The small ACI values in the winter months of both hemispheres are attributed to the non-ice PSCs.

To show the change of aerosol load in the Southern Hemisphere due to the Merapi eruption, we first removed the seasonal cycle from the MIPAS aerosol data. Therefore, we selected a time period from November 2007 to March 2008 with no major SO_2 emission in the Southern Hemisphere UTLS (as shown in Fig. 5) as a "reference state". We calculated the biweekly median ACI between November 2010 and March 2011 and subtracted it from the biweekly ACI median of the "reference state". The results are shown in Fig. 6. Since in the MIPAS retrievals, small ACI values represent large aerosol extinction coefficients and large ACI values represent small aerosol extinction coefficients, in Fig. 6 the positive values indicate an increase of the aerosol load and negative values indicate a decrease of the aerosol load. Reference time periods from November 2003 to March 2004 and November 2005 to March 2006 were also tested and they all showed qualitatively comparable results.

In the first half of November, the zonal median (Fig. 6a) does not show a signal of the Merapi eruption, because during the initial time period, the plume was confined to longitudes around the volcano (see Fig. 3), and the MIPAS tracks did not always sample the maximum concentration, so the median ACI values are large (low concentration or clear air). In the second half of November, the plume was transported zonally around the globe, and hence the largest aerosol increase appeared in the upper troposphere at the latitude of the Mount Merapi (Fig. 6b) and then moved quasi-horizontally southward into the UTLS region at ~30–40 °S (Figs. 6c–d), confirming the simulation result in Fig. 4c–d. The increase of the aerosol load south of 60 °S started to become prominent after December 2010, and the poleward movement is most obvious above the 350 K isentropic surface (Figs. 6e–h). The observations confirm the temporal and spatial characteristics of poleward movement of the aerosol in the simulation in Fig. 4. Later in March 2011, the enhanced aerosol load in the tropics phased out and the aerosol load maxima descended to around the 350 K isentropic surface.

However, the background aerosol level in the tropical upper troposphere and stratosphere is constantly disturbed by tropical and extratropical volcanic eruptions. The reference time period we chose (November 2007 to March 2008) is relatively free of large aerosol sources in the Southern Hemisphere, but the aerosol load in the tropical stratosphere is already elevated by previous volcanic eruptions, e.g.,

Soufriere Hills (May 2006), Tavurvur (October 2006), Piton de la Fournaise (April 2007), Jebel at Tair (September 2007). So the change of the aerosol load in Fig.6 underestimates the increase of aerosol load in the tropical stratosphere after the Merapi eruption. The slow upward transport in the tropics shown in Fig. 4 is about 7 km in five months. It is not visible in Fig. 6, but time series of the MIPAS measurements in the tropical stratosphere reveals a similar upward transport trend (see Fig. A1 in the appendix).

3.4 Quasi-horizontal transport from the tropics to Antarctica

The MPTRAC simulations and the MIPAS measurements show the transport in the "surf zone" that reaches from the subtropics to high latitudes (Holton et al., 1995), where air masses are affected by both fast meridional transport and the slow BDC. The reconstructed emission time series in Fig. 2 and the MIPAS aerosol measurements in Figs. 3 and 6 show that the volcanic plume was injected into the TTL. Hence, the main transport pathway towards Antarctica is the quasi-horizontal mixing in the lower extratropical stratosphere between 350 and 480 K (see Fig. 4 and Fig. 6). Figure 7 illustrates how the volcanic plume between 350 and 480 K approached Antarctica over time. Kunz et al. (2015) derived a climatology of potential vorticity (PV) streamer boundaries on isentropic surfaces between 320 and 500K using ERA-Interim reanalyses for the time period from 1979 to 2011. This boundary is derived from the maximum product of the meridional PV gradient and zonal wind speed on isentropic surfaces, which identifies a PV contour that best represents the dynamical discontinuity on each isentropic surface. It can be used as an isentropic transport barrier and to determine the isentropic cross-barrier transport related to Rossby wave breaking (Haynes and Shuckburgh, 2000; Kunz et al., 2011a,b). In Fig. 7, gray dashed lines mark PV boundaries on the 350 K isentropic surface. On isentropic surfaces below 380 K, the PV boundaries represent the dynamical discontinuity near the core of the subtropical jet stream. Isentropic transport of air masses across these boundaries indicates exchange between the tropics and extratropics due to Rossby wave breaking. On isentropic surfaces above 400 K, PV boundaries represent a transport barrier in the lower stratosphere, in particular, due to the polar vortices in winter (Kunz et al., 2015). For comparison, we also show the 220 DU contour lines of ozone column density (black isolines in Fig. 7), obtained from OMI on satellite Aura, indicating the boundary and size of the ozone hole. The PV boundary on 480 K is in most cases collocated with the area of the ozone hole, showing that both quantities provide a consistent representation of the area of the polar vortex.

The Merapi volcanic plume first reached the transport barrier on the 350 K isentropic surface in mid-November and went close to the transport barrier on the 480 K isentropic surface in December. The

long-lasting polar vortex prevented the volcanic plume from crossing the transport barrier at 480 K in early December. But from mid-December, the polar vortex became more disturbed and displaced from the South Pole, resulting in a shrinking ozone hole. As mentioned in Sect.3.1, the ozone hole broke down at the end of December 2010 and the polar vortex broke down by mid-January 2011.

The fraction of the volcanic plume that crosses the individual transport barriers or the latitude of 60 °S on each isentropic surface are shown in Fig. 8. In both cases, the proportion increased from November 2010 to January 2011. In November and December 2010 the largest plume transport across the transport barriers occurred between the 360 and 430 K isentropic surface (Fig. 8a), with a peak at 380–390 K. In January and February 2011 the peak was slightly elevated to 390–400 K. In November 2010, the volcanic plume did not cross the 480 K transport barrier of the polar vortex at high altitudes, especially above about 450 K. The high-latitude fraction increased from December 2010 to February 2011 as the weakening of the polar vortex made the transport barrier more permeable. In March and April 2011, the total proportion decreased and the peak descended to 370 K in March and further to 360 K in April. The proportion of the volcanic plume south of 60 °S (Fig. 8b) increased slightly from November to December 2010, and then increased significantly from December 2010 to January and February 2011 at all altitudes as the polar vortex displaced and broke down. Finally, the transport to the south of 60 °S started to decrease in March 2011. From November 2010 to February 2011 the peak was around 370–400 K, but in March and April 2011 the peak resided around 350–370 K.

Figure 9a summarizes the simulated poleward transport of the volcanic plume between the isentropic surfaces of 350 and 480 K from November 2010 to March 2011 and the percentage of air parcels south of 60 °S. The percentage was calculated by dividing the number of SO_2 parcels between 350 and 480 K south of 60 °S by the total number of SO_2 parcels released for the forward trajectory simulation. Figure 9b demonstrates the change of aerosol load in the same vertical range for MIPAS aerosol detections. As in Sect. 3.3, we calculated the median ACI between November 2010 and March 2011 and subtracted it from the ACI median of the "reference state" between November 2007 and March 2008. The simulations show that the plume reached 60 °S in December 2010. Correspondingly, the aerosol load south of 60 °S was elevated. The percentage fluctuated, but increased until the end of February 2011, with a maximum percentage of about 4%. A steep increase occurred from mid-December 2010 to end of January 2011, following the displacement and breakdown of the polar vortex. The elevated aerosol load south of 60 °S decreased from March 2011, and part of the plume descended to altitudes below 350 K as shown by Fig. 8b. The MIPAS aerosol measurements in Fig. 9b where a positive ACI difference indicates an increase in the aerosol load, confirm the simulated transport pattern in Fig. 9a. Overall,

simulations and observations indicate the largest increase of the aerosol load in the tropics and mid-latitudes, but also show a significant enhancement over the south polar region after December 2010.

4 Discussion

The results presented in Sect. 3 show that the main transport pathway for the poleward transport of the Merapi volcanic plume to Antarctica was between the isentropic surfaces of 350 and 480 K (about 10 to 20 km), covering the TTL and the lower stratosphere at mid- and high latitudes. For this long-range transport on timescales of a few months, fast isentropic transport associated with quasi-horizontal mixing played the main role in transporting the volcanic aerosol from the TTL to the Antarctic lower stratosphere. The Merapi eruption occurred in austral spring and fast poleward transport was facilitated by the weakening of the subtropical jet and active Rossby wave breaking events. The polar vortex was relatively stable when the Merapi erupted, but by the time the volcanic plume reached the south polar region, the polar vortex was displaced from the South Pole and distorted because more wave systems propagated into the polar stratosphere and warmed the polar region, so that the volcanic plume was transported from the tropics deep into Antarctica.

Based on the simulation results in Sect. 3.4, up to 4% of the volcanic plume air parcels was transported from the TTL to the lower stratosphere in the south polar region till the end of February 2011. Based on previous research on the Merapi case, we assigned a total mass of 0.44 Tg to all SO_2 parcel released, which means the Merapi eruption contributed about 8800 tons of sulfur to the polar lower stratosphere within 4 months after the eruption, assuming that the sulfate aerosol converted from the SO_2 remained in the plume. Although the MPTRAC model we used to simulate the 3D movement of air parcels in the volcanic plumes can estimate the conversion of SO_2 to sulfate aerosol during the transport process, however, it does not resolve the chemical processes of aerosol formation. Hence, the estimated 8800 tons of sulfur are the maximum value since processes as e.g. wet deposition remove sulfur from the atmosphere. But in the lower stratosphere, the atmosphere is relatively dry and clean compared with the lower troposphere, so the sulfate aerosol has a lower posibility to interact with clouds or to be washed out. In fact, in the polar lower stratosphere usually sedimentation and downward transport by the BDC are the main removal processes. Clouds and washout processes usually cannot be expected in the lower stratosphere. However, the amount of sulfate aerosol in the plume could also be affected by other mechanisms that speed up the loss of sulfur, for example, coagulation in the volcanic plume, or the

absorption of sulfur onto fine ash particles. But for the moderate eruption Merapi in 2010, sulfuric particle growth may not be as significant as it is in a large volcanic eruption, so the scavenging efficiency of sulfur will be low. So generally, our estimation may be larger than the actual value, but this number may be considered as the upper limit of the contribution of the Merapi eruption.

Besides, a kinematic trajectory model like MPTRAC, in which reanalysis vertical wind is used as vertical velocity, typically shows higher vertical dispersion in the equatorial lower stratosphere compared with a diabatic trajectory model (Schoeberl et al., 2003; Wohltmann and Rex, 2008; Liu et al., 2010; Ploeger et al., 2010, 2011). However, the ERA–Interim reanalysis data used in this study to drive the model may constrain the vertical dispersion much better than older reanalyses (Liu et al., 2010; Hoffmann et al., 2017). The meridional transport in this study was mainly quasi-horizontal transport in the mid- and high latitude UTLS region, so the effect of the vertical speed scheme is limited.

The aerosol transported to the polar lower stratosphere will finally descend with the downward flow and have a chance to become a nonlocal source of sulfur for Antarctica by dry and wet deposition, following the general precipitation patterns. Quantifying the sulfur deposition flux onto Antarctica is beyond the scope of this study, though. Model results of Solomon et al. (2016) suggest that the Merapi eruption made a small but significant contribution to the ozone depletion over Antarctica in the vertical range of 100–200 hPa, roughly between 10 and 14 km. This altitude range is in agreement with our results, where we found transport into the Antarctic stratosphere between 10 and 20 km. When the volcanic plume was transported to Antarctica in December 2010, the polar synoptic temperature at these low height levels was already too high for the formation of PSCs. The additional ozone depletion found by Solomon et al. (2016) together with the fact that sulfate aerosol was transported from the Merapi into the Antarctic stratosphere between November and February where no PSCs are present during polar summer, may support the study that suggested that significant ozone depletion can also occur on cold binary aerosol (Drdla and Müller, 2012). The Merapi eruption in 2010 could be an interesting case study for more sophisticated geophysical models to study the aftermath of volcanic eruptions on polar processes.

5 Summary and conclusion

In this study, we analyzed the poleward transport of volcanic aerosol released by the Merapi eruption in 2010 from the tropics to the Antarctic lower stratosphere. The analysis was based on AIRS SO_2 measurements, MIPAS sulfate aerosol detections and MPTRAC transport simulations. First, we

estimated altitude-resolved SO_2 injection time series during the explosive eruption period using AIRS data together with a backward trajectory approach. Second, the long-range transport of the volcanic plume from the initial eruption to April 2011 was simulated based on the derived SO_2 injection time series. Then the evolution and the poleward migration of the volcanic plume were analyzed using the forward trajectory simulations and MIPAS aerosol measurements. The simulations are compared with and verified by the MIPAS aerosol measurements.

Results of this study suggest that the volcanic plume from the Merapi eruption was transported from the tropics to the south of 60 °S within a time scale of one month. Later on, in the UTLS region a fraction of the volcanic plume (~4%) crossed 60 °S, even further to Antarctica until the end of February 2011. As a result, the aerosol load in the Antarctic lower stratosphere was significantly elevated. This relatively fast meridional transport of volcanic aerosol was mainly carried out by quasi-horizontal mixing from the TTL to the extratropical lower stratosphere. Based on the simulations, most of the quasi-horizontal mixing occurred between the isentropic surfaces of 360 to 430 K. This transport was in turn facilitated by the weakening of the subtropical jet and the breakdown of the polar vortex in the seasonal transition from austral spring to summer. The polar vortex in late austral spring 2010 was relatively strong compared to the climatological mean state. However, in December 2010 the polar vortex was displaced off the South Pole and later on broke down when the plume went to the high latitudes, so the volcanic plume did not penetrate the polar vortex but entered the South Pole with the breakdown of the polar vortex.

Overall, after the Merapi eruption, the largest increase of aerosol load occurred in the Southern Hemisphere midlatitudes and a relatively small but significant fraction of the volcanic plume (4%) was further transported to the Antarctic lower stratosphere within 4 months after the eruption. As a maximum estimation, it contributed up to 8800 tons of sulfur to the Antarctic stratosphere, which indicates that long-range transport under favorable meteorological conditions can make moderate tropical volcanic eruptions an important remote source of sulfur to Antarctica.

Code and data availability. AIRS data are distributed by the NASA Goddard Earth Sciences Data Information and Services Center. The SO_2 index data used in this study (Hoffmann et al., 2014) are available for download at https://datapub.fz-juelich.de/slcs/airs/volcanoes/ (last access: 26 March 2018). Envisat MIPAS Level-1B data are distributed by the European Space Agency. The ERA–Interim reanalysis data (Dee et al., 2011) were obtained from the European Centre for Medium-Range Weather Forecasts. The code of the Massive-Parallel Trajectory Calculations (MPTRAC) model is available

under the terms and conditions of the GNU General Public License, Version 3 from the repository at https://github.com/slcs-jsc/mptrac (last access: 31 January 2018).

Appendix

Figure A1 shows the 9-day running median values of the MIPAS ACI between 10 °N and 10 °S. During the time period of the reference state (November 2007 to March 2008), the aerosol load in the tropical stratosphere from 20 to 25 km is elevated by a couple of previous volcanic eruptions. The aerosol load at this vertical range after the Merapi eruption in 2010 is apparently smaller compared with the reference state.

It should be noted that there are semiannual data oscillations in the MIPAS ACI aerosol detections. This periodic pattern is caused by the aerosol index that uses the atmospheric window region between 960 and 961 cm^{-1}. Around this window region, there are CO_2 laser bands. Due to the semiannual temperature changes at about 50 km (semiannual oscillation), the CO_2 radiance contribution to this window region also oscillates. As this window is generally very clear of other trace gases, this oscillation is not only visible at higher altitudes but also in the lower stratosphere, because the satellite line of sight looks through the whole layer (Wu et al., 2017). But even though with the semiannual data oscillations, the upward transport of the aerosol from the Merapi eruption in the tropical stratosphere is still visible and the vertical speed is estimated to about 7–8 km in five months (November 2010 to March 2011).

Competing interests. The authors declare that they have no conflict of interest.

Acknowledgments. This work was supported by National Natural Science Foundation of China under grant no. 41605023, China Postdoctoral Science Foundation under grant no. 2018T110131 and International Postdoctoral Exchange Fellowship Program 2015 under grant no. 20151006.

Reference

Anstey, J. A., and Shepherd, T. G.: High-latitude influence of the quasi-biennial oscillation, Q. J. R. Meteorol. Soc., 140, 1-21, doi: 10.1002/qj.2132, 2014.

Aumann, H. H., Chahine, M. T., Gautier, C., Goldberg, M. D., Kalnay, E., McMillin, L. M., Revercomb, H., Rosenkranz, P. W., Smith, W. L., Staelin, D. H., Strow, L. L., and Susskind, J.: AIRS/AMSU/HSB on the Aqua mission: design, science objectives, data products, and processing systems, IEEE Trans. Geosci. Remote Sens., 41, 253-264, doi: 10.1109/TGRS.2002.808356, 2003.

Baldwin, M. P., and Dunkerton, T. J.: Propagation of the Arctic Oscillation from the stratosphere to the troposphere, J. Geophys. Res. Atmos., 104, 30937-30946, doi: 10.1029/1999JD900445, 1999.

Bosilovich, M., Akella, S., Coy, L., Cullather, R., Draper, C., Gelaro, R., Kovach, R., Liu, Q., Molod, A., Norris, P., Wargan, K., Chao, W., Reichle, R., Takacs, L., Vikhliaev, Y., Bloom, S., Collow, A., Firth, S., Labow, G., Partyka, G., Pawson, S., Reale, O., Schubert, S. D., and Suarez, M.: MERRA-2: Initial evaluation of the climate, Tech. rep., NASA, series on Global Modeling and Data Assimilation, NASA/TM–2015-104606, Vol. 43, 2015.

Dee, D. P., Uppala, S. M., Simmons, A. J., Berrisford, P., Poli, P., Kobayashi, S., Andrae, U., Balmaseda, M. A., Balsamo, G., Bauer, P., Bechtold, P., Beljaars, A. C. M., van de Berg, L., Bidlot, J., Bormann, N., Delsol, C., Dragani, R., Fuentes, M., Geer, A. J., Haimberger, L., Healy, S. B., Hersbach, H., Holm, E. V., Isaksen, L., Kallberg, P., Kohler, M., Matricardi, M., McNally, A. P., Monge-Sanz, B. M., Morcrette, J. J., Park, B. K., Peubey, C., de Rosnay, P., Tavolato, C., Thepaut, J. N., and Vitart, F.: The ERA-Interim reanalysis: configuration and performance of the data assimilation system, Q. J. R. Meteorol. Soc., 137, 553-597, doi: 10.1002/qj.828, 2011.

Drdla, K., and Müller, R.: Temperature thresholds for chlorine activation and ozone loss in the polar stratosphere, Ann. Geophys., 30, 1055-1073, doi: 10.5194/angeo-30-1055-2012, 2012.

Edmon, H. J. J., Hoskins, B. J., and McIntyre, M. E.: Eliassen-Palm Cross Sections for the Troposphere, J. Atmos. Sci., 37, 2600-2616, doi: 10.1175/1520-0469(1980)037<2600:epcsft>2.0.co;2, 1980.

Fischer, H., Birk, M., Blom, C., Carli, B., Carlotti, M., von Clarmann, T., Delbouille, L., Dudhia, A., Ehhalt, D., Endemann, M., Flaud, J. M., Gessner, R., Kleinert, A., Koopman, R., Langen, J., López-Puertas, M., Mosner, P., Nett, H., Oelhaf, H., Perron, G., Remedios, J., Ridolfi, M., Stiller, G., and Zander, R.: MIPAS: an instrument for atmospheric and climate research, Atmos. Chem. Phys., 8, 2151-2188, doi: 10.5194/acp-8-2151-2008, 2008.

Friberg, J., Martinsson, B. G., Andersson, S. M., and Sandvik, O. S.: Volcanic impact on the climate – the stratospheric aerosol load in the period 2006–2015, Atmos. Chem. Phys., 18, 11149-11169, doi: 10.5194/acp-18-11149-2018, 2018.

Gao, C., Oman, L., Robock, A., and Stenchikov, G. L.: Atmospheric volcanic loading derived from bipolar ice cores: Accounting for the spatial distribution of volcanic deposition, J. Geophys. Res. Atmos., 112, D09109, doi: 10.1029/2006JD007461, 2007.

Griessbach, S., L. Hoffmann, R. Spang and M. Riese: Volcanic ash detection with infrared limb sounding: MIPAS observations and radiative transfer simulations, Atmos. Meas. Tech. 7, 1487-1507, doi: 10.5194/amt-7-1487-2014, 2014.

Griessbach, S., Hoffmann, L., Spang, R., von Hobe, M., Müller, R., and Riese, M.: Infrared limb emission measurements of aerosol in the troposphere and stratosphere, Atmos. Meas. Tech., 9, 4399-4423, doi:10.5194/amt-9-4399-2016, 2016.

Günther, A., Höpfner, M., Sinnhuber, B. M., Griessbach, S., Deshler, T., von Clarmann, T., and Stiller, G.: MIPAS observations of volcanic sulphate aerosol and sulphur dioxide in the stratosphere, Atmos. Chem. Phys., 2017, 1-32, doi: 10.5194/acp-18-1217-2018, 2018.

Haynes, P., and Shuckburgh, E.: Effective diffusivity as a diagnostic of atmospheric transport: 2. Troposphere and lower stratosphere, J. Geophys. Res. Atmos., 105, 22795-22810, doi: 10.1029/2000JD900092, 2000.

Heng, Y., Hoffmann, L., Griessbach, S., Rößler, T., and Stein, O.: Inverse transport modeling of volcanic sulfur dioxide emissions using large-scale simulations, Geosci. Model Dev., 9, 1627-1645, doi:10.5194/gmd-9-1627-2016, 2016.

Hoffmann, L., Griessbach, S., and Meyer, C. I.: Volcanic emissions from AIRS observations: detection methods, case study, and statistical analysis, in: Remote Sensing of Clouds and the Atmosphere XIX and Optics in Atmospheric Propagation and Adaptive Systems XVII, edited by: Comeron, A.,

Kassianov, E. I., Schafer, K., Picard, R. H., Stein, K., and Gonglewski, J. D., Proceedings of SPIE, Spie-Int Soc Optical Engineering, Bellingham, doi: 92421410.1117/12.2066326, 2014.
Hoffmann, L., Hertzog, A., Rößler, T., Stein, O., and Wu, X.: Intercomparison of meteorological analyses and trajectories in the Antarctic lower stratosphere with Concordiasi superpressure balloon observations, Atmos. Chem. Phys., 17, 8045-8061, doi: 10.5194/acp-17-8045-2017, 2017.
Hoffmann, L., Rößler, T., Griessbach, S., Heng, Y., and Stein, O.: Lagrangian transport simulations of volcanic sulfur dioxide emissions: Impact of meteorological data products, J. Geophys. Res. Atmos., 121, 4651-4673, doi: 10.1002/2015JD023749, 2016.
Hofmann, D. J., Rosen, J. M., and Gringel, W.: Delayed production of sulfuric acid condensation nuclei in the polar stratosphere from El Chichon volcanic vapors, J. Geophys. Res. Atmos., 90, 2341-2354, doi:10.1029/JD090iD01p02341, 1985.
Hofmann, D. J., Rosen, J. M., and Harder, J. W.: Aerosol measurements in the winter/spring Antarctic stratosphere: 1. Correlative measurements with ozone, J. Geophys. Res. Atmos., 93, 665-676, doi:10.1029/JD093iD01p00665, 1988.
Holton, J. R., Haynes, P. H., McIntyre, M. E., Douglass, A. R., Rood, R. B., and Pfister, L.: Stratosphere-troposphere exchange, Rev. Geophys., 33, 403-439, doi: 10.1029/95RG02097, 1995.
Holton, J. R., and Tan, H. C.: The Influence of the Equatorial Quasi-Biennial Oscillation on the Global Circulation at 50 mb, J. Atmos. Sci., 37, 2200-2208, doi: 10.1175/1520-0469(1980)037<2200:tioteq>2.0.co;2, 1980.
Höpfner, M., Pitts, M. C., and Poole, L. R.: Comparison between CALIPSO and MIPAS observations of polar stratospheric clouds, J. Geophys. Res. Atmos., 114, doi:10.1029/2009JD012114, 2009.
Ivy, D. J., Solomon, S., Kinnison, D., Mills, M. J., Schmidt, A., and Neely, R. R.: The influence of the Calbuco eruption on the 2015 Antarctic ozone hole in a fully coupled chemistry-climate model, Geophys. Res. Lett., 44, 2556-2561, doi: 10.1002/2016GL071925, 2017.
Jäger, H.: Long-term record of lidar observations of the stratospheric aerosol layer at Garmisch-Partenkirchen, J. Geophys. Res. Atmos., 110, D08106, doi: 10.1029/2004JD005506, 2005.
Jäger, H., and Wege, K.: Stratospheric ozone depletion at northern midlatitudes after major volcanic eruptions, J. Atmos. Chem., 10, 273-287, doi: 10.1007/bf00053863, 1990.
Kalnay, E., Kanamitsu, M., Kistler, R., Collins, W., Deaven, D., Gandin, L., Iredell, M., Saha, S., White, G., Woollen, J., Zhu, Y., Chelliah, M., Ebisuzaki, W., Higgins, W., Janowiak, J., Mo, K. C., Ropelewski, C., Wang, J., Leetmaa, A., Reynolds, R., Jenne, R., and Joseph, D.: The NCEP/NCAR 40-Year Reanalysis Project, Bull. Am. Meteorol. Soc. 77, 437-472, doi: 10.1175/1520-0477(1996)077<0437:tnyrp>2.0.co;2, 1996.
Khaykin, S. M., Godin-Beekmann, S., Keckhut, P., Hauchecorne, A., Jumelet, J., Vernier, J. P., Bourassa, A., Degenstein, D. A., Rieger, L. A., Bingen, C., Vanhellemont, F., Robert, C., DeLand, M., and Bhartia, P. K.: Variability and evolution of the midlatitude stratospheric aerosol budget from 22 years of ground-based lidar and satellite observations, Atmos. Chem. Phys., 17, 1829-1845, doi: 10.5194/acp-17-1829-2017, 2017.
Kunz, A., Konopka, P., Müller, R., and Pan, L. L.: Dynamical tropopause based on isentropic potential vorticity gradients, J. Geophys. Res. Atmos., 116, D01110, doi: 10.1029/2010JD014343, 2011a.
Kunz, A., Pan, L. L., Konopka, P., Kinnison, D. E., and Tilmes, S.: Chemical and dynamical discontinuity at the extratropical tropopause based on START08 and WACCM analyses, J. Geophys. Res. Atmos., 116, D24302, doi: 10.1029/2011JD016686, 2011b.
Kunz, A., Sprenger, M., and Wernli, H.: Climatology of potential vorticity streamers and associated isentropic transport pathways across PV gradient barriers, J. Geophys. Res. Atmos., 120, 3802-3821, doi: 10.1002/2014jd022615, 2015.

Levelt, P. F., Oord, G. H. J. v. d., Dobber, M. R., Malkki, A., Huib, V., Johan de, V., Stammes, P., Lundell, J. O. V., and Saari, H.: The ozone monitoring instrument, IEEE Trans. Geosci. Remote Sens., 44, 1093-1101, doi: 10.1109/TGRS.2006.872333, 2006.

Liu, Y. S., Fueglistaler, S., and Haynes, P. H.: Advection-condensation paradigm for stratospheric water vapor, J. Geophys. Res. Atmos., 115,D24307, doi: 10.1029/2010JD014352, 2010.

Mazzera, D. M., Lowenthal, D. H., Chow, J. C., and Watson, J. G.: Sources of PM10 and sulfate aerosol at McMurdo station, Antarctica, Chemosphere, 45, 347-356, doi: https://doi.org/10.1016/S0045-6535(00)00591-9, 2001.

McCormick, M. P., Steele, H. M., Hamill, P., Chu, W. P., and Swissler, T. J.: Polar Stratospheric Cloud Sightings by SAM II, J. Atmos. Sci., 39, 1387-1397, doi: 10.1175/1520-0469(1982)039<1387:pscsbs>2.0.co;2, 1982.

Newman, P. A., and Nash, E. R.: Quantifying the wave driving of the stratosphere, J. Geophys. Res. Atmos.,105, 12485-12497, doi: 10.1029/1999JD901191, 2000.

Olsen, M. A., Douglass, A. R., Schoeberl, M. R., Rodriquez, J. M., and Yoshida, Y.: Interannual variability of ozone in the winter lower stratosphere and the relationship to lamina and irreversible transport, J. Geophys. Res. Atmos., 115, 10.1029/2009jd013004, 2010.

O'Sullivan, D., and Dunkerton, T. J.: The influence of the quasi-biennial oscillation on global constituent distributions, J. Geophys. Res. Atmos., 102, 21731-21743, doi: 10.1029/97JD01689, 1997.

Pallister, J. S., Schneider, D. J., Griswold, J. P., Keeler, R. H., Burton, W. C., Noyles, C., Newhall, C. G., and Ratdomopurbo, A.: Merapi 2010 eruption—Chronology and extrusion rates monitored with satellite radar and used in eruption forecasting, J. Volcanol. Geotherm. Res., 261, 144-152, doi: http://dx.doi.org/10.1016/j.jvolgeores.2012.07.012, 2013.

Ploeger, F., Konopka, P., Gunther, G., Grooss, J. U., and Muller, R.: Impact of the vertical velocity scheme on modeling transport in the tropical tropopause layer, J. Geophys. Res. Atmos., 115, 14, doi: 10.1029/2009jd012023, 2010.

Ploeger, F., Fueglistaler, S., Grooss, J. U., Gunther, G., Konopka, P., Liu, Y. S., Muller, R., Ravegnani, F., Schiller, C., Ulanovski, A., and Riese, M.: Insight from ozone and water vapour on transport in the tropical tropopause layer (TTL), Atmos. Chem. Phys., 11, 407-419, doi: 10.5194/acp-11-407-2011, 2011.

Portmann, R. W., Solomon, S., Garcia, R. R., Thomason, L. W., Poole, L. R., and McCormick, M. P.: Role of aerosol variations in anthropogenic ozone depletion in the polar regions, J. Geophys. Res. Atmos., doi: 101, 22991-23006, doi:10.1029/96JD02608, 1996.

Rößler, T., Stein, O., Heng, Y., Baumeister, P., and Hoffmann, L.: Trajectory errors of different numerical integration schemes diagnosed with the MPTRAC advection module driven by ECMWF operational analyses, Geosci. Model Dev., 11, 575-592, doi: 10.5194/gmd-11-575-2018, 2018.

Sand, M., Samset, B. H., Balkanski, Y., Bauer, S., Bellouin, N., Berntsen, T. K., Bian, H., Chin, M., Diehl, T., Easter, R., Ghan, S. J., Iversen, T., Kirkevåg, A., Lamarque, J. F., Lin, G., Liu, X., Luo, G., Myhre, G., Noije, T. V., Penner, J. E., Schulz, M., Seland, Ø., Skeie, R. B., Stier, P., Takemura, T., Tsigaridis, K., Yu, F., Zhang, K., and Zhang, H.: Aerosols at the poles: an AeroCom Phase II multi-model evaluation, Atmos. Chem. Phys., 17, 12197-12218, doi: 10.5194/acp-17-12197-2017, 2017.

Schoeberl, M. R., Douglass, A. R., Zhu, Z. X., and Pawson, S.: A comparison of the lower stratospheric age spectra derived from a general circulation model and two data assimilation systems, J. Geophys. Res. Atmos., 108, 16, doi: 10.1029/2002jd002652, 2003.

Sembhi, H., Remedios, J., Trent, T., Moore, D. P., Spang, R., Massie, S., and Vernier, J. P.: MIPAS detection of cloud and aerosol particle occurrence in the UTLS with comparison to HIRDLS and CALIOP, Atmos. Meas. Tech., 5, 2537-2553, doi: 10.5194/amt-5-2537-2012, 2012.

Shuckburgh, E., Norton, W., Iwi, A., and Haynes, P.: Influence of the quasi-biennial oscillation on isentropic transport and mixing in the tropics and subtropics, J. Geophys. Res. Atmos., 106, 14327-14337, doi: 10.1029/2000JD900664, 2001.

Sigl, M., Winstrup, M., McConnell, J. R., Welten, K. C., Plunkett, G., Ludlow, F., Buntgen, U., Caffee, M., Chellman, N., Dahl-Jensen, D., Fischer, H., Kipfstuhl, S., Kostick, C., Maselli, O. J., Mekhaldi, F., Mulvaney, R., Muscheler, R., Pasteris, D. R., Pilcher, J. R., Salzer, M., Schupbach, S., Steffensen, J. P., Vinther, B. M., and Woodruff, T. E.: Timing and climate forcing of volcanic eruptions for the past 2,500 years, Nature, 523, 543-549, doi: 10.1038/nature14565http://www.nature.com/nature/journal/v523/n7562/abs/nature14565.html#supplementary-information, 2015.

Solomon, S.: Stratospheric ozone depletion: A review of concepts and history, Rev. Geophys., 37, 275-316, doi: 10.1029/1999RG900008, 1999.

Solomon, S., Daniel, J. S., Neely, R. R., Vernier, J.-P., Dutton, E. G., and Thomason, L. W.: The Persistently Variable "Background" Stratospheric Aerosol Layer and Global Climate Change, Science, 333, 866-870, doi: 10.1126/science.1206027, 2011.

Solomon, S., Garcia, R. R., Rowland, F. S., and Wuebbles, D. J.: On the depletion of Antarctic ozone, Nature, 321, 755, doi: 10.1038/321755a0, 1986.

Solomon, S., Ivy, D. J., Kinnison, D., Mills, M. J., Neely, R. R., and Schmidt, A.: Emergence of healing in the Antarctic ozone layer, Science, doi: 10.1126/science.aae0061, 2016.

Solomon, S., Sanders, R. W., Garcia, R. R., and Keys, J. G.: Increased chlorine dioxide over Antarctica caused by volcanic aerosols from Mount-Pinatubo, Nature, 363, 245–248, doi: https://doi.org/10.1038/363245a0, 1993.

Spang, R., Riese, M., and Offermann, D.: CRISTA-2 observations of the south polar vortex in winter 1997: A new dataset for polar process studies, Geophys. Res. Lett., 28, 3159–3162, doi: 10.1029/2000GL012374, 2001.

Stohl, A., Forster, C., Frank, A., Seibert, P., and Wotawa, G.: Technical note: The Lagrangian particle dispersion model FLEXPART version 6.2, Atmos. Chem. Phys., 5, 2461-2474, doi:10.5194/acp-5-2461-2005, 2005.

Stone, K. A., Solomon, S., Kinnison, D. E., Pitts, M. C., Poole, L. R., Mills, M. J., Schmidt, A., Neely, R. R., Ivy, D., Schwartz, M. J., Vernier, J.-P., Johnson, B. J., Tully, M. B., Klekociuk, A. R., König-Langlo, G., and Hagiya, S.: Observing the Impact of Calbuco Volcanic Aerosols on South Polar Ozone Depletion in 2015, J. Geophys. Res. Atmos., 122, 11,862-811,879, doi: 10.1002/2017JD026987, 2017.

Surono, Jousset, P., Pallister, J., Boichu, M., Buongiorno, M. F., Budisantoso, A., Costa, F., Andreastuti, S., Prata, F., Schneider, D., Clarisse, L., Humaida, H., Sumarti, S., Bignami, C., Griswold, J., Carn, S., Oppenheimer, C., and Lavigne, F.: The 2010 explosive eruption of Java's Merapi volcano—A '100-year' event, J. Volcanol. Geotherm. Res., 241, 121-135, doi: http://dx.doi.org/10.1016/j.jvolgeores.2012.06.018, 2012.

Tilmes, S., Muller, R., and Salawitch, R.: The sensitivity of polar ozone depletion to proposed geoengineering schemes, Science, 320, 1201-1204, doi: 10.1126/science.1153966, 2008.

Toohey, M., Krüger, K., Niemeier, U., and Timmreck, C.: The influence of eruption season on the global aerosol evolution and radiative impact of tropical volcanic eruptions, Atmos. Chem. Phys., 11, doi: 12351-12367, 10.5194/acp-11-12351-2011, 2011.

Vernier, J. P., Thomason, L. W., Pommereau, J. P., Bourassa, A., Pelon, J., Garnier, A., Hauchecorne, A., Blanot, L., Trepte, C., Degenstein, D., and Vargas, F.: Major influence of tropical volcanic eruptions on the stratospheric aerosol layer during the last decade, Geophys. Res. Lett., 38, L12807, doi: 10.1029/2011GL047563, 2011.

Vogel, B., Pan, L. L., Konopka, P., Gunther, G., Muller, R., Hall, W., Campos, T., Pollack, I., Weinheimer, A., Wei, J., Atlas, E. L., and Bowman, K. P.: Transport pathways and signatures of mixing in the extratropical tropopause region derived from Lagrangian model simulations, J. Geophys. Res. Atmos., 116, 16, doi: 10.1029/2010jd014876, 2011.

von Glasow, R., Bobrowski, N., and Kern, C.: The effects of volcanic eruptions on atmospheric chemistry, Chem. Geol., 263, 131-142, doi: http://dx.doi.org/10.1016/j.chemgeo.2008.08.020, 2009.

Watson, P. A. G., and Gray, L. J.: How Does the Quasi-Biennial Oscillation Affect the Stratospheric Polar Vortex?, J. Atmos. Sci., 71, 391-409, doi: 10.1175/jas-d-13-096.1, 2014.

Wohltmann, I., and Rex, M.: Improvement of vertical and residual velocities in pressure or hybrid sigma-pressure coordinates in analysis data in the stratosphere, Atmos. Chem. Phys., 8, 265-272, doi: 10.5194/acp-8-265-2008, 2008.

Wu, X., Griessbach, S., and Hoffmann, L.: Equatorward dispersion of a high-latitude volcanic plume and its relation to the Asian summer monsoon: a case study of the Sarychev eruption in 2009, Atmos. Chem. Phys., 17, 13439-13455, doi: 10.5194/acp-17-13439-2017, 2017.

Zuev, V. V., Zueva, N. E., Savelieva, E. S., and Gerasimov, V. V.: The Antarctic ozone depletion caused by Erebus volcano gas emissions, Atmos. Environ., 122, 393-399, doi: https://doi.org/10.1016/j.atmosenv.2015.10.005, 2015.

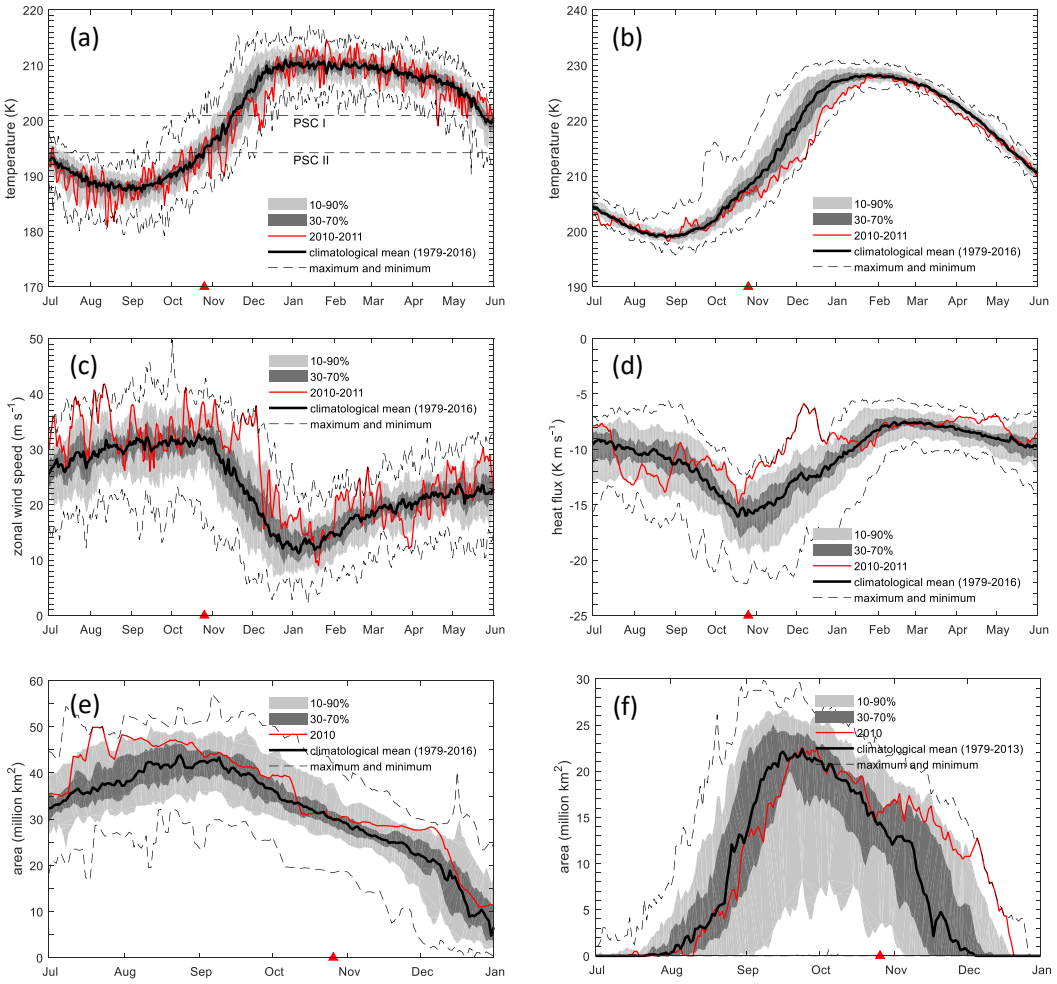

Figure 1: (a) Minimum temperature south of 50 ℃S at 150 hPa; (b) temperature averaged over the polar cap for latitudes south of 60 ℃S at 150 hPa; (c) zonal wind speed at 60 ℃S at 150 hPa; (d) eddy heat flux averaged between 45 ℃S and 75 ℃S for the 45-day period prior to the date indicated at 150 hPa; (e) the area of the polar vortex for 1 July–31 December 2010 on the 460 K isentropic surface; (f) ozone hole area for 1 July 2010–31 December 2010. Temperatures for PSC existence in (a) are determined by assuming a nitric acid concentration of 6 ppbv and a water vapor concentration of 4.5 ppmv. (a)–(f) are based on Modern-Era Retrospective analysis for Research and Applications reanalysis version 2 (MERRA2) data (Bosilovich et al., 2015). The ozone hole area in (f) is determined from OMI ozone satellite measurements (Levelt et al., 2006). The red triangles indicate the time of the Merapi eruption.

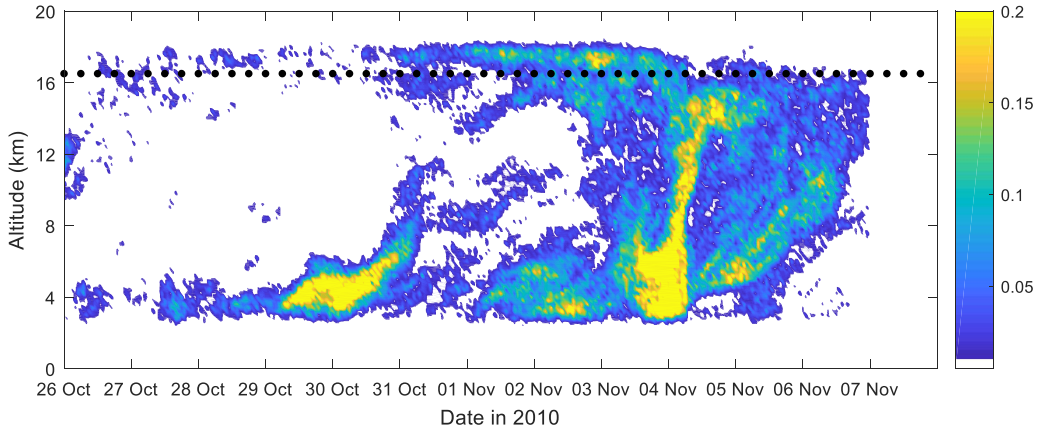

Figure 2: Merapi SO_2 emission time series (unit: kg m^{-1} s^{-1}) derived from AIRS measurements using a backward trajectory approach (see text for details). The emission data are binned every 1 h and 0.2 km. The ticks for the horizontal axis mark 0 UTC on each day. Black dots denote the height of the thermal tropopause (based on the ERA–Interim reanalysis).

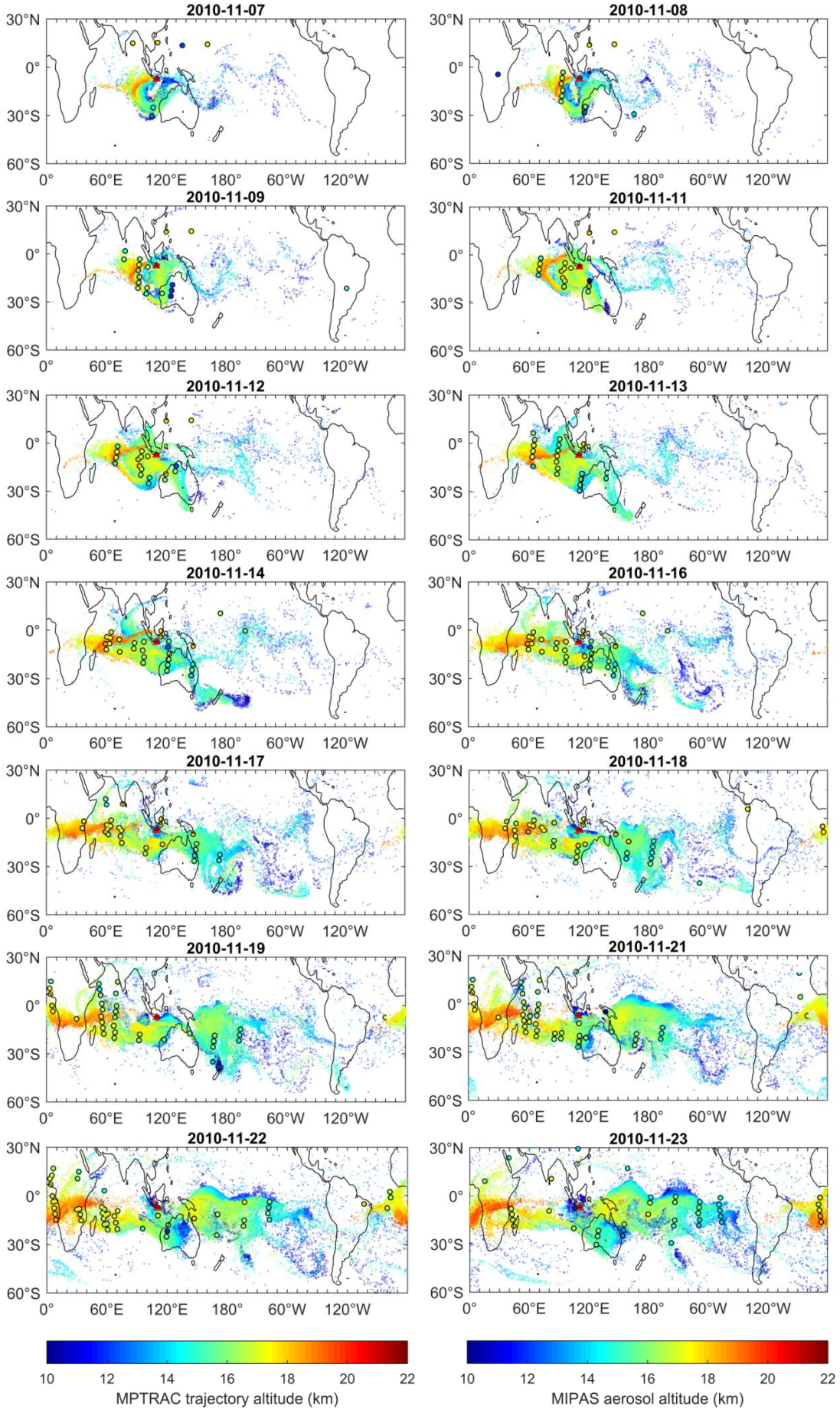

Figure 3: Distribution of the volcanic plume (showing only air parcels higher than 10 km, shading) from MPTRAC simulations (shown for 00:00UTC on selected days) and MIPAS aerosol detections (ACI < 7) within ±6 h (color-filled circles). The altitudes of all

air parcels, regardless of their SO_2 values, are shown. The red triangle denotes the location of Mount Merapi.

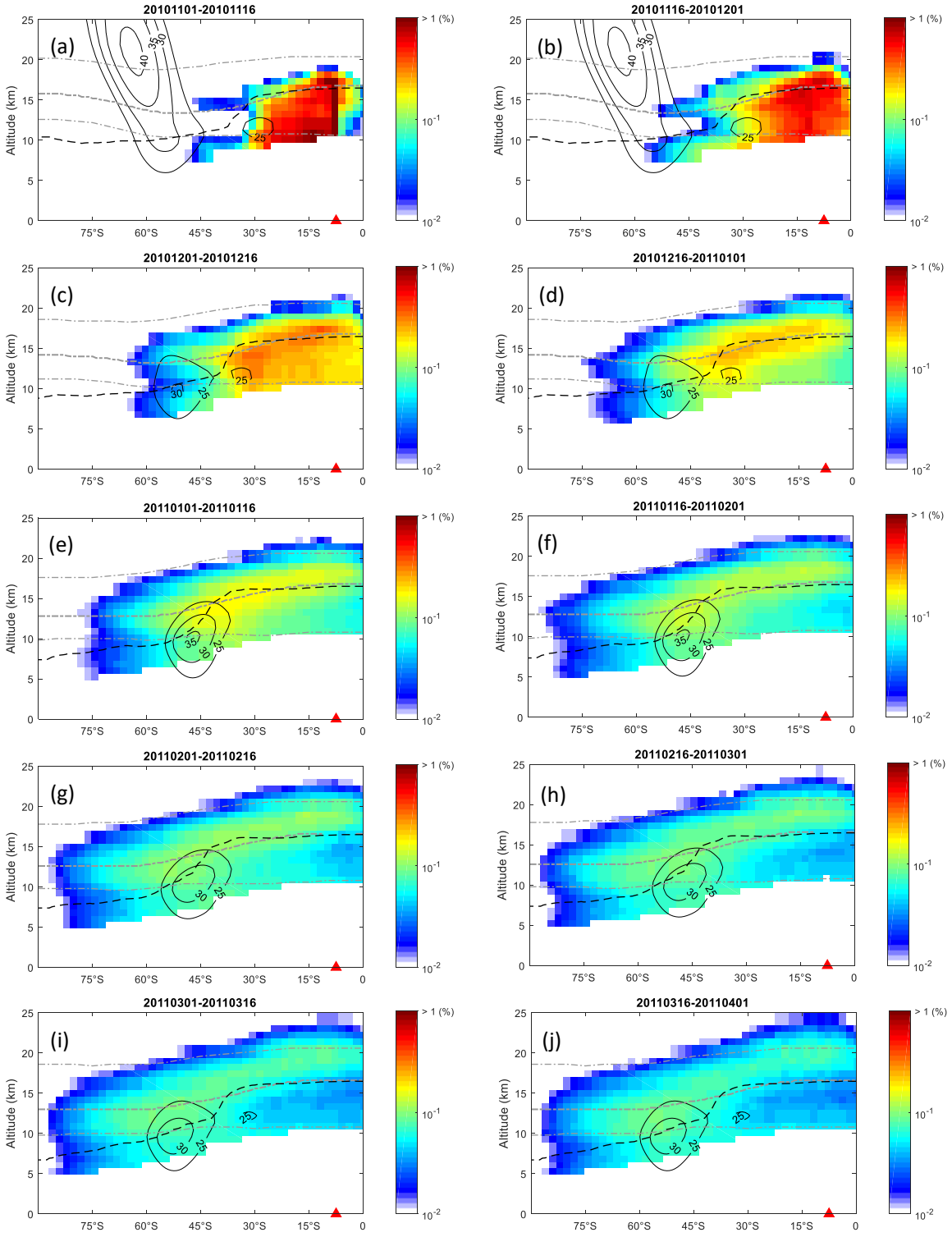

Figure 4: Percentage (%) of air parcels in proportion to the total number of air parcels released in the Lagrangian forward simulation, overlaid with monthly mean zonal winds (black contours), the thermal tropopause (black dashed line), the 380 K potential temperature isoline (thick gray dashed line) and 350 and 480 K potential temperature isolines (thin gray dashed lines). Results are binned every 2 °in latitude and 1 km in altitude. The red triangle denotes the latitude of the Mount Merapi. Please see title of each figure for the time period covered.

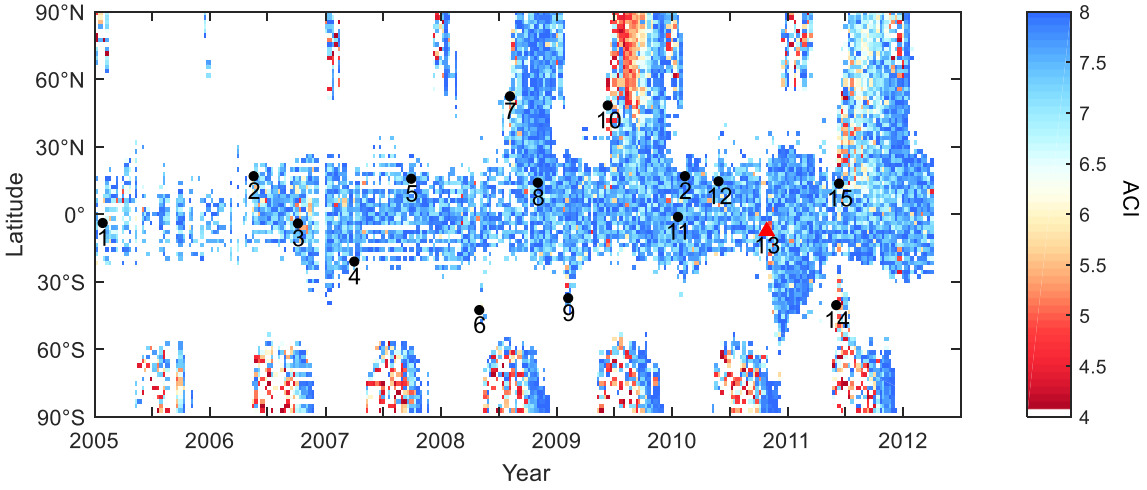

Figure 5: Median value of MIPAS ACI detections between 12–18 km (bin size: 10 days and 2 °in latitude) from January 2005 to April 2012. Only ACI values from 4 to 8 are shown. The red triangle indicates the eruption of Mount Merapi (No. 13). The black filled circles indicate 1 Manam, 2 Soufriere Hills, 3 Tavurvur (Rabaul), 4 Piton de la Fournaise, 5 Jebel at Tair, 6 Chaitén, 7 Kasatochi, 8 Dalaffilla, 9 Australian bushfire, 10 Sarychev Peak, 11 Nyamuragira, 12 Pacaya, 14 Puyehue-Cordón Caulle, 15 Nabro.

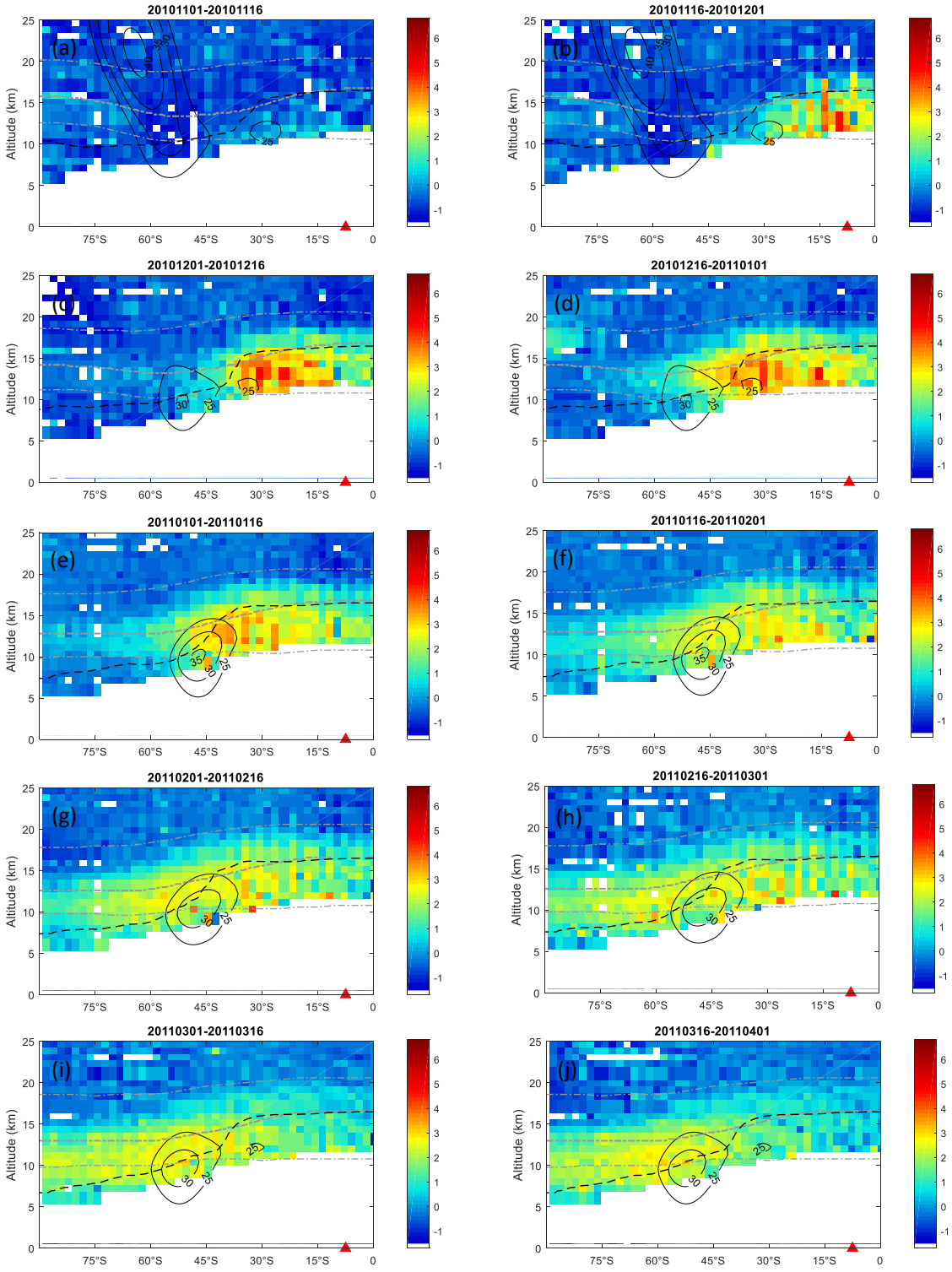

Figure 6: The change of MIPAS ACI values after the eruption of Merapi in 2010, overlaid with monthly mean zonal winds (black contours), the thermal tropopause (black dashed line), the 380 K potential temperature isoline (thick gray dashed line) and 350 and 480 K potential temperature isolines (thin gray dashed lines). Positive values indicate an increase of the aerosol load and negative values indicate a decrease of the aerosol load. Results are binned every 2 °in latitude and 1 km in altitude. The red triangle denotes the latitude of the Mount Merapi. Please see title of each figure for the time period covered.

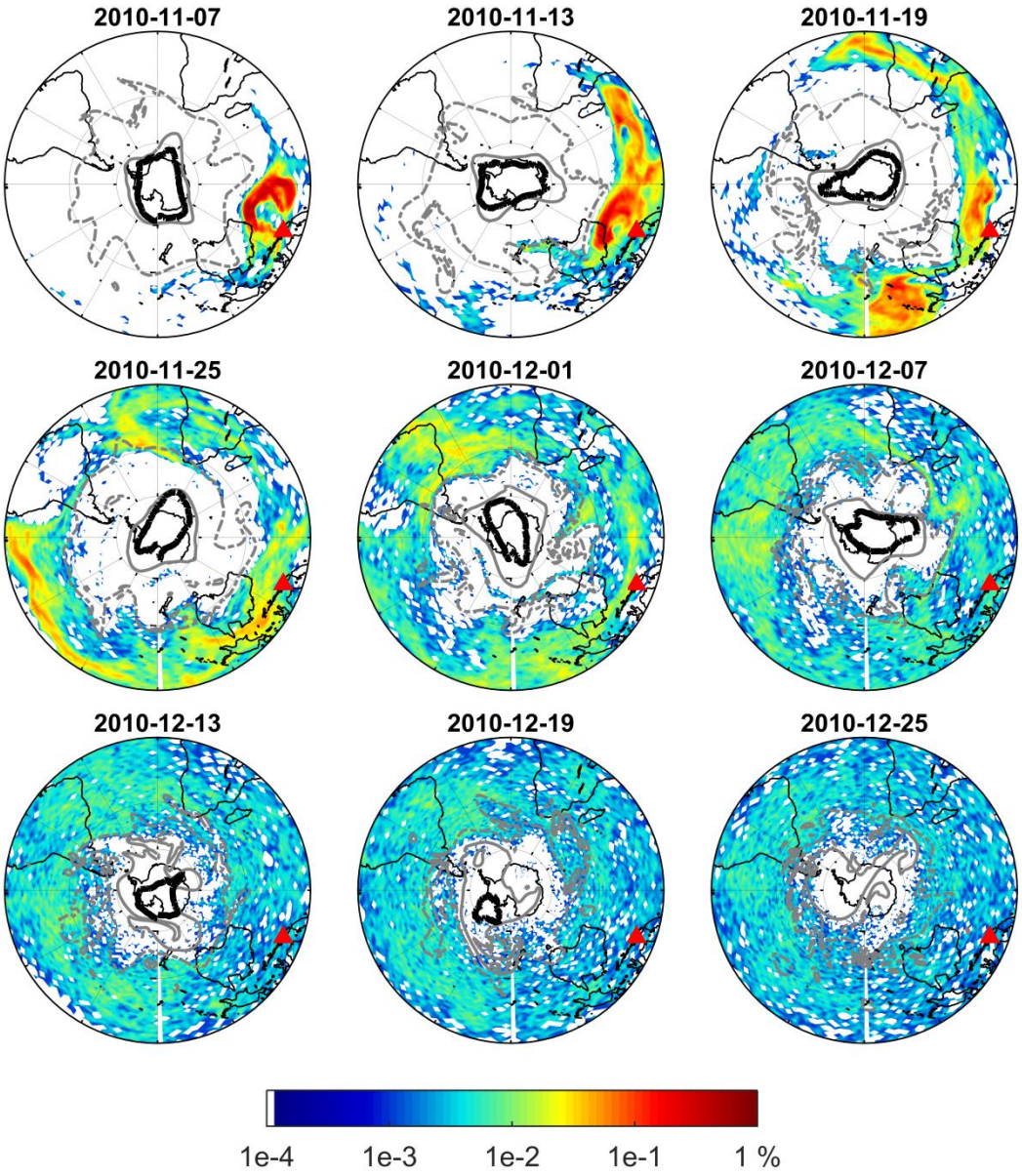

Figure 7: Percentage (%) of air parcels between the isentropic surfaces of 350 and 480 K in proportion to the total number of air parcels released in the Lagrangian forward simulation. All results are at 12:00 UTC on selected dates and binned every 2 ° in longitude and 1 ° in latitude. The black contours indicate the 220 DU contour lines of daily mean ozone column density provided by OMI. PV contours marked with gray dashed and solid lines show PV boundaries on the 350 and 480 K isentropic surfaces respectively (Kunz et al., 2015). The red triangle denotes the location of Mount Merapi.

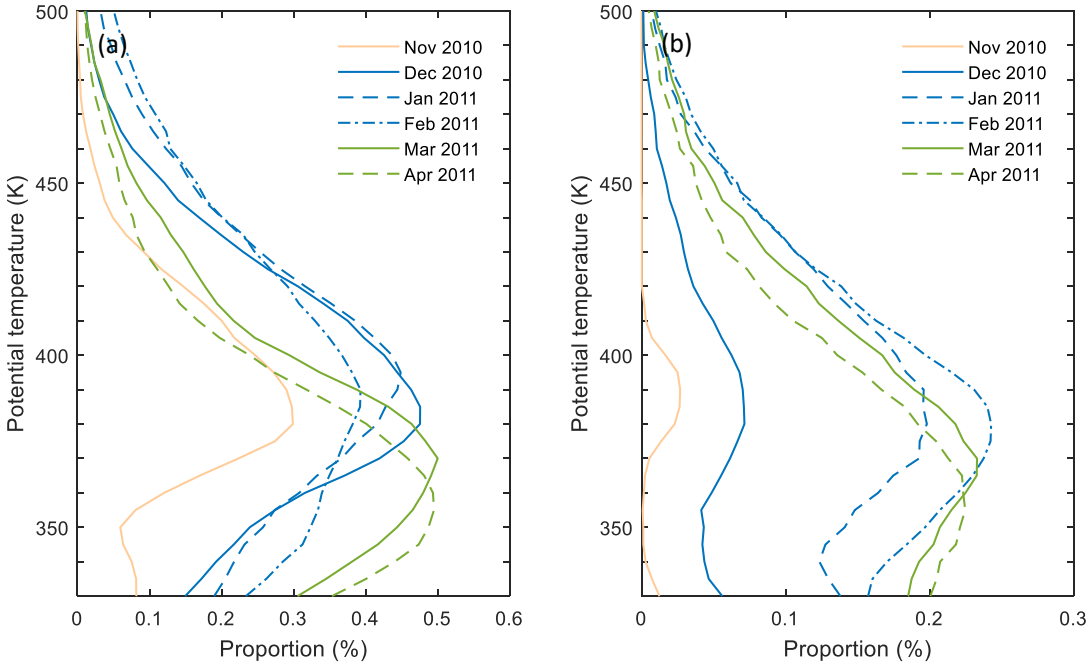

Figure 8: (a) Proportion (%) of the air parcels poleward of the PV-based transport boundaries at the end of each month; (b) proportion (%) of the air parcels south of 60 ℃S.

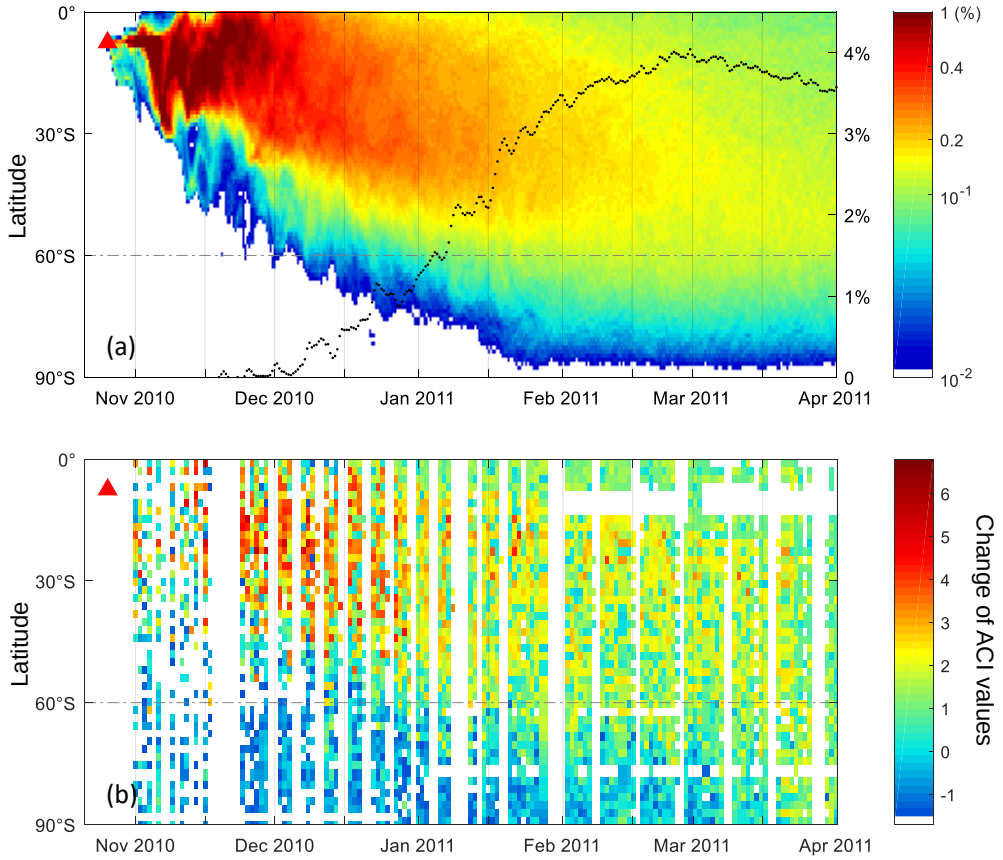

Figure 9: Time and latitude evolution of the (a) percentage (%) of air parcels between the isentropic surfaces of 350 and 480 K from the Lagrangian simulations (shading, only percentages larger than 0.05% are shown; bin size: 12h and 1 ° in latitude) and the proportion (%) of air parcels south of 60 °S (black dots); (b) the change of MIPAS ACI values after the eruption of Merapi in 2010 between 350 and 480 K. Positive values indicate an increase and negative values indicate a decrease of the aerosol load (bin size: 24h and 2 ° in latitude). The red triangle denotes the time and latitude of the Merapi eruption.

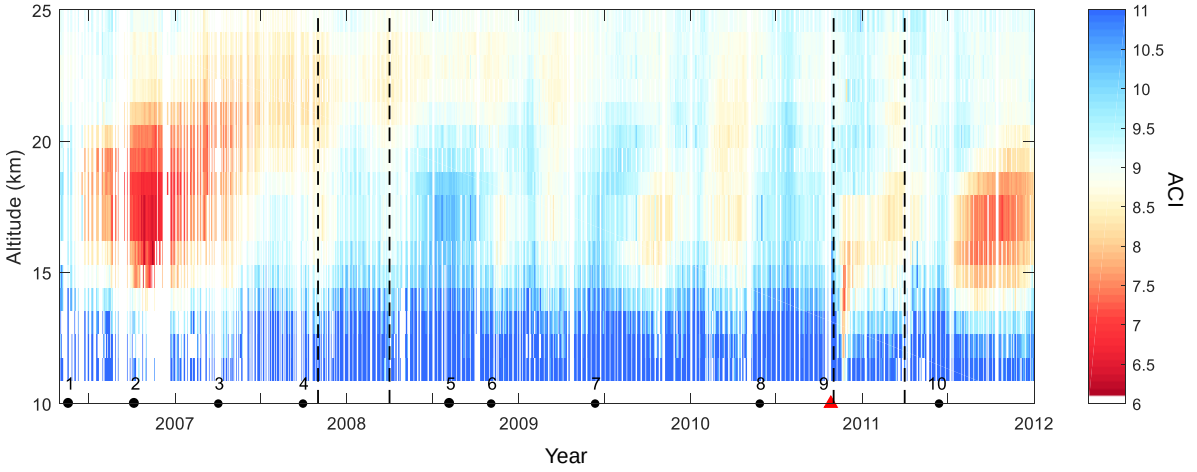

Figure A1: MIPAS 9-day running median of ACI between 10 ℕ and 10 𝕊 from May 2006 to December 2011.The dashed vertical lines indicate the reference state from November 2007 to March 2008, and the investigation period for the Merapi eruption from November 2010 to March 2011. The red triangle indicates the time of the Merapi eruption (No. 9). The black dots indicate 1 Soufriere Hills, 2 Tavurvur (Rabaul), 3 Piton de la Fournaise, 4 Jebel at Tair, 5 Kasatochi, 6 Dalaffilla, 7 Sarychev, 8 Pacaya, 10 Nabro.